

INSTITUTE
FOR
COSMIC RAY RESEARCH
UNIVERSITY OF TOKYO

ANNUAL REPORT
(APRIL 2010 – MARCH 2011)



Editorial Board

YOSHIKOSHI, Takanori

OHASHI, Masatake

OBAYASHI, Yoshihisa

BAI, Lili

TAKENAGA, Yumiko

ITOH, Hideo

©**Institute for Cosmic Ray Research, University of Tokyo**

5-1-5, Kashiwanoha, Kashiwa, Chiba 277-8582, Japan

Telephone: (81) 4-7136-3102

Facsimile: (81) 4-7136-3115

WWW URL: <http://www.icrr.u-tokyo.ac.jp/>

TABLE OF CONTENTS

Preface	
Research Divisions	1
Neutrino and Astroparticle Division	2
High Energy Cosmic Ray Division	15
Astrophysics and Gravity Division	40
Observatories and a Research Center	58
Norikura Observatory	59
Akeno Observatory	64
Kamioka Observatory	65
Research Center for Cosmic Neutrinos	66
Appendix A. ICRR Workshops and Ceremonies	68
Appendix B. ICRR Seminars	68
Appendix C. List of Publications	69
(a) Papers Published in Journals	
(b) Conference Papers	
(c) ICRR Reports	
Appendix D. Doctoral Theses	75
Appendix E. Public Relations	75
(a) ICRR News	
(b) Public Lectures	
(c) Visitors	
Appendix F. Inter-University Researches	78
Appendix G. List of Committee Members	82
(a) Board of Councillors	
(b) Advisory Committee	
(c) Inter-University Research Advisory Committee	
Appendix H. List of Personnel	83

PREFACE

This report summarizes the scientific activities of the Institute for Cosmic Ray Research (ICRR) of the University of Tokyo in the Japanese FY 2010.

ICRR is an inter-university research institute for studies of cosmic rays. The headquarters of ICRR is located in Kashiwa, Chiba prefecture, Japan. In order to promote various cosmic-ray-related studies efficiently, ICRR has three research divisions; Neutrino and Astroparticle division, High Energy Cosmic Ray division, and Astrophysics and Gravity division. ICRR has 3 observatories in Japan; Kamioka Observatory (Kamioka underground, Gifu prefecture), Norikura Observatory (2770 meters above sea level, Mt. Norikura, Gifu prefecture), and Akeno Observatory (Yamanashi prefecture), together with 1 research center; Research Center for Cosmic Neutrinos (Kashiwa, Chiba prefecture). In addition, there are 3 major experimental facilities outside of Japan. They are located in Utah in USA, Yangbajing in Tibet, China, and Woomera in Australia.

More than 300 researchers from various Japanese institutions are involved in the research programs of ICRR. It should be noted that most of the scientific outputs from this institute are the results of the collaborative efforts by many institutions. In order to produce outstanding results, it is very important to carry out an experiment by an international collaboration composed of top-level researchers all over the world. Hence, most of the experimental collaborations that ICRR is involved are international ones. For example, the number of collaborators in the Super-Kamiokande experiment is about 130; among them 60 are from abroad (USA, Korea, China, Poland and Spain).

Many exciting scientific activities of ICRR are described in this report. One of the highlights is the initial results from the T2K long-baseline neutrino oscillation experiment, which studies neutrino oscillations in detail including the third mixing angle θ_{13} . Another highlight is the start of the construction of Large-scale Cryogenic Gravitational wave Telescope (LCGT), which intends to detect gravitational waves for the first time and open a new field of "gravitational wave astronomy".

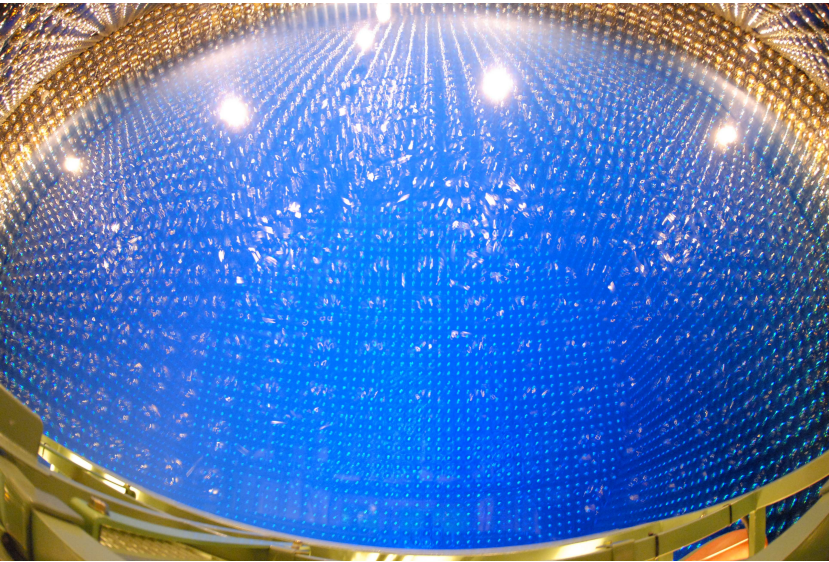
We hope that this report is useful for the understanding of the current research activities of ICRR. Finally, we appreciate very much the strong support of our colleagues in this research field, the University of Tokyo and the Japanese Ministry of Education, Culture, Sports, Science and Technology. They are indispensable for the continuing, and exciting scientific outcome of ICRR.



Takaaki Kajita,
Director,
Institute for Cosmic Ray Research,
The University of Tokyo



The ICRR building at Kashiwa, Chiba, Japan.



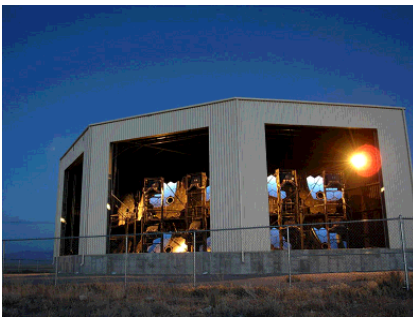
The inner detector of Super-Kamiokande-III during the full reconstruction. The purified water is under filling.



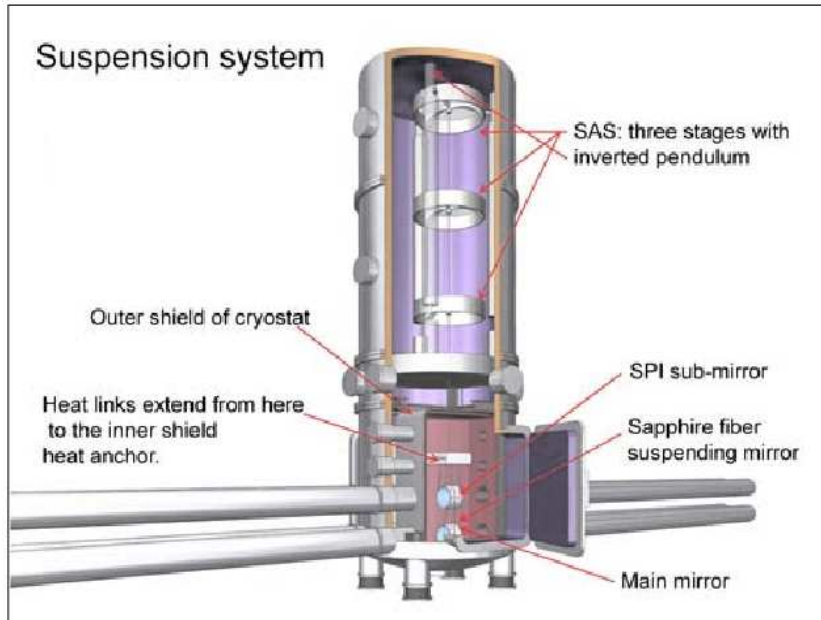
The system of four imaging atmospheric Cherenkov telescopes of 10m diameter of CANGAROO project for detection of very high energy gamma-rays. The whole system is in operation since March 2004 in Woomera, South Australia.



Tibet-III air shower array (37000 m²) at Yangbajing, Tibet (4300 m in altitude).



Air fluorescence telescopes (left) and a scintillator surface detector (right) of the Telescope Array experiment in Utah, USA to explore the origin of extremely high energy cosmic rays.



Cryogenic mirror suspension system for Large Scale Cryogenic Gravitational Wave Telescope.

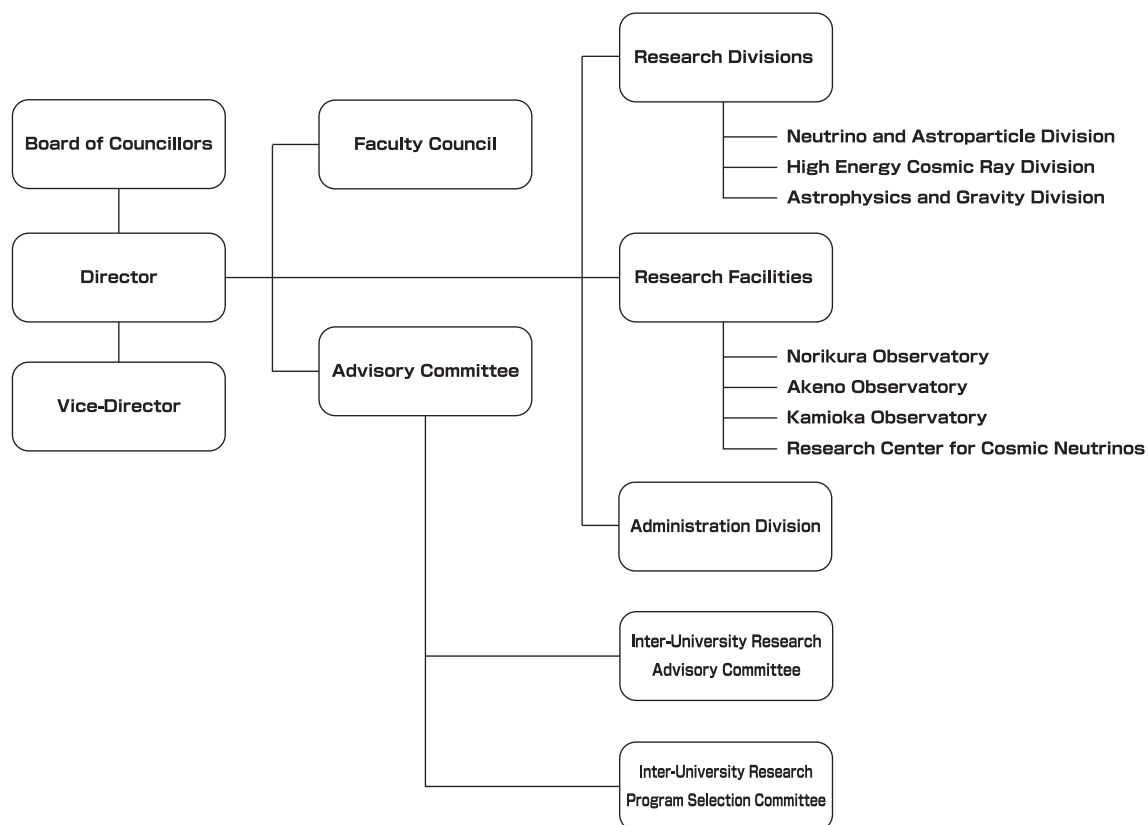


Wide-view telescope of 2.5 m diameter (left telescope) in Arizona, USA for the Sloan Digital Sky Survey project.



A public lecture held by Research Center for Cosmic Neutrinos.

Organization



Number of Staff Members (As of April 1, 2010)

	Scientific Staff	Technical Staff	Research Fellows	Administrators and Secretaries	Total
Neutrino and Astroparticle Div.	22	5	4	14	45
High Energy Cosmic Ray Div.	15	14	4	5	38
Astrophysics and Gravity Div.	10	0	3	1	14
Administration	1	0	0	11	12
Total	48	19	11	31	109

FY 2005–2010 Budget

	2005	2006	2007	2008	2009	2010
Personnel expenses	465 000	566 000	624 000	632 000	590 000	576 000
Non-personnel expenses	1 822 000	812 000	1 253 000	1 121 000	1 292 000	1 048 000
Total	2 287 000	1 378 000	1 877 000	1 753 000	1 882 000	1 624 000

(in 1 000 yen)

RESEARCH DIVISIONS

Neutrino and Astroparticle Division

Overview

Super-Kamiokande Experiment

Hyper-Kamiokande

T2K Experiment

XMASS Experiment

High Energy Cosmic Ray Division

Overview

CANGAROO and TeV Gamma-Ray Projects

TA: Telescope Array Experiment

Tibet AS γ Project

Ashra Project

High Energy Astrophysics Group

Astrophysics and Gravity Division

Overview

Gravitational Wave Group

LCGT Project

CLIO Project

Sloan Digital Sky Survey

Primary Cosmic Ray Group

Theory Group

Particle Phenomenology

Astrophysics and Cosmology

NEUTRINO AND ASTROPARTICLE DIVISION

Overview

This division aims to study particle physics with prime interests in physics of neutrinos and proton decay, and astroparticle physics with the use of underground experimental facilities.

Our most important facility is the Super-Kamiokande (SK) detector. It is a 50kton water Cherenkov detector using 11,129 50 cm-diameter photomultipliers (PMTs) for its inner detector and 1,885 20 cm-diameter PMTs for its outer detector. The data taking of SK started in April 1996. The most important physics results are the discovery of neutrino oscillation in atmospheric neutrinos in 1998 and thereby demonstrating that neutrinos have a finite mass, and the accurate measurement of the solar neutrino flux from the decay of ^8B which served to confirm the long-conjectured neutrino oscillation hypothesis in solar neutrinos beyond doubt. The search for nucleon decay at SK gives the current best limit which strongly constrains the grand unification scenario of particle interactions. SK has been monitoring for neutrinos from supernova bursts. If a supernova burst occurs at a distance from the center of our galaxy, SK will be able to detect about 8,000 neutrino events. A high intensity neutrino beam experiment using the J-PARC accelerator (T2K) was started in 2009. The T2K experiment uses the SK detector as the far detector. The third oscillation pattern (the effect of the mixing angle θ_{13}) and the high precision measurement of oscillation parameters are main physics subjects in T2K. In 2010, the first results of the T2K experiment were released as described below.

Another activity of the Neutrino and Astroparticle division is a multi-purpose experiment using liquid xenon aiming at the detection of cold dark matter, neutrino absolute mass using neutrinoless double beta decay, and low energy solar neutrinos. The construction of a 800 kg liquid xenon detector which is dedicated for the dark matter search was finished in 2010 and the commissioning of the detector was started.

Recent progress of research activities in the Neutrino and Astroparticle division is presented here.

Super-Kamiokande experiment

Supernova neutrinos

Kamiokande and IMB observed the neutrino burst from supernova 1987a. This observation confirmed that the energy released by neutrinos is about several $\times 10^{53}$ ergs. However, the observed number of events were only 11 by Kamiokande and 8 by IMB, respectively. Super-Kamiokande would be able to detect several thousand neutrino events if a supernova happened near the center of our galaxy. Such an observation would enable us to investigate in detail the mechanics of the supernova explosion. Galactic supernovae are searched for almost in real time at SK. The online data acquisition system running in the mine sends data to the offline computer system in the surface building of Kamioka observatory. As

soon as a block of data (usually a block corresponds to several minutes) is transferred to the offline system, a program called SNWATCH searches for time clustered events. Current criteria of SNWATCH are (1) more than or equal to 7 events within 0.5sec, (2) more than or equal to 8 events within 2sec, and (3) more than or equal to 13 events within 10sec. When at least one of these criteria are met, SNWATCH reconstructs vertex position and energy of the events together with neighboring cosmic ray muons. In most cases, these clusters are due to spallation products whose vertex positions are aligned with their parent cosmic ray muon. If SNWATCH finds an event cluster whose vertex spread is larger than a given criterion, an alarm signal is sent to experts by an e-mail. Then, the experts check whether it is a real supernova signal or not by looking at various plots which are uploaded to a secured site accessible from the Internet (including i-mode keitai). Such alarms happen almost once per month. They are usually due to the accidental coincidence of two cosmic ray induced clusters. We have a supernova drill at least once per year. So far, no real supernova neutrino burst signal has been observed at Super-Kamiokande.

In the drill, the SNWATCH conveners and the executive committee members meet via TV conference system, and discuss to make a decision for a prompt announcement to outside researchers and the press. We practice this drill as if a real supernova happened. We also have SK shift training by illuminating an LED in the SK detector a few times every month. SK shift members are notified by a dummy alarm that SNWATCH makes when the LED is illuminated. The shift members then call to the SNWATCH experts and give a report. The SK collaborators will be ready for the real supernovae through the drill and the training.

We also search for neutrinos from old supernovae, which are called Supernova Relic Neutrinos (SRNs). The SRN signal is the diffuse supernova neutrino background from all the supernovae in the past. This signal has never been detected, but it is expected to be detectable in the 16-30 MeV energy region, which is the gap between the energy ranges of solar neutrinos and atmospheric neutrinos. We have applied carefully tuned data selection to enhance the SRN candidates, improving the efficiency of our search by over 20% compared to the 2003 SK-I study, which currently provides the world's best limit on SRN flux. Our improved data selection also allows us to now search the 16-18 MeV positron energy region, which was previously unusable due to spallation background. Our updated search utilizes SK-II and SK-III data as well as SK-I, considers two new background channels, and performs a sophisticated maximum likelihood search in multiple regions of the Cherenkov angle distribution to extract the most accurate flux limit possible (Fig.1). Multiple systematic errors are considered. A flux limit of between 2.7 and 3.0 $\bar{\nu} \text{cm}^{-2} \text{s}^{-1}$ (positron energy > 16 MeV) is our new result, with the exact value depending on the shape of the neutrino spectrum

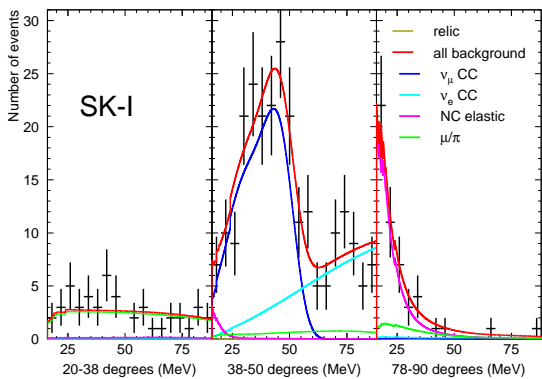


Fig. 1. SK-I best fit result, assuming Ando et al's LMA model. The relic best fit is negative, so a relic fit of 0 is shown. SK-II and SK-III have small but positive relic best fits.

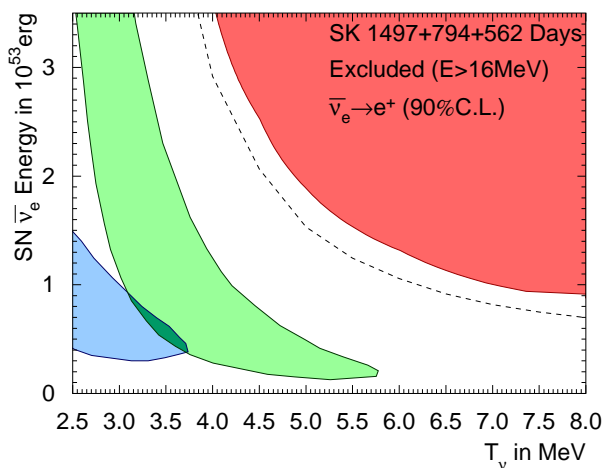


Fig. 2. Results plotted as an exclusion contour in SN neutrino luminosity vs. neutrino temperature parameter space. The green and blue contours show IMB and Kamiokande allowed areas for 1987a data, respectively. The red shows our new 90% c.l. result. The dashed line shows the individual 90% c.l. results of each temperature considered separately, which is not a true 2-D exclusion contour.

assumed. This new result will replace the 2003 study to be the most accurate measure of the SRN signal ever performed. Furthermore, a new method of presenting the SRN flux limit is also ready which is of great use to theorists and does not depend on any particular model (Fig.2).

Super-Kamiokande R&D gadolinium project

As mentioned above, although at SK a few SRN events a year are expected, SRNs have not been detected yet because the large backgrounds constrain our search. The main goal of our research is to reduce these backgrounds and be able to detect SRNs. The observation of SRNs in general or neutrinos from distant supernovae in particular, would give us some information about the universe, for example the core collapse rate from SRNs, and the neutrino itself too, for example about



Fig. 3. In the new cavern the Gd pre-mixing and pre-treatment 15 ton tank (front left), the selective filtration system (front right) and the 200 ton tank (rear of the hall) have been installed.

its lifetime. Since most of the neutrinos that can be detected at SK undergo inverse beta decay, electron anti-neutrinos are the most copiously detected neutrinos:



Presently, the SK detector can only detect the positrons efficiently but if we could detect the neutrons, we could greatly reduce the backgrounds that constrain our SRN search. This could be attained by the coincidence detection of positron and neutron (in space, vertices within tens of cm and in time, with the neutron capture delayed about 20 μ sec). By adding 0.2% of gadolinium (Gd) sulfate into the water tank we could achieve this goal. Gadolinium has a neutron capture cross section of 49,000 barns (about 5 orders of magnitude larger than of protons) and emits a gamma cascade of 8 MeV that can be easily detected at SK.

We want to show that adding Gd into the SK water, SK will become an electron anti-neutrino detector, able to tag inverse beta decays, while keeping all its previous capabilities in the other analyses like solar and atmospheric neutrinos. The EGADS (Evaluation Gadolinium's Action on Detector Systems) project was funded in 2009 and since then a new hall near the SK detector has been excavated and a 200 ton tank with its ancillary equipment has been installed, see Fig.3. The idea is to mimic the conditions at SK inside the 200 ton tank. It has been equipped with a selective water filtration system, that will filter out water impurities while keeping Gd in the water, a Gd pre-mixing and pre-treatment 15 ton tank and a device to measure the water attenuation length (UDEAL). Since the middle of January, the 200 ton tank has been filled with pure water. The water system, which has been running stably since the beginning of February has proven to keep a high water quality, see Fig.4. Soon we will test adding gadolinium sulfate to the pre-mixing 15 ton tank and circulate the water through the water system. The next step will be to add gadolinium sulfate to the 200 ton tank and by the end of 2011 we expect to mount 240 50-cm photomultipliers, thus entering in the last phase of this exciting project.

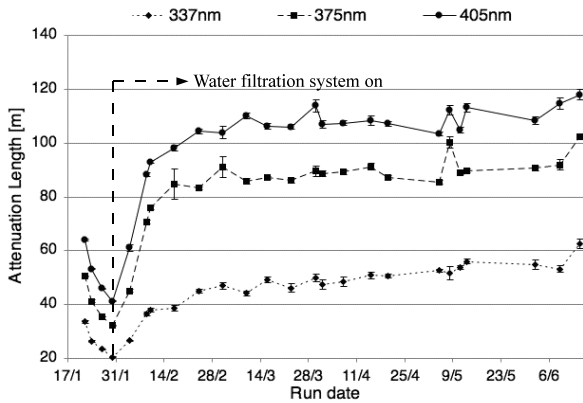


Fig. 4. Water attenuation length for pure water from the 200 ton tank for three wave lengths: 337nm, 375nm and 405nm. The water attenuation length decreases first and then increases as soon as the water filtration system ran continuously.

Source	Total flux
Energy scale	± 1.4
Energy resolution	± 0.2
Theoretical uncertainty of ${}^8\text{B}$ spectrum	$\pm 0.2^{(+1.1)}_{(-1.0)}$
Trigger efficiency	± 0.5
Angular resolution	$\pm 0.67(\pm 1.2)$
Vertex shift	$\pm 0.54(\pm 1.3)$
Event quality cuts	$\pm 0.65^{(+2.1)}_{(-1.6)}$
Spallation	± 0.2
External event cut	± 0.25
Small cluster hits cut	± 0.5
Background shape	± 0.1
Signal extraction method	± 0.7
Livetime	± 0.1
Cross section	± 0.5
Total	$\pm 2.1^{(+3.5)}_{(-3.2)}$

Table 1. Systematic uncertainty summary for the total flux in %. SK-I values are also shown in parentheses for the largely improved systematic sources in the current SK-III analysis.

Solar neutrinos

SK detects solar neutrinos through elastic neutrino-electron scattering, $\nu + e \rightarrow \nu + e$, where the energy, direction and time of the recoil electron are measured. Due to its large fiducial mass of 22.5 kiloton, SK gives the most precise measurement of the solar neutrinos' flux with accurate information of the energy spectrum and time variations. To achieve this high precision, precise calibrations are performed for the energy scale, energy resolution, angular resolution and the vertex position resolution using a LINAC and ${}^{16}\text{N}$ radioisotope generated by a DT neutron generator.

This year, the SK-III data analysis was finalized with a livetime of 298 days for the total electron energy range between 5 MeV and 6.5 MeV, and 548 days for the range between 6.5 MeV and 20 MeV [1]. The SK-III data have a lower background level in the low energy region than the SK-

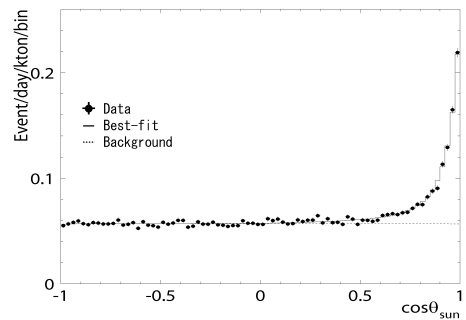


Fig. 5. Solar angle distribution of the SK-III final sample. The livetime is 298 days for the energy range from 5 to 6.5 MeV and 548 days for the energy range from 6.5 to 20 MeV. Data points are fitted using the ${}^8\text{B}$ spectrum calculated by Winter *et al.*. The best fit curve is indicated by the solid curve.

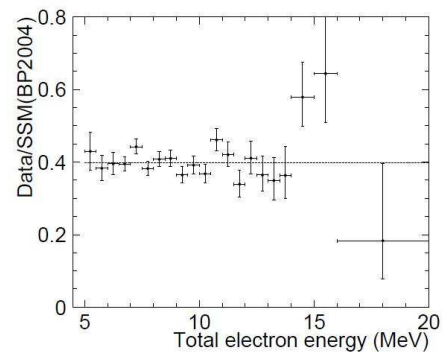


Fig. 6. Energy spectrum of solar neutrino flux in SK-III data from 5 MeV to 20 MeV. Each point shows the ratio of the data and the expected flux calculated from the SSM. The line indicates the averaged value of the SK-III data.

I data because the amount of the Rn contamination within the fiducial volume has been reduced by changing the water flow inside the tank and keeping the water with relatively rich radioactivity from entering into the fiducial volume. Also because pure water was supplied through a RO (reverse osmosis) system which seems to have removed radium content in water. Detector simulation and event reconstruction tools have been improved in this analysis, which give lower systematic uncertainties (See Table 1). Among the improvements in the detector simulation, the position dependence of the water transparency in the tank was newly implemented and the reflectivity of the sheet, optically separating the inner detector from the outer detector, was carefully measured and updated. An example of refinement in the reconstruction tools is the improvement in the direction fitter, which yields a 10 % better angular resolution. With all those improvements, the systematic uncertainties for total flux of the SK-III data becomes $\pm 2.1\%$, which is reduced from ${}^{+3.5}_{-3.2}\%$ of the SK-I data [2].

Fig. 5 shows the result of the solar angle distribution for the SK-III final sample. After subtracting background and fitting with the ${}^8\text{B}$ energy spectrum by Winter *et al.* [3], we obtained the ${}^8\text{B}$ flux value of $2.32 \pm 0.04(\text{stat.}) \pm 0.05(\text{sys.}) \times 10^6 \text{cm}^{-2}\text{s}^{-1}$, which is consistent with the previous SK-I and II results. The energy spectrum of the solar neutrino flux for

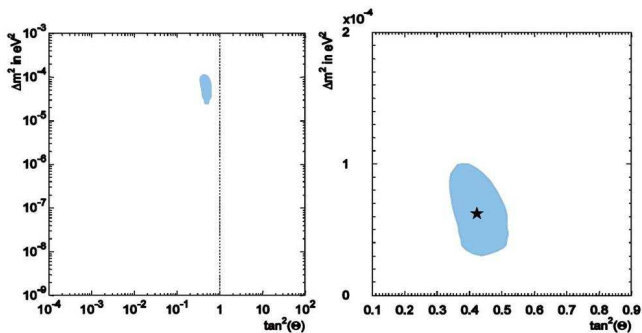


Fig. 7. Allowed region for neutrino oscillation parameters, Δm^2 and $\tan^2\theta$ from solar analysis. The left figure shows the results from the SK-I, II and III combined analysis with the ^8B flux constrained by SNO NC measurement. The right figure presents the result of global analysis including SK and other solar experiments (SNO, Borexino, Homestake, GALLEX-GNO and SAGE).

the SK-III data is shown in Fig. 6. The energy range used for the analysis is from 5 to 20 MeV. As shown in the figure, the ratio of the data and the expected flux from the Standard Solar Model (SSM) [4] scatters almost flat at 0.4, and the energy spectrum distortion which is expected from the LMA solution is not observed yet.

Oscillation analysis has also been done including the SK-III solar neutrino data. The two flavor analysis for the determination of the solar oscillation parameters, θ_{12} and Δm_{12}^2 was done with the combined SK-I, II and III data. In the analysis, the total ^8B flux is constrained by the SNO NC measurement [5][6]. The result is shown in Fig. 7. As shown in the left figure, the LOW solution is excluded and the LMA solution is only allowed to explain the solar neutrino oscillation. Note that this result was obtained using SK results only (not global analysis) with the ^8B flux constraint.

We have also done the same analysis using the data from SK and other solar experiments, i.e. SNO [5][6][7][8], Borexino [9], and radiochemical experiments (Homestake [10], SAGE [11] and GALLEX-GNO [12]). The allowed region from the global analysis is shown in Fig. 7 (right). The best-fit parameters are $\tan^2\theta_{12} = 0.44 \pm 0.33$ and $\Delta m_{21}^2 = (7.6 \pm 0.2) \times 10^{-5} \text{eV}^2$.

In addition to the two flavor analysis, three flavor analysis was also done. We used three oscillation parameters, Δm_{12}^2 , θ_{12} and θ_{13} as free parameters and set a fixed value of $2.4 \times 10^{-3} \text{eV}^2$ for Δm_{23}^2 . Fig. 8 shows the allowed region for $\sin^2\theta_{13}$ and $\tan^2\theta_{12}$ from the three flavor analysis of SK and other solar experiments together with the KamLAND three flavor analysis [13]. The allowed region for the combined analysis from the solar global and KamLAND analyses is also indicated. The limit of $\sin^2\theta_{13}$ is 0.060 at 95% C.L. for the solar global analysis. After combination with the KamLAND result, the best fit value of $\sin^2\theta_{13}$ is found to be $0.025^{+0.018}_{-0.016}$ and upper bound is obtained as $\sin^2\theta_{13} < 0.059$ at 95% C.L. These results will be published soon.

Since SK-IV was started with new electronics and online system in October 2008, we continue taking the solar neutrino data without large unscheduled downtime. By the end of March 2011, data of about 754.1 days livetime were col-

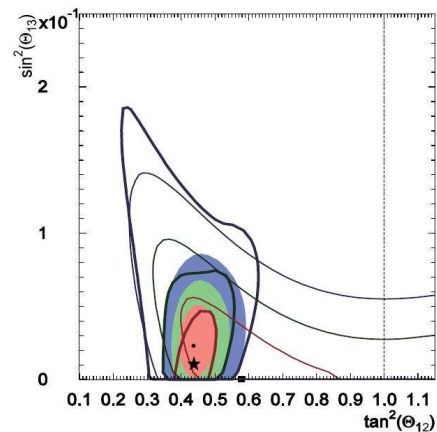


Fig. 8. Allowed region for $\sin^2\theta_{13}$ and $\tan^2\theta_{12}$ from the three flavor analysis. The thick lines and the star mark show the allowed regions and the best fit point of the global solar analysis. The thin lines and the square mark show the allowed regions and the best fit point of our KamLAND analysis. The filled areas and the filled circle mark show the allowed regions and the best fit point of the combined analysis. For all regions, the innermost area (red), the middle area (green) and the outermost area (blue) show 68.3, 95, 99.7 % C.L. respectively.

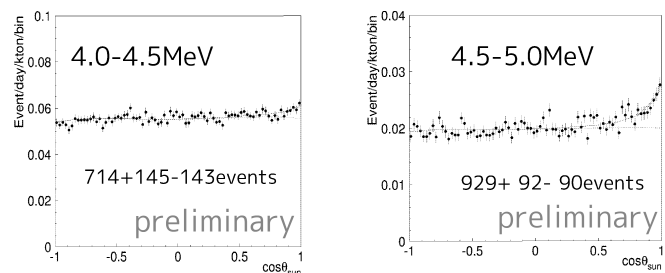


Fig. 9. Solar angle distributions of 754.1 days SK-IV data sample for solar neutrino with energy between 4.0-4.5 MeV (left) and 4.5-5.0 MeV (right).

lected. In SK-IV period, we have introduced a precise temperature control system for the inlet water to avoid water convection which causes Rn rich water to enter the fiducial volume. In Fig. 9, the solar angle distribution in the 4.5-5.0 MeV energy region and that in the 4.0-4.5 MeV energy region are shown. They show that the solar neutrinos even below 5 MeV are clearly observed in SK-IV. High quality ^8B solar neutrino data are being accumulated and the SK-IV data analysis is now ongoing.

Atmospheric neutrinos

Cosmic ray interactions in the atmosphere produce neutrinos. The prediction of the absolute flux has an uncertainty of at least $\pm 20\%$. However, the flavor ratio of the atmospheric neutrino flux, $(\nu_\mu + \bar{\nu}_\mu)/(\nu_e + \bar{\nu}_e)$, has been calculated to an accuracy of better than 5%. Another important feature of atmospheric neutrinos is that the fluxes of upward and downward going neutrinos are expected to be nearly equal for $E_\nu > (\text{a few GeV})$ where the effect of the geomagnetic field on primary cosmic rays is negligible. The livetime and ob-

served number of atmospheric neutrino events during the four SK run periods are summarized in Table 2. Fully contained (FC) events deposit all of their Cherenkov light in the inner detector, while partially contained (PC) events have exiting tracks which deposit some Cherenkov light in the outer detector. The neutrino interaction vertex is required to be reconstructed within a 22.5 kiloton fiducial volume, defined to be > 2 m from the PMT wall.

The FC events are classified into “sub-GeV” ($E_{vis} < 1330$ MeV) and “multi-GeV” ($E_{vis} > 1330$ MeV). These events are further separated into sub-samples based on the number of observed Cherenkov rings. Single- and multi-ring are then divided into electron-like (e-like) or muon-like (μ -like) samples depending on pattern identification of the most energetic Cherenkov ring. The sub-GeV samples are additionally divided based on their number of decay-electrons and their likelihood of being a π^0 .

The PC events are separated into “OD stopping” and “OD through-going” categories based on the amount of light deposit by the exiting particle in the OD.

Energetic atmospheric ν_μ 's passing through the Earth interact with rock surrounding the detector and produce muons via charged current interactions. These neutrino events are observed as upward going muons. Upward going muons are classified into two types. One is “upward through-going muons” which have passed through the detector, and the other is “upward stopping muons” which come into and stop inside the detector. The upward through-going muons are subdivided into “showering” and “non-showering” based on whether their Cherenkov pattern is consistent with light emitted from an electro-magnetic shower produced by a very high energy muon.

The livetime and number of observed events for the first three SK periods are summarized in Table 3.

Table 2. Atmospheric neutrino livetimes and the number of observed FC and PC events for each SK run period. (*)Numbers for SK-IV are preliminary since data taking is still ongoing.

	Livetime(days)	FC	PC
SK-I	1,489	12,232	896
SK-II	799	6,584	429
SK-III	518	4,356	343
SK-IV*	763	6,187	485

Table 3. Atmospheric neutrino induced upward-going muon livetime and the number of observed events for the first three SK run periods. (*)Numbers for SK-IV are preliminary since data taking is still ongoing.

	Livetime(days)	through-going	stopping
SK-I	1,646	1,856	458
SK-II	828	889	228
SK-III	636	735	210
SK-IV*	763	924	223

The zenith angle and lepton momentum distributions for each of the above samples compared with the atmospheric neutrino Monte Carlo predictions are shown in Fig. 10. The

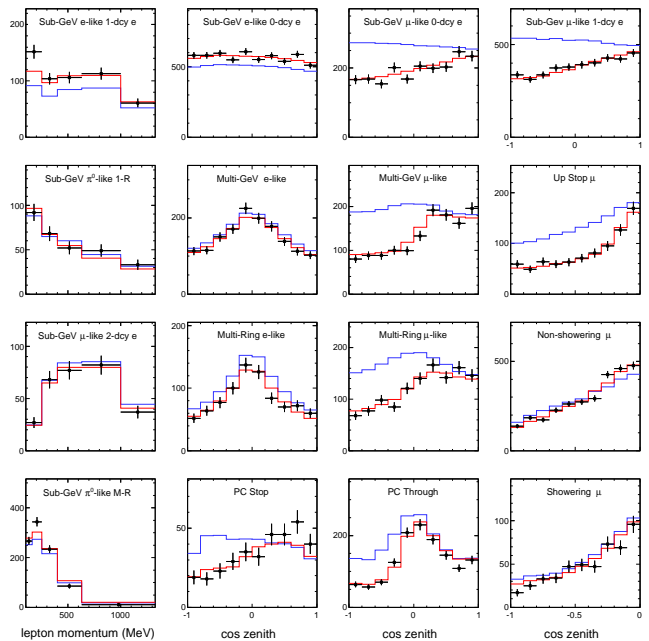


Fig. 10. The zenith angle and lepton momentum distributions for each data sample. $\cos \Theta = 1$ indicates downward-going particles. The blue histograms show the MC prediction without neutrino oscillation and the red histograms show the MC prediction for $\nu_\mu \leftrightarrow \nu_\tau$ oscillations with $\sin^2 2\theta = 1.0$ and $\Delta m^2 = 2.1 \times 10^{-3} \text{eV}^2$.

prediction is based on the recent precise measurements of primary cosmic rays by BESS, AMS and a three dimensional calculation of the neutrino flux by Honda *et al.* The μ -like data from SK exhibit a strong up-down asymmetry in their zenith angle (Θ) distribution while no significant asymmetry was observed in the e -like data. The data were compared with the Monte Carlo expectation without neutrino oscillations and the best-fit expectation for $\nu_\mu \leftrightarrow \nu_\tau$ oscillations. The oscillated Monte Carlo reproduces the zenith angle distributions of the data well.

We carried out $\nu_\mu \rightarrow \nu_\tau$ 2-flavor oscillation analysis using the entire SK-I, II and III atmospheric neutrino data set. Red contours in Figure 11 show the allowed neutrino oscillation parameter regions for $\nu_\mu \leftrightarrow \nu_\tau$ oscillations. The best fit oscillation parameters are $\sin^2 2\theta = 1.0$ and $\Delta m^2 = 2.2 \times 10^{-3} \text{eV}^2$. The allowed oscillation parameter range is $\sin^2 2\theta > 0.96$ and $\Delta m^2 = (1.8 - 2.6) \times 10^{-3} \text{eV}^2$ at 90 % C.L.

The atmospheric neutrino data are well described by neutrino oscillations. The survival probability of a ν_μ is given by a sinusoidal function of L/E , where L is the distance traveled by the neutrino and E is the neutrino energy. We also performed an oscillation analysis binning the data in the combined variable L/E . Low energy or horizontal-going events are rejected in this analysis since they have either large scattering angles or large $dL/d\Theta_{\text{zenith}}$. This creates a sample with good resolution in the L/E variable that is used to search for the maximum in the oscillation probability sinusoid. The obtained allowed oscillation parameter regions are shown in Figure 11. This result is consistent with that of the oscillation analysis using the zenith angle binning. The observed L/E

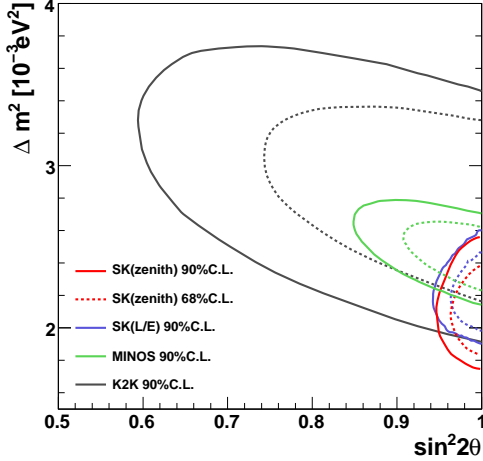


Fig. 11. Allowed region of $\nu_\mu \rightarrow \nu_\tau$ neutrino oscillation parameters obtained by SK using contained atmospheric neutrino events and upward-going muon events. Solid and dashed contours correspond to 90 and 68% C.L. respectively. Red contours are obtained by the zenith angle analysis and blue contours are obtained by the L/E analysis (see text). Allowed regions by long-baseline neutrino oscillation experiment K2K and MINOS are shown in black and green contours, respectively.

distribution gives the first direct evidence that the neutrino survival probability obeys the sinusoidal function predicted by neutrino flavor oscillations.

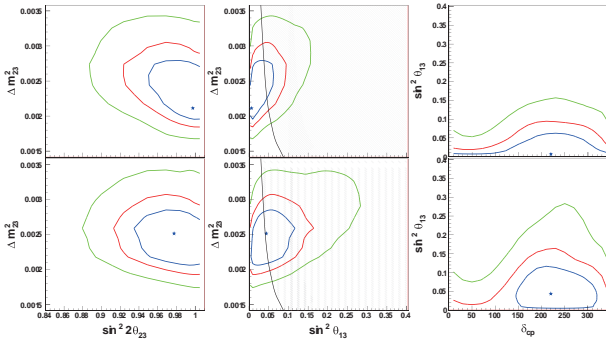


Fig. 12. The allowed regions for $(\Delta m^2, \sin^2 2\theta_{23})$; left, $(\Delta m^2, \sin^2 \theta_{13})$; middle, and $(\sin^2 \theta_{13}, \delta_{CP})$; right for the normal (upper figure) and inverted (lower figure) hierarchy. The blue, red, and green contours correspond to 68, 90 and 99% C.L. allowed regions obtained by this analysis, respectively. The shaded regions corresponds to the area excluded at 90% C.L. by the CHOOZ experiment.

Two flavor neutrino oscillations which assume that $\theta_{13}=0$ and $\Delta m_{12}^2 \ll \Delta m_{23}^2$ successfully describe the SK atmospheric neutrino data with maximum mixing angle ($\theta_{23}=\pi/4$). However, nonzero θ_{13} may be observable in the excess of multi-GeV electron neutrino events, and to a lesser extent in the oscillations of multi-GeV muon neutrinos. Additionally, the effects of the solar oscillation parameters and non-maximal mixing are observable as a sub-leading oscillation effect on the event rate of the Sub-GeV electron-like samples. If the CP violating term δ_{CP} is also considered, there are additional sub-dominant oscillation effects predicted across many of the

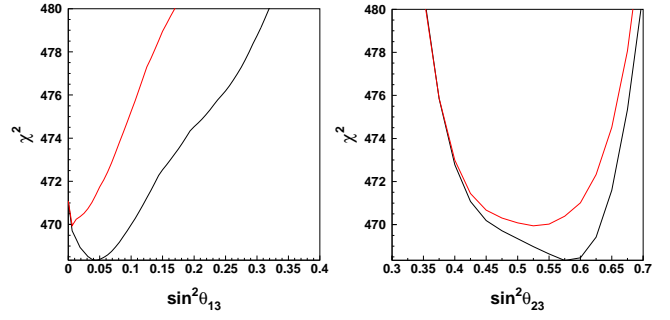


Fig. 13. χ^2 distribution as a function of (left): $\sin^2 \theta_{13}$ and (right): $\sin^2 \theta_{23}$. The normal hierarchy and inverted hierarchy cases are plotted with red and black lines, respectively.

SK atmospheric neutrino samples.

We have performed an extended oscillation analysis including all the mixing parameters and the CP violating term. The matter effect in the Earth is also considered in this calculation and both the normal and inverted mass hierarchies are tested. Figure 12 shows the allowed regions for $(\Delta m^2, \sin^2 2\theta_{23})$, $(\Delta m^2, \sin^2 \theta_{13})$, and $(\sin^2 \theta_{13}, \delta_{CP})$ for the normal and inverted mass hierarchies. A comparison of χ^2 between normal and inverted hierarchy case is shown in Figure 13. The best fit parameter sets are $(\Delta m_{23}^2, \sin^2 \theta_{23}, \sin^2 \theta_{13}, \delta_{CP}) = (2.11 \cdot 10^{-3} eV^2, 0.525, 0.006, 220^\circ)$ for the normal hierarchy and $(2.51 \cdot 10^{-3} eV^2, 0.575, 0.044, 220^\circ)$ for the inverted hierarchy case. All fits are consistent with the two flavor oscillation results and CHOOZ experiment's upper limit on θ_{13} . No indication for either mass hierarchy is seen in the data. [14].

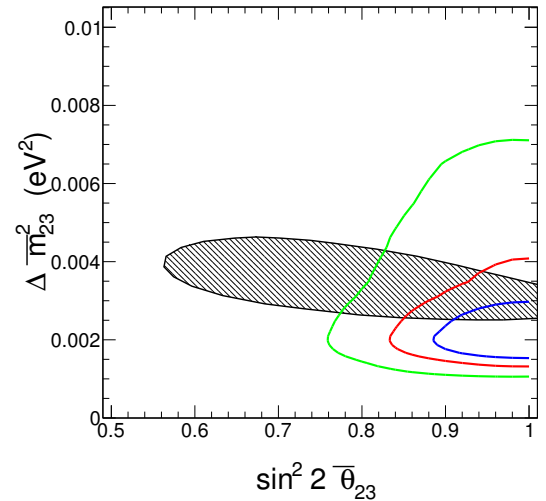


Fig. 14. Allowed regions for the anti-neutrino mixing parameters. The blue, red and green contours correspond to the 68%, 90%, and 99% C.L. allowed regions respectively. Shaded region shows the allowed regions by MINOS experiment [15].

Recently MINOS experiment reported the indication of the larger Δm^2 in anti-neutrino ($\bar{\nu}_\mu$) oscillation [15]. We also performed a CPT violation test of the atmospheric neutrino data using separated two-neutrino disappearance model, which allows neutrino and anti-neutrino to oscillate with different parameter sets of $(\Delta m^2, \theta)$ and $(\Delta \bar{m}^2, \bar{\theta})$, respectively.

According to the fitting result, the allowed region for anti-neutrino mixing parameters is shown in Figure 14, and the best fit parameters are $(\Delta m^2, \Delta \bar{m}^2, \sin^2 2\theta, \sin^2 2\bar{\theta}) = (2.1 \times 10^{-3} \text{ eV}^2, 2.0 \times 10^{-3} \text{ eV}^2, 1.0, 1.0)$. The atmospheric mixing parameters for anti-neutrino oscillations are consistent with those for neutrinos and therefore no evidence for CPT violation is found.

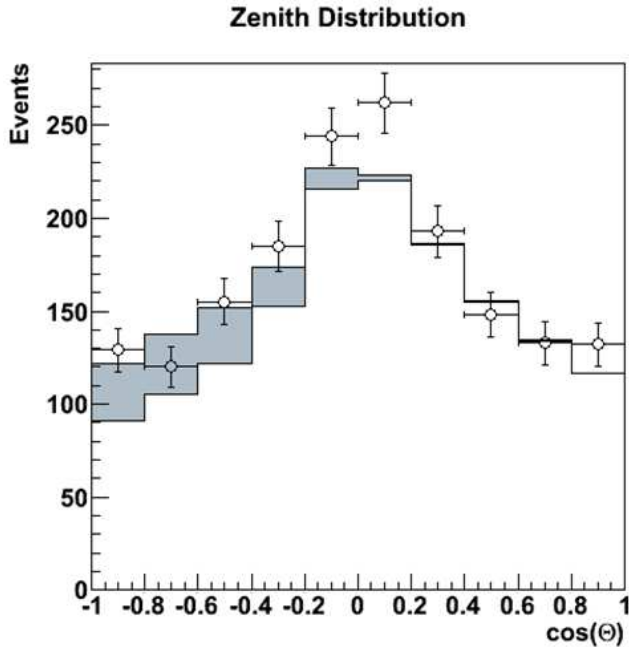


Fig. 15. Zenith angle distribution of tau-selected events by neural network method. SK-I, II, III dataset is used. Zenith angle $\cos(\theta)=-1$ (1) indicates upward-going (downward-going) direction. The data (dot with error bar) and the best-fit MC including tau signal (shaded region) and background from atmospheric neutrinos (ν_e and ν_μ) are shown.

Tau events, which are produced via ν_τ charge current (CC) interactions oscillated from ν_μ , are expected to be observed in SK. It would bring the direct evidence of $\nu_\mu \rightarrow \nu_\tau$ oscillation, however, the detection of ν_τ CC events in SK is challenging; the interaction rate of ν_τ charged current events is low since the neutrino energy threshold is 3.5 GeV and the atmospheric neutrino flux above this energy is relatively low. Also tau events are difficult to be identified individually because they tend to produce multiple particles. Tau analysis is performed employing neural network technique to discriminate tau events of hadronic decay from backgrounds of atmospheric ν_e and ν_μ events. Figure 15 shows the zenith angle distribution of tau-selected events. Tau events are expected to appear in the upward-going events because they originates $\nu_\mu \rightarrow \nu_\tau$ oscillation. The zenith angle shape of data is fitted with the MC expectation including tau signal and background with their normalizations free. According to the fitting result, the signal excess is estimated to 213.6 ± 45 (stat) $^{+13.2}_{-29.75}$ (syst) events, and the detection significance correspond to 3.8σ .

We have observed 763 days of atmospheric neutrinos data with SK-IV. The quality of the observed data are consistent with the previous SK-I, II, III results. Due to the electronics upgrade, several performance are expected to be improved,

such as the performance of Michel electrons tagging, the energy resolution in multi-GeV electron sample, etc. The further analysis including SK-IV data are going on.

Search for nucleon decay

Proton decays and bound neutron decays (nucleon decays in general) is the most dramatic prediction of Grand Unified Theories in which three fundamental forces of elementary particles are unified into a single force. Super-Kamiokande (SK) is the world's largest detector to search for nucleon decays and it has accumulated data of 91.7 kt-yrs (SK-I), 49.2 kt-yrs (SK-II), 31.9 kt-yrs (SK-III), and 32.9 kt-yrs (SK-IV), resulting in 206 kt-yrs data in total. Various nucleon decay modes have been looked for in the period from SK-I to SK-IV data but we have found no significant signal excess so far.

A proton decay into one positron and one neutral pion ($p \rightarrow e^+ \pi^0$) is one of the most popular decay modes. This decay mode is mediated by super-heavy gauge bosons and discovery of the signal would give us the information of the mass of the gauge mesons. To discriminate the signal from the atmospheric neutrino background, we reconstruct the number of particles (Cherenkov rings) and reconstruct the total visible energy corresponding to parent proton mass and total momentum corresponding to the proton's Fermi momentum. The signal efficiency of SK-IV is estimated to be 45.0 % and the background induced by the atmospheric neutrino interactions is estimated to be 0.05. The BG rate was confirmed by an artificial neutrino beam by using 1-kton water Cherenkov detector [16]. There are no candidate events in data from SK-I to SK-IV, on the other hand, expected background in total (from SK-I to SK-IV) is 0.42. Then we obtained a lower limit on the partial lifetime of the proton; $\tau/B_{p \rightarrow e^+ \pi^0} > 1.2 \times 10^{34}$ years at 90% confidence level.

In addition, we looked for SUSY favored decay modes which include K mesons in the final state, $p \rightarrow \bar{\nu} K^+$, $n \rightarrow \bar{\nu} K^0$, $p \rightarrow \mu^+ K^0$, and $p \rightarrow e^+ K^0$. In $p \rightarrow \bar{\nu} K^+$ search, we have analyzed data until SK-IV. In this mode, we tag the signal by decay products from K^+ . The momentum of K^+ is below the Cherenkov threshold, and is stopped in the water and decay into $\mu^+ \nu$ or $\pi^+ \pi^0$ with monochromatic momenta. On the other hand, the residual nucleus after proton decay emits γ ray (40% probability) and it is also useful to tag the proton decay signal. In SK-IV, SK electronics has been replaced and all of hits information are recorded by DAQ. As a result, the decay electron tagging efficiency is improved and the selection efficiencies of $p \rightarrow \bar{\nu} K^+$ are improved. The efficiency of the prompt γ tagging method is increased from 7.2 % (SK-I) to 8.2 % (SK-IV), and the efficiency of the $\pi^+ \pi^0$ method is increased from 6.5 % to 7.9 %.

Figure 16 shows one analysis method in which we search for muon with the monochromatic momentum 236 MeV/c. It shows the comparison of the muon momentum distributions for single-ring μ -like events between data, atmospheric ν MC, and proton decay MC, and there are no significant excess in data. We have analyzed the data from SK-I to SK-IV, there are no candidates in the prompt γ method and the $\pi^+ \pi^0$ method. Therefore we conclude that there is no evidence of nucleon decays and we calculated partial lifetime limits taking into ac-

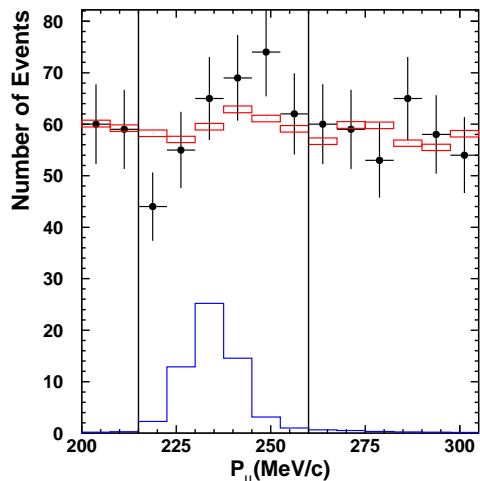


Fig. 16. The comparison between data and fitting results of the muon momentum distribution for single-ring μ -like events. The filled circles show data with statistical errors. The solid line shows $p \rightarrow \bar{\nu}K^+$ MC. The dashed line shows the best fitted atmospheric neutrino MC with free normalization.

count systematic uncertainties. Obtained limit is 3.9×10^{33} years at 90% confidence level for $p \rightarrow \bar{\nu}K^+$.

Moreover, we have performed extensive study for events; $p \rightarrow \mu K^0$ using decay products from K_L^0 , in which we have included K_S^0 decays in the previous paper. Now just SK-I data has been analyzed and the results of all SK data will be coming up soon.

Bibliography

- [1] Super-Kamiokande Collaboration, “Solar neutrino results in Super-Kamiokande-III”, *Phys. Rev. D* 83 (2011) 052010.
- [2] Super-Kamiokande Collaboration, “Solar neutrino measurements in Super-Kamiokande-I”, *Phys. Rev. D* 73 (2006) 112001.
- [3] W. T. Winter *et al.*, “The ^8B neutrino spectrum”, *Phys. Rev. C* 73 (2006) 025503.
- [4] J.N.Bahcall and M.H.Pinsonneault, “What Do We (Not) Know Theoretically about Solar Neutrino Fluxes?”, *Phys. Rev. Lett.* 92 (2004) 121301.
- [5] B. Aharmim *et al.*, “Independent Measurement of the Total Active ^8B Solar Neutrino Flux Using an Array of ^3He Proportional Counters at the Sudbury Neutrino Observatory”, *Phys. Rev. Lett.* 101 (2008) 011301.
- [6] B. Aharmim *et al.*, “Low Energy Threshold Analysis of the Phase I and Phase II Data Sets of the Sudbury Neutrino Observatory” *Phys. Rev. C* 81 (2010) 055504.
- [7] B. Aharmim *et al.*, “Determination of the ν_e and Total ^8B Solar Neutrino Fluxes with the Sudbury Neutrino Observatory Phase I Data Set”, *Phys. Rev. C* 75 (2007) 045502.
- [8] S.N.Ahmed *et al.*, “Electron Energy Spectra, Fluxes, and Day-Night Asymmetries of ^8B Solar Neutrinos from the 391-Day Salt Phase SNO Data Set”, *Phys. Rev. C* 72 (2005) 055502.
- [9] C.Arpesella *et al.*, “Direct Measurement of the ^7Be Solar Neutrino Flux with 192 Days of Borexino Data”, *Phys. Rev. Lett.* 101 (2008) 091302.
- [10] B.T.Cleveland *et al.*, “Measurement of the Solar Electron Neutrino Flux with the Homestake Chlorine Detector Bruce T. Cleveland”, *Astrophys. J.* 496 (1998) 505.
- [11] J.N.Abdurashitov *et al.*, “Measurement of the solar neutrino capture rate with gallium metal”, *Phys. Rev. C* 60 (1999) 055801.
- [12] M.Altmann *et al.*, “GNO solar neutrino observations: results for GNO I”, *Phys. Lett. B* 490 (2000) 16.
- [13] S. Abe *et al.*, “Precise Measurement of Neutrino Oscillation Parameters with KamLAND”, *Phys. Rev. Lett.* 100 (2008) 221803.
- [14] R. Wendell, C. Ishihara *et al.* [Super-Kamiokande Collaboration], “Atmospheric neutrino oscillation analysis with subleading effects in Super-Kamiokande I, II, and III”, *Phys. Rev. D* 81 (2010) 092004.
- [15] P. Adamson *et al.* [MINOS collaboration], “First direct observation of muon antineutrino disappearance,” arXiv:1104.0344 [hep-ex].
- [16] S. Mine *et al.* [K2K Collaboration], “Experimental study of the atmospheric neutrino backgrounds for proton decay to positron and neutral pion searches in water Cherenkov detectors,” *Phys. Rev. D* 77, 032003 (2008) [arXiv:0801.0182 [hep-ex]].
- [17] H. Nishino *et al.* [Super-Kamiokande Collaboration], “Search for Proton Decay via $p \rightarrow e^+\pi^0$ and $p \rightarrow \mu^+\pi^0$ in a Large Water Cherenkov Detector,” *Phys. Rev. Lett.* 102, 141801 (2009) [arXiv:0903.0676 [hep-ex]].

Hyper-Kamiokande

Feasibility study has been performed for the next generation nucleon decay and neutrino detector Hyper-Kamiokande that aims to explore unification of elementary particles and full picture of neutrino masses and mixings. The water Cherenkov detector with the dimension of 1 million tones has capability of exploring nucleon lifetimes about 10 times as long as the limits set by the Super-Kamiokande. For example, the sensitivity for the decay mode $p \rightarrow e^+\pi^0$ is expected to be beyond 1×10^{35} years [1]. The detector also aims to study neutrino properties such as Dirac CP phase, mass hierarchy, octant of θ_{23} , and so on by using a high power accelerator based neutrino beam and atmospheric neutrinos. Figure 1 shows the expected significance to exclude CP conservation $\sin \delta_{CP} = 0$, for the parameter space of θ_{13} and δ_{CP} by using upgraded JPARC neutrino beam with the power of 1.66 MW

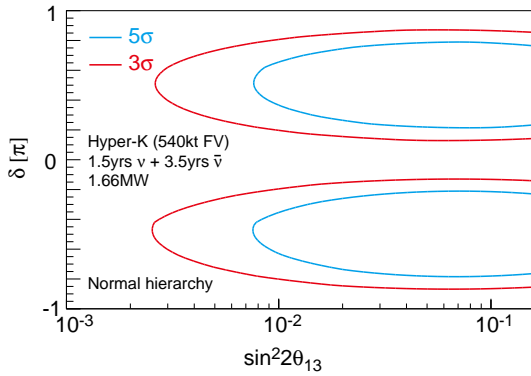


Fig. 1. The expected significance to exclude leptonic CP conservation in θ_{13} and δ parameter space by using upgraded JPARC ν beam and the Hyper-Kamiokande.

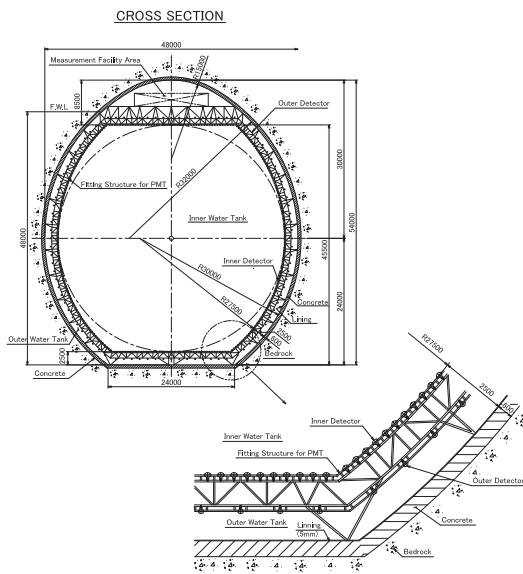


Fig. 2. The preliminary design of the Hyper-Kamiokande water tank.

$\times 5$ years and the Hyper-Kamiokande detector with the fiducial volume of 0.54 Megaton [1].

If the indication of electron neutrino appearance in the T2K experiment [2] is the result of nonzero θ_{13} , we are opening possibility of exploring these remaining neutrino parameters, *i.e.* CP phase and mass hierarchy. The suggested large size of θ_{13} is really encouraging and it will boost the activities toward realization of the future detector. Conceptual design (Fig.2), scheduling, and costing of the detector have been already started.

Bibliography

- [1] M. Shiozawa, “Large Underground Water Cherenkov Detectors”, Proceeding of the XXIV International Conference on Neutrino Physics and Astrophysics (Neutrino2010), June, 2010. to be published in Nuclear Physics B Proceedings Supplement.
- [2] K. Abe *et al.* [T2K Collaboration], “Indica-

tion of Electron Neutrino Appearance from an Accelerator-produced Off-axis Muon Neutrino Beam,” arXiv:1106.2822 [hep-ex].

T2K Experiment

The T2K (Tokai-to-Kamioka) experiment [1] is a long baseline neutrino oscillation experiment. Its main goal is to measure the last unknown lepton sector mixing angle θ_{13} by observing ν_e appearance in a ν_μ beam. It also aims to make a precision measurement of the known neutrino oscillation parameters with precision of $\delta(\Delta m_{23}^2) \sim 10^{-4} \text{ eV}^2$ and $\delta(\sin^2 2\theta_{23}) \sim 0.01$ via ν_μ disappearance studies. In addition to neutrino oscillation studies, the T2K neutrino beam (with $E_\nu \sim 1 \text{ GeV}$) will enable a rich fixed-target physics program of neutrino interaction studies at energies covering the transition between the resonance production and deep inelastic scattering regimes.

T2K adopts the off-axis method [2] to generate the narrow-band neutrino beam using the new MW-class proton synchrotron at J-PARC. In this method the neutrino beam is purposely directed at an angle with respect to the baseline connecting the proton target and the far detector, Super-Kamiokande. The off-axis angle is set at 2.5° so that the narrow-band muon neutrino beam generated toward the far detector has a peak energy at $\sim 0.6 \text{ GeV}$, which maximizes the effect of the neutrino oscillation at 295 km and minimizes the background to electron-neutrino appearance detection.

Details of the T2K experimental setup are described elsewhere [3]. The J-PARC Main Ring (MR) accelerator [4] provides 30 GeV protons with a cycle of 0.3 Hz. Beam bunches are single-turn extracted in $5 \mu\text{s}$ and transported an extraction line arc defined by superconducting combined-function magnets to the production target. The target is a graphite rod with a diameter of 2.6 cm and a length of 90 cm (corresponding to 1.9 interaction length). Charged particles exiting the target are sign selected and focused into the 96 m long decay tunnel by three magnetic horns pulsed at 250 kA.

The near detector site at $\sim 280 \text{ m}$ from the production target houses two detector systems. The on-axis Interactive Neutrino GRID (INGRID), composed of an array of iron/scintillator sandwiches, measures the neutrino beam intensity, direction and profile. The off-axis detector measures the muon neutrino flux and energy spectrum, and intrinsic electron neutrino contamination in the beam in the direction of the far detector, along with measuring rates for exclusive neutrino reactions. These measurements are essential in order to characterize signals and backgrounds that are observed in the Super-Kamiokande far detector. The off-axis detector consists of three large volume time projection chambers (TPCs) [5] interleaved with two fine-grained detectors (FGDs), a π^0 -optimized detector and a surrounding electromagnetic calorimeter. The whole off-axis detector is placed in a 0.2 T magnetic field provided by the recycled UA1 magnet, which also serves as part of a side muon range detector.

The far detector, Super-Kamiokande [6], is a 50 kton water Cherenkov detector located in the Kamioka Observatory. In 2008, the Super-Kamiokande collaboration completed an

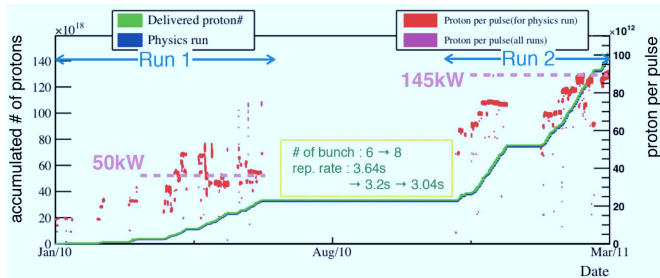


Fig. 1. Accumulated number of protons on target (green/blue lines) and protons per pulse (red/purple dots) during the T2K's first two physics runs.

upgrade to the detector's readout electronics [7]. The new electronics includes a new front-end capable of a higher data processing rate and also improves upon the triggering method. In the new system, the arrival time and charge of each PMT hit is sent to a cluster of PCs that organizes the hit data and searches for event candidates based on programmable software triggers. For the T2K experiment, the DAQ system triggers in time with the beam spills produced by the J-PARC accelerator. Each beam spill is given a GPS timestamp that is immediately sent to the online Super-Kamiokande PCs. Each timestamp is used to define an additional software trigger that records all the PMT hits within $\pm 500 \mu\text{s}$ of the expected beam arrival time (taking a neutrino time-of-flight into account). These spill events are then collected and written to disk. Later the events are fed into offline processing which applies the usual Super-Kamiokande software triggers used to search for neutrino events, and any candidate events found are extracted for further T2K data analysis.

The T2K experiment began accumulating neutrino beam data for physics analysis in January 2010. Figure 1 shows accumulated number of protons on target (p.o.t.), along with number of protons per pulse. The first two physics runs are defined as Run 1 (January–June 2010) and Run 2 (November 2010–March 2011). During this time period, the MR proton beam power was continuously increased and reached 145 kW with 9×10^{13} protons per pulse. The number of bunches was six during Run 1 and eight during Run 2. By the end of Run 2, a total of 2,474,419 spills were retained for analysis after beam and Super-Kamiokande quality cuts, yielding 1.43×10^{20} p.o.t.. The proportion of Super-Kamiokande good spills to the total number of spills selected by beam conditions was 99%. In FY2010, neutrino oscillation studies were performed by using the whole Run 1 data, which correspond to 3.23×10^{19} p.o.t..

The neutrino flux is predicted by a Monte Carlo (MC) simulation based on experimental data. Pion production is based on the data by the NA61/SHINE experiment [8], which measured hadron production by 30 GeV protons on a graphite target. Other hadronic interactions inside the target are simulated by FLUKA. GEANT3/GCALOR handles particle propagation through the magnetic horns, target hall, decay volume and beam dump. The predicted neutrino flux is predominantly ν_μ with $< 1\%$ ν_e contamination. Pion and kaon production uncertainties dominate the neutrino flux prediction uncertainty.

The NEUT MC event generator [9], which has been tuned with recent neutrino interaction data in an energy region compatible with T2K, is used to simulate neutrino interactions in the near and far detectors. An energy-dependent error on charged-current quasi-elastic interactions (CCQE) is assigned to account for the uncertainty in the low energy cross-section, especially for the different target materials between the near and far detectors.

An inclusive ν_μ charged-current (CC) measurement in the off-axis near detector is used to constrain the expected event rate at the far detector. Neutrino interactions in the FGDs with tracks entering the downstream TPC are selected. A dE/dx of the most energetic negative track in the TPC is required to be compatible with a muon. To reduce background from interactions outside the FGDs, there must be no track in the upstream TPC. The analysis selects 1529 events. The measured data/MC ratio is $1.061 \pm 0.028(\text{stat.})$ $^{+0.044}_{-0.038}(\text{det.syst.}) \pm 0.039(\text{phys.syst.})$. The detector systematic errors mainly come from tracking and particle identification efficiencies, and physics uncertainties are related to the interaction modeling.

At Super-Kamiokande, a fully-contained fiducial volume (FCFV) sample is extracted by requiring no event activity in either the OD or in the $100 \mu\text{s}$ before the event trigger time, at least 30 MeV electron-equivalent energy deposited in the ID (defined as visible energy E_{vis}), and the reconstructed vertex in the 22.5 kton fiducial region. The Run 1 data have 23 such FCFV events. All of them are within the time range from -2 to $10 \mu\text{s}$ around the beam trigger time. The accidental contamination from non-beam related events (predominantly from atmospheric neutrino interactions) is estimated to be less than 10^{-2} events.

The electron neutrino appearance analysis produces a Super-Kamiokande event sample enhanced in ν_e CCQE interactions arising from $\nu_\mu \rightarrow \nu_e$ oscillations. The main background are intrinsic ν_e contamination in the beam and neutral-current (NC) interactions with a misidentified π^0 . The selection criteria for this analysis were fixed from MC studies before the data were collected, optimized for the initial running conditions. The analysis relies on the well-established Super-Kamiokande reconstruction techniques developed for other data samples [10]. Among 23 FCFV events, ten events are reconstructed with a single ring, and two of those are electron-like (e -like). Both events satisfy a visible energy cut $E_{\text{vis}} > 100 \text{ MeV}$, but one of these has a delayed-electron signal and is rejected. To suppress misidentified π^0 mesons, the reconstruction of two rings is forced by comparison of the observed and expected light patterns calculated under the assumption of two showers [11], and a cut on the two-ring invariant mass $M_{\text{inv}} < 105 \text{ MeV}/c^2$ is imposed. The remaining one event is not rejected. Finally, the neutrino energy E_V^{rec} is computed using the reconstructed momentum and direction of the ring, by assuming quasi-elastic kinematics and neglecting Fermi motion. The event is remained after requiring $E_V^{\text{rec}} < 1250 \text{ MeV}$, aimed at suppressing events from the intrinsic ν_e component arising primarily from kaon decays. The ν_e appearance signal efficiency is estimated from MC to be 68% while rejection for ν_μ and intrinsic ν_e are $> 99\%$ and 79% , respectively. Figure 2 shows a display of the event satisfies all

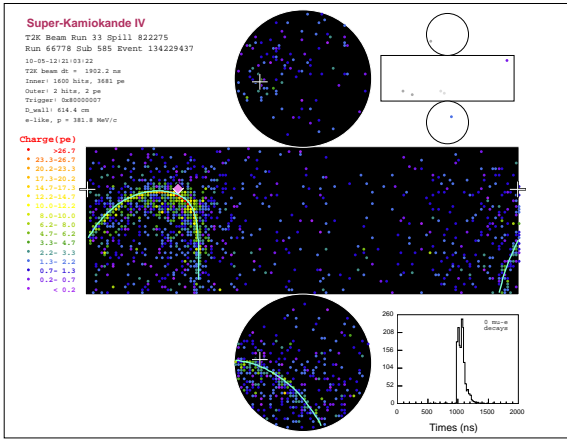


Fig. 2. A display of the observed ν_e candidate event.

Table 1. Contributions from various sources and the total relative uncertainty for $\sin^2 2\theta_{13} = 0$ and 0.1

Source	$\sin^2 2\theta_{13} = 0$	$\sin^2 2\theta_{13} = 0.1$
neutrino flux	$\pm 8.9\%$	$\pm 11.9\%$
near detector	$+5.6\%$ -5.2%	$+5.6\%$ -5.2%
near det. statistics	$\pm 2.7\%$	$\pm 2.7\%$
cross section	$\pm 14.3\%$	$\pm 10.6\%$
far detector	$\pm 15.8\%$	$\pm 9.5\%$
Total $\delta N_{SK}^{exp}/N_{SK}^{exp}$	$+23.9\%$ -23.8%	$+19.5\%$ -19.4%

the ν_e selection criteria.

The expected number of events at Super-Kamiokande (N_{SK}^{exp}) is calculated by using the near detector ν_μ CC interaction rate measurement as normalization, and the ratio of expected events in the near and far detectors, where common systematic errors cancel. The oscillation parameters other than $\sin^2 2\theta_{13}$ are fixed at $\Delta m_{12}^2 = 7.6 \times 10^{-5} \text{eV}^2$, $\Delta m_{23}^2 = 2.4 \times 10^{-3} \text{eV}^2$, $\sin^2 2\theta_{12} = 0.8704$, $\sin^2 2\theta_{23} = 1.0$, and $\delta_{CP} = 0$ unless otherwise noted. The computed N_{SK}^{exp} are 0.34(1.20) events for $\sin^2 2\theta_{13} = 0(0.1)$, which consist of 0.14(0.14) $\nu_\mu + \bar{\nu}_\mu$, 0.18(0.16) intrinsic ν_e , and 0.02(0.9) $\nu_\mu \rightarrow \nu_e$ oscillation events. As shown in Table 1, the total systematic uncertainty on N_{SK}^{exp} depends on θ_{13} . The errors from cross-section modeling are dominated by uncertainties in intranuclear final state interactions (FSI) and by the knowledge of the $\sigma(\nu_e)/\sigma(\nu_\mu)$ ratio, estimated to $\pm 6\%$. The systematic uncertainties due to event selection in Super-Kamiokande were studied with cosmic-ray muons, electrons from muon decays, and atmospheric neutrino events. Main contribution to $\delta N_{SK}^{exp}/N_{SK}^{exp}$ for e.g. $\sin^2 2\theta_{13} = 0.1$ is 5.0% from ring counting, 4.9% from particle identification, and 6.0% from the M_{inv} cut.

The oscillation analysis is based entirely on comparing the number of ν_e candidate events with predictions, varying $\sin^2 2\theta_{13}$ for each δ_{CP} value. At each oscillation parameter point, a probability distribution for the expected number of events is constructed, incorporating systematic errors, which

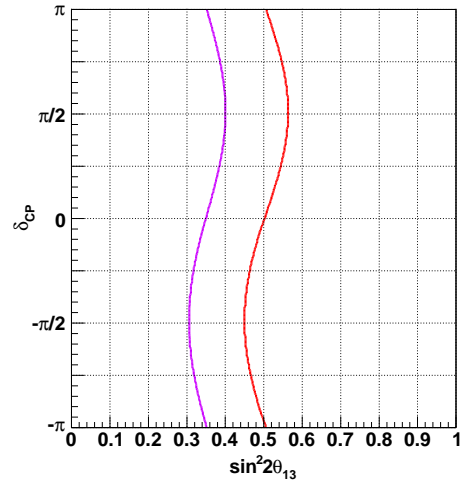


Fig. 3. The 90% C.L. upper limit (red) and sensitivity (purple) on $\sin^2 2\theta_{13}$ for each value of δ_{CP} assuming normal mass hierarchy.

is used to make the confidence interval, following the unified ordering prescription of Feldman and Cousins [12]. Figure 3 shows the upper limit and sensitivity on $\sin^2 2\theta_{13}$ at 90% confidence level (C.L.) for normal mass hierarchy. Though the constraint on θ_{13} obtained from the first T2K data was not as stringent as those set by CHOOZ [13] and MINOS [14] due to their low statistics, our strategy in a ν_e appearance search including high background suppression by the off-axis neutrino beam technique and a nice e/π^0 separation, near/far error cancellation, etc., was verified.

In the ν_μ disappearance study, a ν_μ CCQE enriched sample is selected by applying the following additional cuts on the FCFV sample: (1) single ring, (2) muon-like (μ -like), (3) number of delayed-electron signals is 0 or 1, and (4) reconstructed muon momentum $> 200 \text{MeV}/c$. Eight events remained in the whole Run 1 data, while the expected number of events with a normalization by the near detector ν_μ CC interaction rate measurement is $22.81 \pm 3.19(\text{syst.})$ in the null oscillation case and $6.34 \pm 1.04(\text{syst.})$ in the two-flavor $\nu_\mu \rightarrow \nu_\tau$ oscillation case with $\Delta m_{23}^2 = 2.4 \times 10^{-3} \text{eV}^2$ and $\sin^2 2\theta_{23} = 1.0$. Significance from the null oscillation hypothesis is 2.6σ . Figure 4 shows the reconstructed neutrino energy distribution of the selected events.

By the end of Run 2, we have already accumulated about 5 times as much as the data obtained during Run 1. The result of the ν_e appearance search using these new data with reduced systematic errors will be reported in FY2011, as well as the first result of the T2K ν_μ disappearance analysis. The T2K beam production has been suspended since the Tohoku Earthquake occurred on March 11, 2011. Recovery works on the damaged accelerator and beamline components are in progress in order to resume the neutrino beam data-taking by December, 2011.

Bibliography

- [1] Letter of intent: Neutrino oscillation experiment at JHF, 2003. http://neutrino.kek.jp/jhfnu/loi/loi_JHFcor.pdf.

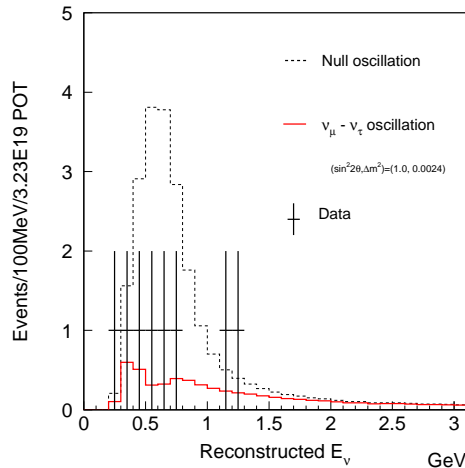


Fig. 4. Reconstructed neutrino energy of the events selected in the ν_μ disappearance analysis.

- [2] D. Beavis, A. Carroll, I. Chiang, *et al.*, Long Baseline Neutrino Oscillation Experiment at the AGS (Proposal E889), 1995. Physics Design Report, BNL 52459.
- [3] K. Abe *et al.* (T2K Collaboration), accepted for publication in Nucl. Instrum. Methods, article in press (2011), doi: 10.1016/j.nima.2011.06.067, arXiv:1106.1238 [physics.ins-det].
- [4] Y. Yamazaki *et al.*, KEK Report 2002-13 and JAERI-Tech 2003-44 and J-PARC-03-01 (2003).
- [5] N. Abgrall *et al.*, Nucl. Instrum. Meth. A637, 25 (2011), arXiv:1012.0865 [physics.ins-det].
- [6] Y. Fukuda *et al.* (Super-Kamiokande Collaboration), Nucl. Instrum. Meth. A501, 418 (2003).
- [7] S. Yamada *et al.* (Super-Kamiokande Collaboration), IEEE Trans. Nucl. Sci. 57, 428 (2010).
- [8] N. Abgrall *et al.* (NA61/SHINE Collaboration), submitted to Phys. Rev. C (2011), arXiv:1102.0983 [hep-ex].
- [9] Y. Hayato, Nucl. Phys. (Proc. Suppl.) B112, 171 (2002).
- [10] Y. Ashie *et al.* (Super-Kamiokande Collaboration), Phys. Rev. D71, 112005 (2005), hep-ex/0501064.
- [11] T. Barszczak, (2005), Ph.D. Thesis (University of California, Irvine), UMI-31-71221.
- [12] G. J. Feldman and R. D. Cousins, Phys. Rev. D57, 3873 (1998).
- [13] M. Apollonio *et al.* (Chooz Collaboration), Eur. Phys. J. C27, 331 (2003), hep-ex/0301017.
- [14] P. Adamson *et al.* (MINOS Collaboration), Phys. Rev. D82, 051102 (2010), arXiv:1006.0996 [hep-ex].

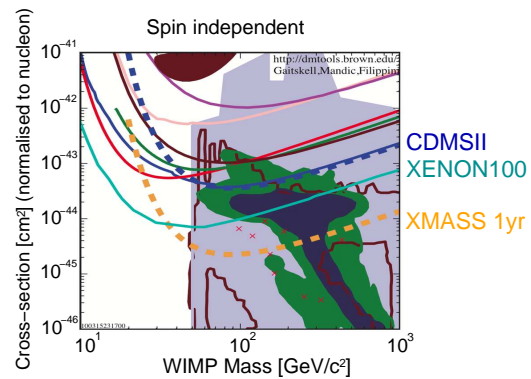


Fig. 1. XMASS sensitivity compared to other experiments. See <http://dmtools.berkeley.edu/>

XMASS experiment

The XMASS experiment aims to detect $^7\text{Be/pp}$ solar neutrinos, neutrino-less double beta decay, and dark matter searches using ultra-pure liquid xenon. The first stage of XMASS experiment is concentrated on dark matter searches using 800 kg liquid xenon detector. The 800 kg detector construction in the Kamioka mine was funded and started in April 2007. Construction work was completed in September 2010 and commissioning run has been started since October 2010.

Several astronomical observations indicate that the universe contains a large amount of nonbaryonic dark matter. One of the most plausible candidates for the nonbaryonic dark matter is a weakly interacting massive particle (WIMP) provided by the supersymmetry in the form of the lightest supersymmetric particle. WIMPs can be directly detected through their elastic scattering off target nuclei in a detector. XMASS searches for the WIMP-xenon nucleus interaction in liquid xenon. Liquid xenon has the several advantages for dark matter searches. Large amount of scintillation light (42,000 photons/MeV), which is as good as NaI(Tl) scintillator enables us to detect small energy signals such as dark matter recoil. Owing to the high atomic number of xenon ($Z = 54$) and the high density of liquid xenon ($\sim 2.9 \text{ g/cm}^3$), target volume can be small and external background gamma-rays can be absorbed within a short distance from the detector wall. With 20 cm self-shielding, gamma-rays from ^{238}U contamination is expected to be reduced more than 3 orders of magnitude in the 5-50 keV electron recoil energy range from the simulation study. Figure 1 shows the expected sensitivity of the XMASS experiment. Our goal is to reach 10^{-45} cm^2 .

Most of the XMASS facilities are located at Hall-C in the Kamioka mine 1,000m underneath the top of Mt. Ikenoyama. The XMASS detector consists of the cylindrical water tank with 72 50cm PMTs (outer detector: OD) and spherical liquid xenon detector with 642 2inch PMTs (inner detector: ID) as shown in figure 2. The spherical liquid xenon detector is contained in a double wall vessel. The vessel consisting of inner and outer vacuum chamber (IVC and OVC) is made from oxygen free high conductivity (OFHC) copper. The gap between IVC and OVC is kept vacuum for thermal isolation. The inner surface of IVC was polished with electro-chemical buffing (ECB) to reduce emanation of hydrogen and radon from copper.

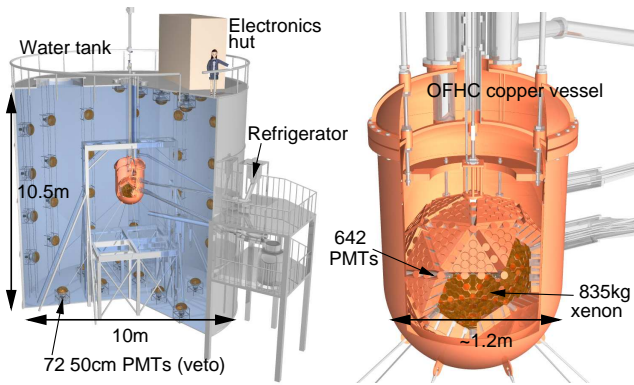


Fig. 2. Schematic view of the water tank and the liquid xenon vessel.



Fig. 3. Photo of IVC (left). The inner surface of upper part (right, top) and lower part (right, bottom).

In July 2010, the vessel was delivered at Kamioka mine, and detector assembling work was started inside the water tank. We made a clean booth inside the water tank and assembling work was done there while the IVC was opened. The radon concentration in the water tank was kept about 200 mBq/m^3 which is 1/100 of that in the atmosphere, and the dust level was less than $1000 \text{ particles/ft}^3$ (Particle size $> 0.5 \mu\text{m}$) during the assembling work. All the ID PMTs had been already mounted in the OFHC copper holder in February 2010 as reported in the last annual report. They were put inside the IVC, and PMT signal and high-voltage cables are connected to the electronics system at the top of the water tank through the vertical pipe and feed-through. The xenon supplying and circulation lines were also connected between the side of vessel and outside of the water tank. The refrigerators, circulation pump, filters, and liquid xenon reservoir were put outside the water tank, and connected each other. The 72 50-cm diameter PMTs were also put on the inner wall of the water tank to tag the incoming cosmic ray muons. All the detector assembling work was completed in September 2010 (figure 4). A calibration system was also mounted inside the IVC. This system enables us to drive a radio active source inside the IVC along one axis with $< \pm 1 \text{ mm}$ accuracy.

Internal background needs to be removed before and also the data taking. ^{85}Kr in xenon is a potential source of the internal contamination. Therefore, we processed one ton xenon with our distillation system [2] to reduce the ^{85}Kr for ten days in September 2010. After distillation, xenon was introduced into the IVC. The gas xenon was passed through SAES get-

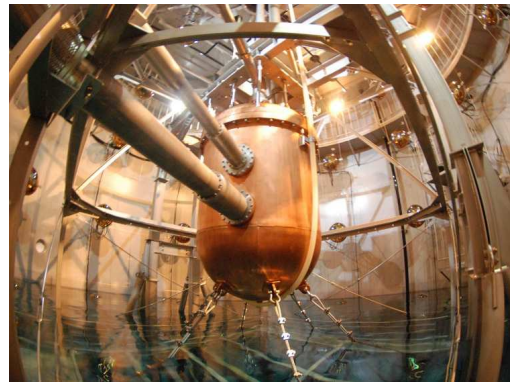


Fig. 4. Photo of liquid xenon vessel inside the water tank as of September 2010.

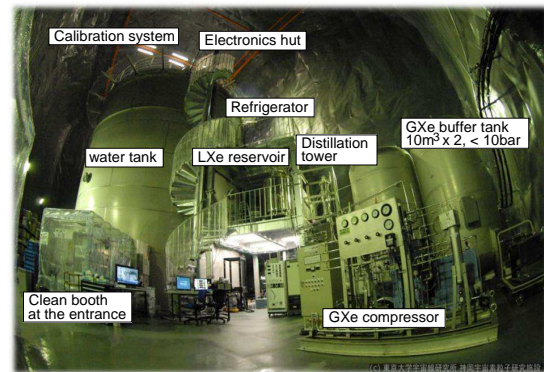


Fig. 5. Photo of Hall-C. All the facilities of XMASS 800 kg detector have been completed.

ter at the 30 L/min of flow rate and liquefied with two 200 W pulse tube refrigerators.

After 1st filling of xenon, we collected liquid xenon from the detector to the reservoir through the stainless particle filter ($10 \mu\text{m}$ mesh) to remove dust. The liquid xenon was evaporated, passed through SAES getter, liquefied with refrigerators, and introduced into the detector again. We purified xenon by the above method two times.

After xenon purification, we have started commissioning run since October 2010. We put several kind of radio active sources at several positions inside the IVC by using calibration system and observed scintillation photons. About 16% improvement of light yield was observed with ^{57}Co source owing to xenon cleaning. Vertex reconstruction study and evaluation of internal contamination (radon, krypton, etc.) have been carried out.

Bibliography

- [1] Y. Suzuki et al., "Low energy solar neutrino detection by using liquid xenon", Aug. 2000, hep-ph/0008296.
- [2] K. Abe et al. (the XMASS collaboration), "Distillation of Liquid Xenon to Remove Krypton", *Astroparticle Physics*, 31 (2009) 290.
- [3] S. Moriyama, "Status of XMASS Experiment", proceedings of identification of dark matter 2010 (IDM2010), July 2010.

HIGH ENERGY COSMIC RAY DIVISION

Overview

There are three major experimental research activities in the High Energy Cosmic Ray Division, the study of high energy gamma rays and the design study of the next generation telescopes by the Cherenkov Cosmic Gamma Ray group, the study of extremely high energy cosmic rays by the Telescope Array (TA) group, and the study of very high energy cosmic rays and gamma rays by the Tibet AS gamma group. Other activities, such as experiments utilizing the Akeno observatory, the Norikura observatory, the Mt. Chacaltaya observatory (jointly operated with Bolivia), and the emulsion-pouring facilities are closely related to inter-university joint research programs. Also an all-sky high resolution air-shower detector (Ashra) has been installed on the Hawaii island. The High Energy Astrophysics Group created in the fiscal year 2009 aims to explore various high energy astrophysical phenomena, through theoretical and observational approaches.

The Cherenkov Cosmic Gamma Ray group operates the CANGAROO telescope system, a set of large imaging atmospheric Cherenkov telescopes, to make observations of high energy air showers originated by TeV gamma rays. The CANGAROO project started as a single telescope with a relatively small mirror (3.8 m in diameter) in 1992. In 1999 a new telescope with a 7 m reflector has been built, and now it has a 10 m reflector with a fine pixel camera. An array of four 10 m telescopes was completed in March 2004 so that more sensitive observations of gamma rays are realized with its stereoscopic imaging capability of Cherenkov light. For further development of Very High Energy Gamma Ray Astronomy, the Cherenkov Cosmic Gamma Ray Group is also working on the design study and development of the next generation international ground-based gamma ray observatory CTA.

At the Akeno observatory, a series of air shower arrays of increasing geometrical sizes were constructed and operated to observe extremely high energy cosmic rays (EHECRs). The Akeno Giant Air Shower Array (AGASA) was operated from 1991 to January 2004 and covered the ground area of 100 km² as the world largest air shower array. In 13 years of operation, AGASA observed a handful of cosmic rays exceeding the theoretical energy end point of the extra-galactic cosmic rays (GZK cutoff) at 10²⁰ eV. The Telescope Array (TA), a large plastic scintillator array with air fluorescence telescopes, has been constructed in Utah, USA, which succeeds AGASA and measures the EHECRs with an order of magnitude larger aperture than that of AGASA to unveil the origin of super-GZK cosmic rays discovered by AGASA. The full-scale TA has started taking data as the largest array viewing the northern sky.

An air shower experiment aiming to search for celestial gamma-ray point sources started in 1990 with Chinese physicists at Yangbajing (Tibet, 4,300 m a.s.l.) and has been successful. This international collaboration is called the Tibet AS γ Collaboration. An extension of the air shower array was

completed in 1995 and an emulsion chamber has been combined with this air shower array since 1996 to study the primary cosmic rays around the knee energy region. After successive extensions carried out in 1999, 2002 and 2003, the total area of the air shower array amounts to 37,000 m². The sun's shadow in cosmic rays affected by the solar magnetic field was observed for the first time in 1992, utilizing its good angular resolution at multi-TeV energy region. From this experiment with better statistics, we expect new information to be obtained on the large-scale structure of the solar and interplanetary magnetic field and its time variation due to the 11-year-period solar activities.

A new type of detector, called Ashra (all-sky survey high resolution air-shower detector), was developed. The first-phase stations were installed near the Mauna Loa summit in the Hawaii Island and high-efficiency observation is continuing. It monitors optical and particle radiation from high-energy transient objects with a wide field-of-view.

The High Energy Astrophysics group is conducting theoretical researches on fundamental processes responsible for nonthermal particle acceleration in various astrophysical environments, including first-order diffusive shock acceleration, second order stochastic acceleration in shock downstream regions, modification of shock structure by pick-up interstellar neutrals, as well as injection processes of suprathermal particles. In addition to these theoretical works, R/D studies for radio observations of pulsars and cosmic ray air showers are also being made.

CANGAROO and TeV Gamma-Ray Projects

CANGAROO-III

[Spokespersons: R.W. Clay, R. Enomoto, and T. Tani-mori]

Collaboration list:

Institute for Cosmic Ray Research, University of Tokyo, Chiba, Japan; School of Chemistry and Physics, University of Adelaide, Australia; Mt Stromlo and Siding Spring Observatories, Australian National University, Australia; Australia Telescope National Facility, CSIRO, Australia; Department of Radiological Sciences, Ibaraki Prefectural University of Health Sciences, Ibaraki, Japan; Faculty of Science, Ibaraki University, Ibaraki, Japan; Department of Physics, Konan University, Hyogo, Japan; Department of Physics, Kyoto University, Kyoto, Japan; Solar-Terrestrial Environment Laboratory, Nagoya University, Aichi, Japan; National Astronomical Observatory of Japan, National Institutes of Natural Sciences, Tokyo, Japan; Department of Physics, Tokai University, Kanagawa, Japan; Department of Physics, Yamagata University, Yamagata, Japan; Faculty of Management Information, Yamanashi Gakuin University, Yamanashi, Japan; Faculty of Medical Engineering and Technology, Kitasato

Table 1. Summary of CANGAROO-III observations carried out in the fiscal year 2010 (April 2010 to March 2011).

Observation Term	Observation Target	Observation Time (hr)
April 2010	HESS J1507–622	23.5
June 2010	HESS J1507–622	20.2
September 2010	RX J1713.7–3946	2.7
November 2010	Crab Nebula	5.1
December 2010	Crab Nebula	8.2
March 2011	Vela X	6.7

University, Kanagawa, Japan; Department of Physics, Hiroshima University, Hiroshima, Japan; Department of Basic Physics, Tokyo Institute of Technology, Tokyo, Japan; Department of Physics, College of Science and Engineering, Ritsumeikan University; Institute of Particle and Nuclear Studies, High Energy Accelerator Research Organization (KEK), Ibaraki, Japan [1].

Status of the Project

CANGAROO is the acronym for the Collaboration of Australia and Nippon (Japan) for a GAMMA Ray Observatory in the Outback. The collaboration started in 1992 with a single Imaging Atmospheric Cherenkov Telescope (IACT) of 3.8 m diameter called CANGAROO-I in the desert area near Woomera, South Australia (136°47'E, 31°06'S, 160 m a.s.l.). As its third-generation experimental setup, the CANGAROO-III stereoscopic IACT system has been in operation since March 2004 with four IACTs of 10 m diameter. Stereoscopic observations of atmospheric Cherenkov light images produced by particle showers caused by high-energy particles bombarding the earth allow effective discrimination of gamma rays from charged cosmic rays which are the overwhelming backgrounds. Two of the four telescopes (called T3 and T4 in the order of construction) have been used in observations, as the first and second telescopes have degraded. A stereoscopic triggering system was installed at the beginning of 2005 and has been working properly, rejecting most single muon events, which are the major background component at low energies. We are continuing observations of various candidates of celestial gamma-ray emitters on moonless, clear nights.

CANGAROO-III Observations

We have carried out six observation shifts in the fiscal year 2010, which are summarized in Table 1. Relatively strong TeV gamma-ray sources with hard spectra have been selected as observation targets considering deteriorated performance of the CANGAROO-III system. A preliminary analysis of the data taken in April and June 2010 from the H.E.S.S. unidentified gamma-ray source HESS J1507–622 [2] has been performed and no statistically significant gamma-ray signal has been found. We therefore estimated preliminary upper limit to the gamma-ray flux from HESS J1507–622, which are consistent with the fluxes detected by H.E.S.S. The results were presented in the Japan Physical Society Meeting held in

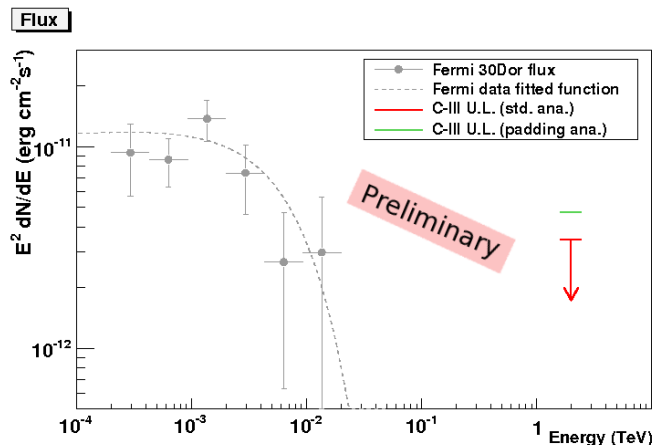


Fig. 1. Preliminary 2σ upper limits to the TeV gamma-ray flux from 30 Doradus in LMC obtained by CANGAROO-III. The red line represents the result of the standard analysis, whereas the green line is that of the analysis with software padding, in which artificial noise is added to pixels offline in order to equalize noise levels between on- and off-source data [4]. The gray points represent the fluxes detected by *Fermi* LAT [3].

September 2010. The presentation also included preliminary results for the data previously taken from 30 Doradus, which is a starburst region in the Large Magellanic Cloud (LMC) from which an extended GeV gamma-ray signal has been detected by *Fermi* LAT [3], and the Sculptor dSph galaxy, which is a dwarf spheroidal galaxy in the vicinity of the Milky Way Galaxy and possibly causes gamma-ray emission due to dark matter annihilations because of its mass concentration. However, no statistically significant TeV gamma-ray signals have been detected from these objects and flux upper limits have been presented. Figure 1 shows the upper limits to the flux from 30 Doradus in comparison with the *Fermi* GeV spectrum.

Bibliography

- [1] Collaboration website: <http://vesper.icrr.u-tokyo.ac.jp/>.
- [2] F. Acero et al., *Astron. Astrophys.*, **525**, A45 (2011).
- [3] A. A. Abdo et al., *Astron. Astrophys.*, **512**, A7 (2010).
- [4] M. F. Cawley, *Proc. Towards a Major Atmospheric Cherenkov Detector II*, ed. R. C. Lamb (Calgary), 172 (1993).

CTA Project (Cherenkov Telescope Array)

[CTA-Japan Spokespersons: T. Totani and M. Teshima]

Collaboration list:

Institute for Cosmic Ray Research, University of Tokyo, Chiba, Japan; Department of Physics, Yamagata University, Yamagata, Japan; Faculty of Science, Ibaraki University, Ibaraki, Japan; Institute of Particle and Nuclear Studies, High Energy Accelerator Research Organization (KEK), Ibaraki, Japan; Department of Physics, Tokyo University of Science, Chiba, Japan Department of Physics, The University of

Tokyo, Tokyo, Japan; Interactive Research Center of Science, Tokyo Institute of Technology, Tokyo, Japan; Department of Physics, Aoyama Gakuin University, Tokyo, Japan; Faculty of Science and Engineering, Waseda University, Tokyo, Japan; Department of Physics, Saitama University, Saitama, Japan; Institute of Space and Astronautical Science, JAXA, Kanagawa, Japan; Department of Physics, Tokai University, Kanagawa, Japan; Department of Radiation Oncology, Tokai University, Kanagawa, Japan; Faculty of Medical Engineering and Technology, Kitasato University, Kanagawa, Japan; Faculty of Management Information, Yamanashi Gakuin University, Yamanashi, Japan; Department of Physics, Nagoya University, Aichi, Japan; Solar-Terrestrial Environment Laboratory, Nagoya University, Aichi, Japan; Kobayashi-Maskawa Institute, Nagoya University, Aichi, Japan; Department of Astronomy, Kyoto University, Kyoto, Japan; Department of Physics, Kyoto University, Kyoto, Japan; Yukawa Institute for Theoretical Physics, Kyoto University, Kyoto, Japan; Department of Earth and Space Science, Osaka University, Japan; Department of Physics, Kinki University, Osaka, Japan; Department of Physics, Konan University, Hyogo, Japan; Department of Physics, Hiroshima University, Hiroshima, Japan; Hiroshima Astrophysical Science Center, Hiroshima University, Hiroshima, Japan; Faculty of Integrated Arts and Sciences, The University of Tokushima; Department of Applied Physics, University of Miyazaki, Miyazaki, Japan; Graduate School of Science and Technology, Kumamoto University, Kumamoto, Japan; Center for Cosmology and Astroparticle Physics, Ohio State University, Ohio, USA; Technical University of Dortmund, Dortmund, Germany [1].

CTA Project

During the past few years, Very High Energy (VHE) gamma ray astronomy has made spectacular progress and has established itself as a vital branch of astrophysics. To advance this field even further, we propose the Cherenkov Telescope Array (CTA) [2], the next generation VHE gamma ray observatory, in the framework of a worldwide, international collaboration. CTA is the ultimate VHE gamma ray observatory, whose sensitivity and broad energy coverage will attain an order of magnitude improvement above those of current Imaging Atmospheric Cherenkov Telescopes (IACTs). By observing the highest energy photons known, CTA will clarify many aspects of the extreme Universe, including the origin of the highest energy cosmic rays in our Galaxy and beyond, the physics of energetic particle generation in neutron stars and black holes, as well as the star formation history of the Universe. CTA will also address critical issues in fundamental physics, such as the identity of dark matter particles and the nature of quantum gravity.

VHE gamma rays from 100GeV to 10TeV can be observed with ground-based IACTs. The history of VHE gamma ray astronomy began with the discovery of VHE gamma rays from the Crab Nebula by the Whipple Observatory in 1989. To date, the current generation IACTs featuring new technologies, such as H.E.S.S., MAGIC, VERITAS, and CANGAROO, have discovered more than 100 Galactic and extragalactic sources of various types.

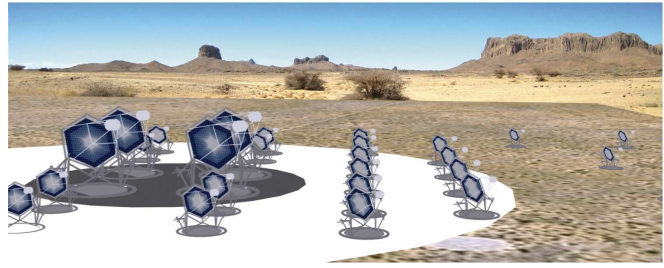


Fig. 2. Artist view of the CTA observatory. CTA consists of three types of telescopes, Large Size Telescopes (23m diameter), Mid Size Telescopes (12m) and Small Size Telescopes (6m), and covers the broad energy band from 20GeV to 100TeV.

CTA is designed to achieve superior sensitivity and performance, utilizing established technologies and experience gained from the current IACTs. The project is presently in its preparatory phase, with international efforts from Japan, the US and EU. It will consist of several 10s of IACTs of three different sizes (Large Size Telescopes, Mid Size Telescopes, and Small Size Telescopes). With a factor of 10 increase in sensitivity ($1\text{m Crab} \sim 10^{-14}\text{erg s}^{-1}\text{cm}^{-2}$), together with a much broader energy coverage from 20GeV up to 100TeV, CTA will bring forth further dramatic advances for VHE gamma ray astronomy. The discovery of more than 1000 Galactic and extragalactic sources is anticipated with CTA.

CTA will allow us to explore numerous diverse topics in physics and astrophysics. The century-old question of the origin of cosmic rays is expected to be finally settled through detailed observations of supernova remnants and other Galactic objects along with the diffuse Galactic gamma ray emission, which will also shed light on the physics of the interstellar medium. Observing pulsars and associated pulsar wind nebulae will clarify physical processes in the vicinity of neutron stars and extreme magnetic fields. The physics of accretion onto supermassive black holes, the long-standing puzzle of the origin of ultrarelativistic jets emanating from them, as well as their cosmological evolution, will be addressed by extensive studies of active galactic nuclei (AGN). Through dedicated observing strategies, CTA will also elucidate many aspects of the mysterious nature of gamma ray bursts (GRBs), the most energetic explosions in the Universe. Detailed studies of both AGNs and GRBs can also reveal the origin of the highest energy cosmic rays in the Universe, probe the cosmic history of star formation including the very first stars, as well as provide high precision tests of theories of quantum gravity. Finally, CTA will search for signatures from elementary particles constituting dark matter with the highest sensitivity yet. Realization of the rich scientific potential of CTA is very much feasible, thanks to the positive experience gained from the current IACTs.

The CTA-Japan consortium [1] is aiming at contributing in particular to the construction of the Large Size Telescopes (LSTs) and is involved in their development. The LST covers the low energy domain from 20GeV to 1000GeV and is especially important for studies of high redshift AGNs and GRBs. The diameter and area of the mirror are 23m and 400m^2 , respectively, in order to achieve the lowest possible energy threshold of 20GeV. All optical elements/detectors re-

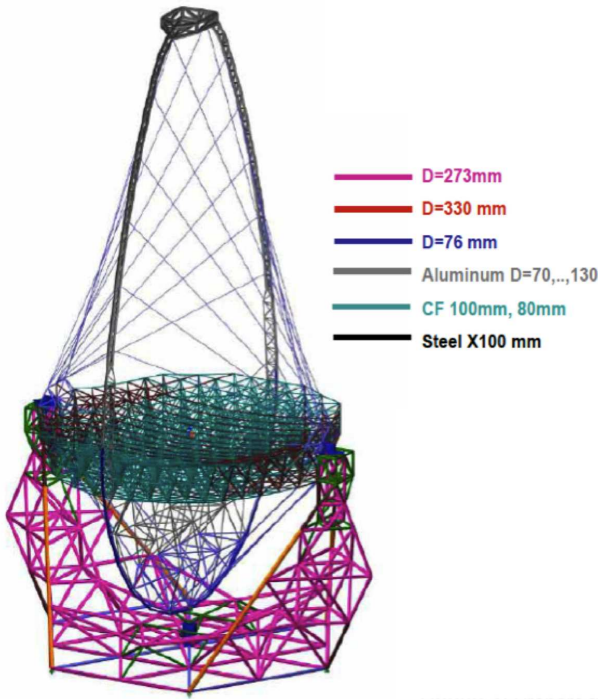


Fig. 3. Large Size Telescope (23m diameter) designed by Max-Planck-Institute for Physics. CTA Japan is contributing to the design and prototyping of the imaging camera at the focal plane, ultrafast readout electronics, and high precision segmented mirrors.

quire high specifications, for example, high reflectivity, high collection efficiency, high quantum efficiency and ultra fast digitization of signal, etc. For this purpose, CTA-Japan is developing high quantum efficiency photomultipliers, ultrafast readout electronics and high precision segmented mirrors. On the strength of their experience gained from construction of the MAGIC telescope, the Max-Planck-Institute for Physics in Munich is responsible for the design of the 23m diameter telescope structure, based on a carbon fiber tube space frame. The LSTs require very fast rotation (180 degrees/20seconds) for promptly observing GRBs.

The Cherenkov Cosmic Gamma Ray group is also operating two current observatories; one is MAGIC [4] on La Palma, Canary Islands, in the Northern hemisphere, and the other is CANGAROO [5] at Woomera, Australia, in the Southern hemisphere. These two facilities are used not only for scientific observations but also for technological development toward the future observatory CTA.

Bibliography

- [1] CTA Consortium website: <http://www.cta-observatory.jp/> and <http://www.cta-observatory.org/>.
- [2] **Design Concepts for The Cherenkov Telescope Array**, The CTA Consortium, (2010), available at arXiv1008.3703.
- [3] **Status of Very High Energy Gamma Ray Astronomy and Future Prospects**, M. Teshima, The Astronomical



Fig. 4. Camera cluster for the Large Size Telescope (LST) developed by CTA-Japan. This cluster consists of seven high quantum efficiency photomultipliers (R11920-100), CW High Voltages, pre-amplifier, Slow Control Board, DRS4 Ultra fast waveform recording system and Trigger. The LST camera can be assembled with 400 of these clusters, cooling plates and camera housing.

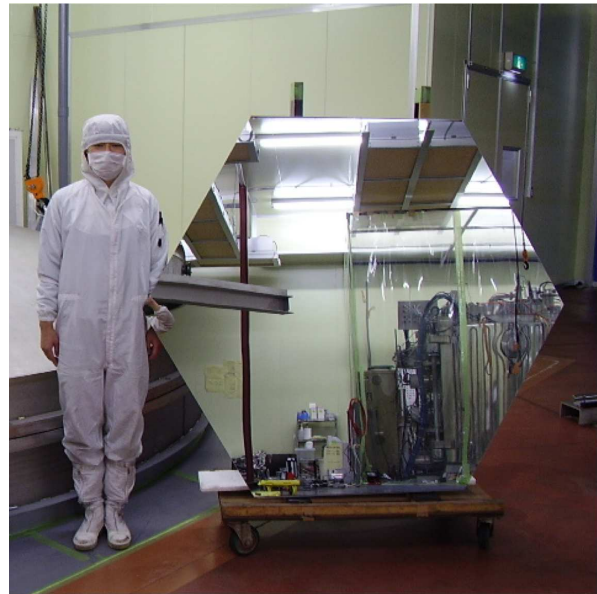


Fig. 5. Prototype of the high precision segmented mirror for the Large Size Telescope (LST) developed by CTA-Japan in cooperation with Sanko Co.LTD. The mirror is made of a 60mm thick aluminum honeycomb sandwiched by 3mm thin glass on both sides. A surface protection coat consisting of the materials SiO₂ and HfO₂ will be applied to enhance the reflectivity and to elongate the lifetime.

Herald, 104 (2011) 333-342.

- [4] MAGIC Collaboration website: <http://magic.mppmu.mpg.de/>.
- [5] CANGAROO Collaboration website: <http://vesper.icrr.u-tokyo.ac.jp/>.

Other Activities

As a test bench of domestic R & D activities for future ground-based gamma-ray observatory projects, a used Cherenkov telescope of a 3 m diameter has been obtained and repaired. We have placed it at the Akeno observatory in November 2010, as shown in Figure 6. Some prototype imaging cameras and electronics systems are planned to be



Fig. 6. 3 m Cherenkov telescope installed at the Akeno observatory as a test bench for future ground-based gamma-ray observatories.

installed to this telescope, and test observations will be carried out in the near future.

TA: Telescope Array Experiment

Spokespersons:

M. Fukushima / ICRR, University of Tokyo
P. Sokolsky / Dept. of Physics, University of Utah

Collaborating Institutions:

Chiba Univ., Chiba, Japan; Chungnam Nat. Univ., Daejeon, Korea; Ehime Univ., Matsuyama, Japan; Ewha W. Univ., Seoul, Korea; Hiroshima City Univ., Hiroshima, Japan; Hanyang Univ., Seoul, Korea; ICRR, Univ. of Tokyo, Kashiwa, Japan; INR, Moscow, Russia; IPMU, Univ. of Tokyo, Kashiwa, Japan; Kanagawa Univ., Yokohama, Japan; KEK/IPNS, Tsukuba, Japan; Kinki Univ., Higashi-Osaka, Japan; Kochi Univ., Kochi, Japan; Nat. Inst. of Rad. Sci., Chiba, Japan; Osaka City Univ., Osaka, Japan; Rutgers Univ., Piscataway, NJ, USA; Saitama Univ., Saitama, Japan; Tokyo City Univ., Tokyo, Japan; Tokyo Inst. of Tech., Tokyo, Japan; Tokyo Univ. of Science, Noda, Japan; ULB, Brussels, Belgium; Univ. of Utah, Salt Lake City, UT, USA; Univ. of Yamanashi, Kofu, Japan; Waseda Univ., Tokyo, Japan; Yonsei Univ., Seoul, Korea

Overview and Status of TA

The TA [1] is the detector that consists of the surface array of plastic scintillator detectors (a la AGASA) and fluorescence detectors (a la HiRes). The aim of the TA is to explore the origin of extremely-high energy (EHE) cosmic rays by measuring energy, arrival direction and mass composition. It is located in the West Desert of Utah, 140 miles south of Salt Lake City (lat. 39.3°N, long. 112.9°W, alt. ~1400 m). The

construction of the TA was performed mainly by the Grants-in-Aid for Scientific Research (Kakenhi) of Priority Areas “The Origin of Highest Energy Cosmic Rays” (JFY2003-JFY2008) and the US National Science Foundation (NSF). All the three fluorescence stations started the observation in November 2007. Major construction of the surface detector array was completed in February 2007, and the array of the surface detectors started the full operation in March 2008. The TA is operated by the international collaboration of researchers from US, Russia, Korea and Japan. The main fund for the TA operation is the Grants-in-Aid for Scientific Research (Kakenhi) of Specially Promoted Research “Extreme Phenomena in the Universe Explored by Highest Energy Cosmic Rays” (JFY2009-JFY2013).

Surface Detector Array

The surface detector (SD) array consists of 507 plastic scintillators on a grid of 1.2 km spacing. It covers the ground area of about 700 km².

The counter is composed of two layers of plastic scintillator overlaid on top of each other. One layer of scintillator is 1.2 cm thick and 3 m² in area. Light from each layer is collected by 104 wave length shifter fibers 5 m long, which are installed in grooves on the surface. Both ends of the fibers are bundled and optically connected to one photomultiplier for each layer. Power of each SD is supplied by a solar panel and battery. The communication between SDs and the host at the communication tower is performed by wireless LAN.

Fluorescence Telescope

The TA has three fluorescence detector (FD) stations. The fluorescence station in the southeast is located at the Black Rock Mesa (BRM) site. The southwestern station is located at the Long Ridge (LR) site and the station in the north is located at the Middle Drum (MD) site.

Twelve reflecting telescopes were newly constructed and installed at each of the BRM and LR stations and cover the sky of 3°-34° in elevation and 108° in azimuth looking toward the center of the surface detector array.

The MD station was constructed using refurbished equipment from the old HiRes-1 observatory. Fourteen reflecting telescopes cover the sky of 3°-31° in elevation and 114° in azimuth.

We also built a laser shooting facility (Central Laser Facility: CLF), which is located at an equal-distance (20.85 km) from three fluorescence stations for atmospheric monitor. The Rayleigh scattering at high altitude can be considered as “standard candle” observable at all the stations.

A LIDAR (LIght Detection And Ranging) system located at the BRM station is used for the atmospheric monitoring. It consists of a pulsed Nd:YAG laser and a telescope attached to an alto-azimuth. The back-scattered light is received by the telescope to analyze the extinction coefficient along the path of the laser.

For monitoring the cloud in the night sky, we installed an infra-red CCD camera at the BRM station, and take data of the night sky every hour during FD observation.

In order to confirm absolute energy scale of the fluorescence detector in situ, we installed a compact electron linear

accelerator (Electron Light Source: ELS) [2] at the BRM FD site. A beam of 10^9 electrons with energy of 40 MeV and a duration of $1 \mu\text{s}$ well simulates a shower energy deposition of $\sim 4 \times 10^{16}$ eV 100 m away from the station, which corresponds to a shower of $\sim 4 \times 10^{20}$ eV 10 km away. The calibration is performed by comparing the observed fluorescence signal with the expected energy deposition calculated by the GEANT simulation [3]. We began to start up the ELS in June 2010, and we shot electron beam vertically up into the atmosphere from the ELS for the first time and took the images with FD on September 3rd, 2010. Fig. 1 shows the image of the pseudo shower by the electron beam together with the image by Geant MC simulation.

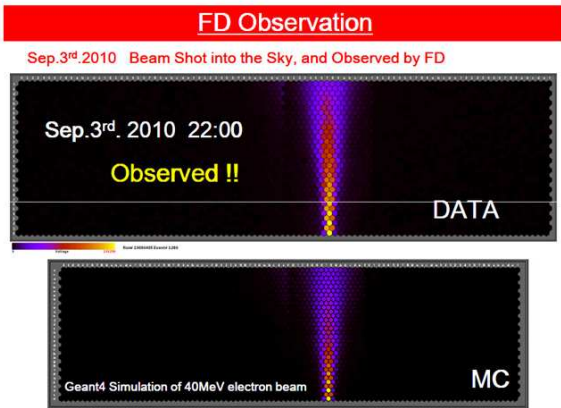


Fig. 1. The image of the pseudo shower by the electron beam that was shot from the ELS at the BRM FD site for the first time on September 3rd, 2010 (upper). The image by Geant MC simulation (lower).

Status of TA Observation

Fig. 2 shows the rate of operation of the surface detectors from May 2008 through March 2011. There were periods for which the fraction of operation decreased because of maintenance and bad weather. The average rate of operation is close to 100%.

Fig. 3 shows the observation hours for the BRM and LR fluorescence detectors from November 2007 through February 2011. We observe during moonless night, and the observation time per night in winter is longer than that in summer.

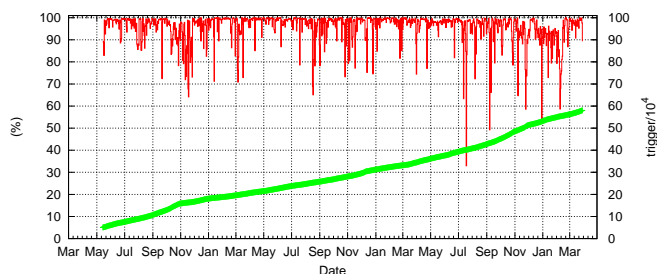


Fig. 2. The rate of operation of the surface detectors in red and the integrated number of triggered air shower events in green from March 2008 through March 2011.

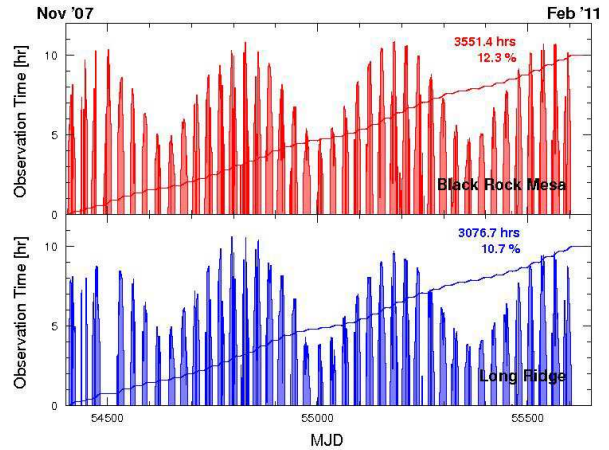


Fig. 3. Observation hours per night and integrated observation hours for the BRM (upper) and LR (lower) fluorescence detector sites from November 2007 through February 2011. The horizontal axes represent modified Julius day (MJD).

Energy spectrum

The Auger group and the HiRes group published the results of energy spectrum, which are consistent with GZK cut-off with their energy scales determined by the method of fluorescence telescope [4, 5]. We present energy spectra using three different methods: the MD monocular FD analysis, hybrid analysis, and SD analysis.

Energy spectrum by the MD monocular FD analysis

The analysis of monocular FD data at the MD station provides a direct comparison between the TA and HiRes energy spectra. The MD spectrum uses the data collected over a three-year period between December 2007 and September 2010. The MD spectrum is based on the monocular observation technique and is analyzed using the profile-constrained geometry reconstruction technique developed by the HiRes-1. The preliminary monocular energy spectrum from the MD fluorescence detector is shown in Fig. 4. The TA MD monocular energy spectrum is in good agreement with the HiRes spectra. The details of the analysis of the MD FD data is described in [6].

Energy spectrum by hybrid analysis

The hybrid events which are detected both by FD and SD are useful to compare the reconstructed results from FD and SD. In addition, we improve the reconstruction of FD events more precisely by using information both of FD and SD for hybrid events than FD monocular analysis alone. Here we use timing information from one SD. When we use only data of the fluorescence detectors, the aperture depends on energy of primary cosmic rays, but hybrid analysis has the merit that the aperture is kept constant above 10^{19} eV by the size of the surface detector array and the systematic error of the aperture becomes smaller. The hybrid event candidates were searched for by the condition that the trigger time difference between FD and SD is less than $200 \mu\text{s}$ from May 2008 through September 2009. We found 1978 hybrid events. The effective aperture after the quality cuts is obtained from the Monte Carlo simulation code COSMOS [7] with QGSJET-II model for pure pro-

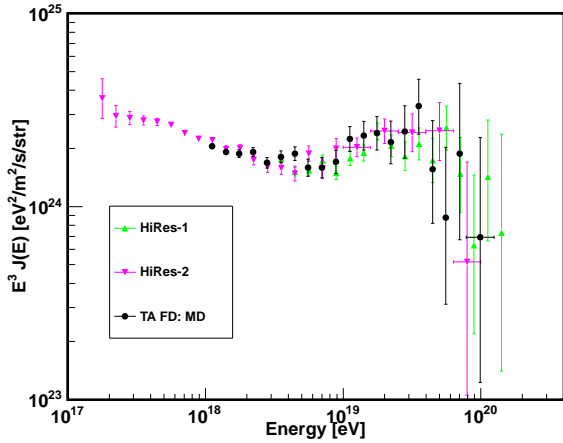


Fig. 4. The preliminary monocular energy spectrum from the TA MD fluorescence detector (black circles). Green triangles and purple downward triangles represent those for the HiRes-1 and HiRes-2 detectors, respectively.

ton including calibration factors for the whole period. The exposure of the hybrid analysis is approximately $4 \times 10^{15} \text{ m}^2 \text{ sr s}$ above 10^{19} eV . After the reconstruction procedure, 124 events remain above $10^{18.65} \text{ eV}$. The total systematic uncertainties are 19% in energy measurement, and 10% in flux from cloud monitoring. The preliminary energy spectrum from the hybrid analysis is shown in Fig. 5. The energy spectrum by this analysis is consistent with the other TA results. The details of the hybrid analysis are described in [8].

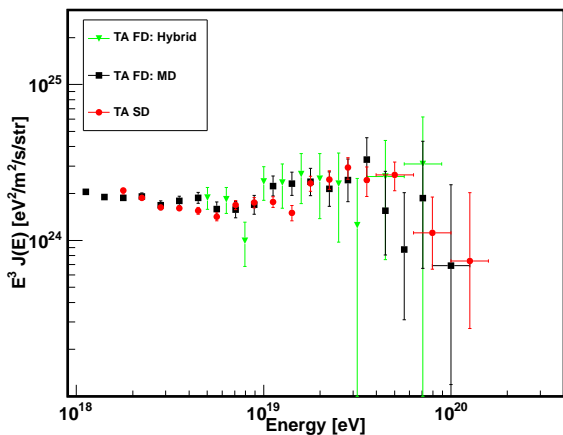


Fig. 5. The preliminary TA energy spectra measured by three different methods. Green downward triangles denote the spectrum by hybrid analysis. Black squares denote the spectrum by the MD monocular FD analysis. Red circles denote the spectrum by the data of the surface detectors with “energy scaled to FD energy”.

Energy spectrum by using the data of the surface detectors

We measure the energy spectrum by using the SD data from May 2008 through February 2010. The exposure is approximately $1500 \text{ km}^2 \text{ sr yr}$ which is equivalent to the total exposure of the AGASA.

There are two types of fits in SD event reconstruction: the fit to determine the geometry of the shower and the fit to determine the lateral density distribution. Monte Carlo data were generated by CORSIKA air shower simulation program [9] with QGSJET-II proton model. The detector simulation with front-end electronics and trigger was constructed with Geant4 simulation. The fit result of the Monte Carlo data by the parameters tuned by the observed data is also good in the same way as that of the observed data.

The basic idea of the energy reconstruction is to use the charge density at a distance of 800 m from shower core (S_{800}) as an energy estimator. The correlation of S_{800} and zenith angle with primary energy from Monte Carlo study is used for the first estimation of the primary energy of the data.

We compare the energy scales of FD and SD using hybrid events. The scatter plot of the energies of well-reconstructed 331 events is shown in Fig. 6. It shows that the energy of SD is 27% larger than that of FD. We choose the energy scale of FD, and the SD energy is rescaled by 27%.

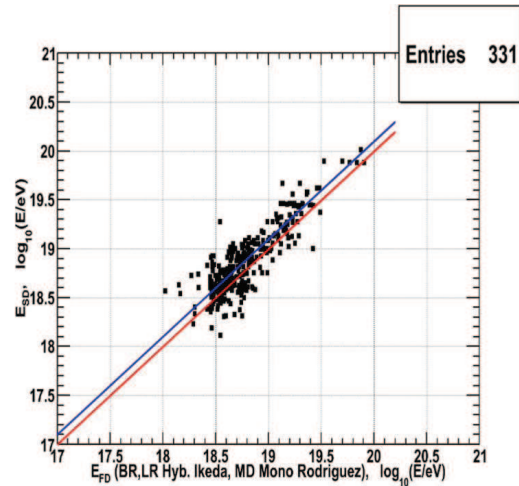


Fig. 6. The preliminary result of the comparison of the energies between FD and SD. The red line corresponds to $E_{SD} = E_{FD}$. The blue line corresponds to $E_{SD} = 1.27 \times E_{FD}$.

After the reconstruction procedure, 6264 events with zenith angles below 45° remain. We obtain the energy spectrum from the number of events in each energy bin by using the effective aperture obtained from the Monte Carlo data. The preliminary energy spectrum is shown in Fig. 5. An excess of UHECRs exceeding the prediction by GZK, which had been observed by AGASA in 1998, was not confirmed. We performed a fit using power laws in three regions, and found the two breaks at $\log E$ (E in eV) of 19.75 and 18.71, which correspond to the GZK suppression [10, 11] and the ankle, respectively. We observed five events above the break point at $10^{19.75} \text{ eV}$ while the expected number of events along the continuous spectrum is 18.4. This result provides evidence for the flux suppression with the significance of 3.5σ . The details of the SD analysis are described in [12].

The obtained preliminary energy spectra by three different methods from the TA experiment are shown together with other experiments in Fig. 7.

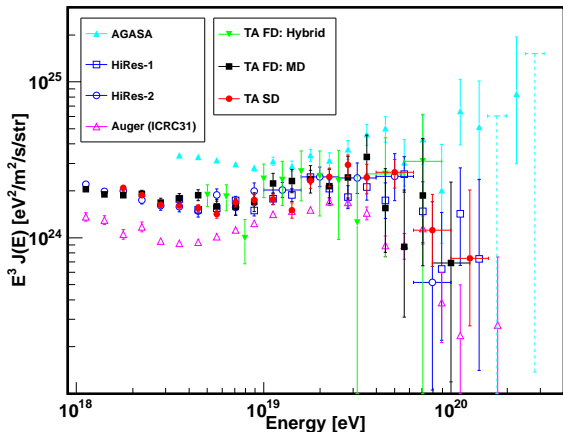


Fig. 7. The preliminary spectra from the Telescope Array together with the spectra from other experiments. The green closed downward triangles represent the TA hybrid spectrum, the black closed squares the monocular FD spectrum from the MD station, and the red closed circles the TA SD spectrum. The light-blue closed triangles represent the AGASA spectrum, the blue open squares the HiRes-1 spectrum, the blue open circles the HiRes-2 spectrum, and the purple open triangles the PAO spectrum. The light-blue dotted bars are 90% C.L. upper limits for the AGASA.

Measurement of mass composition by shower maximum depth (X_{\max})

The basic idea to determine the mass composition of UHECRs is to use the dependence of the atmospheric depth of shower maximum on the primary energy and mass composition.

For composition in EHE region, the Auger data suggests a change to a heavier composition [13] while the HiRes data is consistent with constant elongation rate which stays with proton [14].

The data set from November 2007 through September 2010 is used in this analysis. The events observed simultaneously at two new FD stations are analyzed for the shower geometry by stereo technique and for the longitudinal development in the same way as hybrid technique to measure the atmospheric depth of shower maximum (X_{\max}).

The Monte Carlo data are generated by CORSIKA with the particle types of proton and iron, and the interaction models of QGSJET-01 and SIBYLL. The resolution of energy is 8% and that of X_{\max} is 23 g/cm² at energy around 10^{19.0} eV from QGSJET-01 proton Monte Carlo simulation. We notice that the measured X_{\max} has a bias from the limit of the field of view. Since this bias also depends on the model, the reconstructed X_{\max} from the observed data and Monte Carlo data are compared by applying the same analysis procedure. An example of the distribution of X_{\max} for the TA stereo data along with QGSJET-01 Monte Carlo data is shown in Fig. 8. The distribution of X_{\max} of the observed data is in good agreement with that of the Monte Carlo data for protons.

The evolution of the average X_{\max} with energy was measured and compared with the Monte Carlo data in the energy range from 10^{18.2} to 10^{20.0} eV as shown in Fig. 9. The observed TA data are in good agreement with the QGSJET-01 pure proton prediction. The details of the mass composition

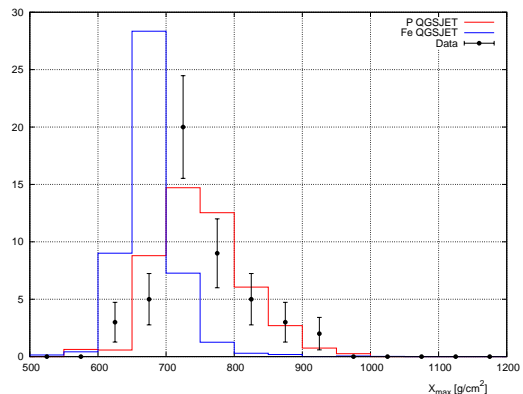


Fig. 8. The preliminary reconstructed X_{\max} distribution for the TA stereo data (points) along with QGSJET-01 Monte Carlo data in the energy region from 10^{18.8} to 10^{19.0} eV. The red and blue histograms are the proton and iron predictions, respectively.

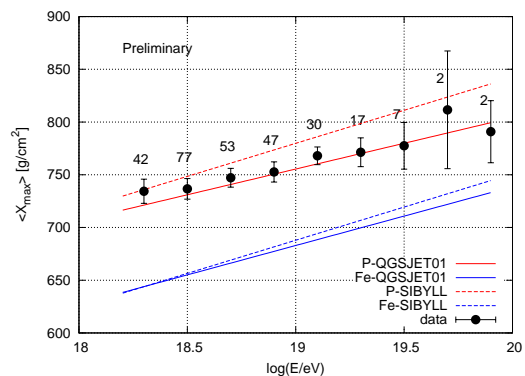


Fig. 9. The preliminary result of the average reconstructed X_{\max} as a function of energy. The black points are the TA stereo data. The upper set of red lines are predictions for pure protons with the interaction models of QGSJET-01 (solid line) and SIBYLL (dashed line). The lower set of blue lines are under the assumption of iron.

study are described in [15].

Search for UHE photons

Several models were proposed for the interpretation of the origin of highest energy cosmic rays. There is a possibility that cosmic rays were generated and accelerated in very active region up to highest energy cosmic rays (bottom-up model), and were observed at the earth through GZK process. If highest energy cosmic rays are generated and accelerated at the sources such as AGN, there is a possibility that UHE photons with energy around 10¹⁹ eV are generated by resonant π^0 production in GZK-type process. It is also expected that large amount of UHE photons with energy above 10¹⁹ eV could be generated by non-accelerated model (top-down model) such as unknown super-heavy particles. It is expected that UHE photons with energy above 10¹⁹ eV interact in deeper atmosphere than UHE hadrons. Then the curvature of air shower front of photons around the ground is larger than that of hadrons.

Fig. 10 shows the curvature of air shower front for the data of the surface detectors taken from May 2008 through October 2009. We obtained the limit on the integral flux of

photons with energy above 10^{19} eV to be

$$3.4 \times 10^{-2} \text{ km}^{-2} \text{ sr}^{-1} \text{ yr}^{-1}$$

at 95% confidence level as shown in Fig. 11 [16].

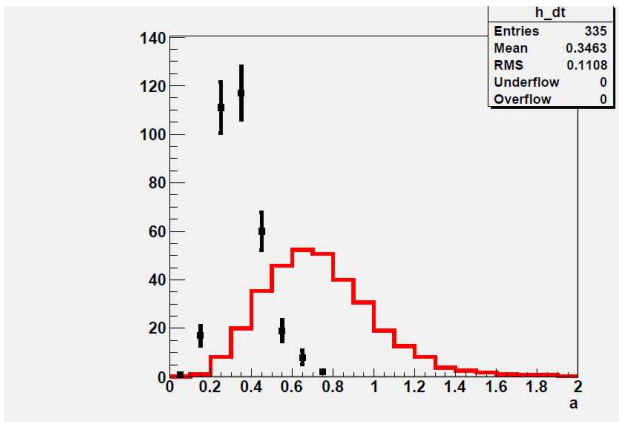


Fig. 10. The preliminary result of the distribution of the curvature of shower front of UHE cosmic rays (Linsley curvature parameter) for zenith angle from 45° to 60° . Black points denote the distribution of curvature of the TA data. The histogram corresponds to the expected distribution of the curvatures for the photons that are generated by the spectrum with power index of -2.

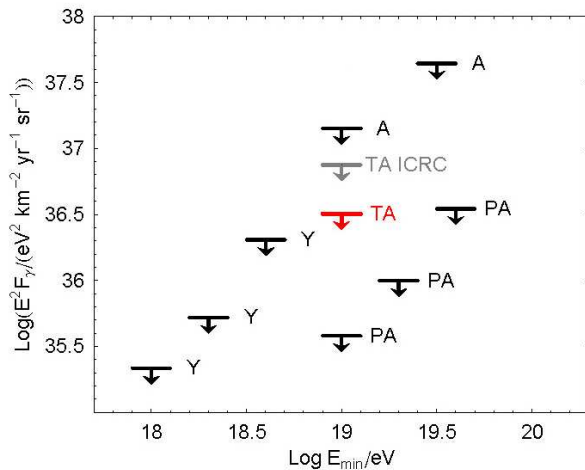


Fig. 11. Upper limits on the integral flux of UHE photons for different experiments: the latest preliminary TA result (TA) in red, TA at ICRC09 (TA ICRC) in gray, AGASA (A), Auger (PA), and Yakutsk (Y).

Arrival directions of UHE cosmic rays

We present the analysis of UHECRs for correlations with the large-scale structure (LSS), correlations with AGN and small-scale anisotropy. The analysis is based on the SD data collected for zenith angles less than 45° from March 2008 through September 2010.

Correlations with LSS

At large angular scales, the anisotropy in the PAO data was claimed [17], and that in the HiRes data was not confirmed [18].

We use the 2MASS Galaxy Redshift Catalog (XSCz) [19] that is derived from the 2MASS Extended Source Catalog (XSC) with redshifts that have either been derived from the 2MASS photometric measurements or measured spectroscopically. We use the galaxies at distances from 5 to 250 Mpc and with Ks magnitudes less than 12.5. This catalog provides the most accurate information about three-dimensional galaxy distribution. We assume that UHECRs are protons. We also assume that the effects of the Galactic and extragalactic magnetic fields are approximated by a Gaussian smearing angle. The flux map calculated with these assumptions at the energy threshold of 57 EeV is shown in Fig. 12. The rectangular region around the Galactic center ($|b| < 10^\circ$ and $|l| < 90^\circ$) is excluded from the analysis because the underlying galaxy catalog is incomplete. We choose an a priori confidence level of 95%, which means that the two distributions are incompatible at the 95% C.L. if the KS-test probability (p-value) is smaller than 0.05. The data both above 40 EeV and 57 EeV are compatible with LSS model. For isotropic model, the data above 40 EeV are compatible while the data above 57 EeV are incompatible at the 95% C.L. [20, 21]

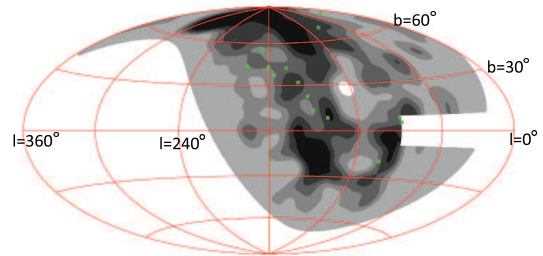


Fig. 12. The sky map of expected flux from LSS model together with observed arrival directions of UHECRs with energies above 57 EeV (green points) in the Galactic coordinates. Darker gray region indicates larger flux and each band contains 1/5 of the total flux. The region $|b| < 10^\circ$ and $|l| < 90^\circ$ is excluded from the analysis. The smearing angle is 6° .

Correlations with AGN

The Pierre Auger Collaboration reported correlations between the arrival directions of UHECRs with energies above 57 EeV and positions of nearby AGN [22]. The probability that the correlations for angular separations less than 3.1° has occurred by chance is 1.7×10^{-3} . However, the HiRes group reported that no correlations have been found [23]. To test AGN hypothesis, we use nearby AGN from Véron 2006 catalog [24], with the cut on redshift $0 < z < 0.018$. As is seen from Fig. 13 [20], the preliminary TA result is compatible both with isotropic distribution and the AGN hypothesis.

Small-scale anisotropy

The small-scale clusters of UHECR arrival directions were observed by the AGASA experiment at the angular scale of 2.5° [25, 26]. On the other hand, the result of small-scale anisotropy by the HiRes experiment is consistent with an isotropic distribution [27]. Following the analysis of the AGASA, we used the events with energies above 10 EeV and 40 EeV. Fig. 14 shows the distribution of separation angles for

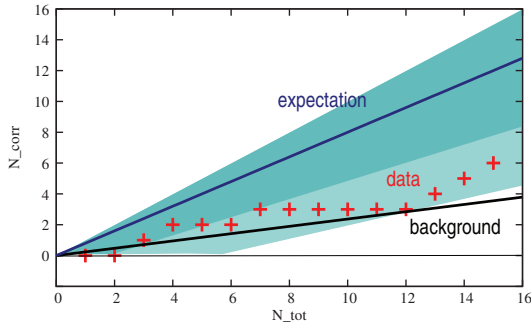


Fig. 13. The preliminary result of the correlations with AGN. The horizontal axis is the number of observed events and the vertical axis is the number of correlated events with AGN. The red crosses are the TA data. The turquoise shaded area shows 1σ region and the light-blue shaded area shows 2σ region. The black solid line is the prediction from isotropic distribution and the blue solid line is the prediction from the result of the Pierre Auger Observatory [22].

any two cosmic rays with energies above 40 EeV normalized by solid angle. Then we count the number of pairs separated by less than 2.5° . For the events with energies above 10 EeV, we find 311 pairs while 323 are expected for the isotropic model. For the events with energies above 40 EeV, we find one pair while 0.8 are expected for the isotropic model. No significant autocorrelations (clustering) at small scales were found in the data sets [20, 28].

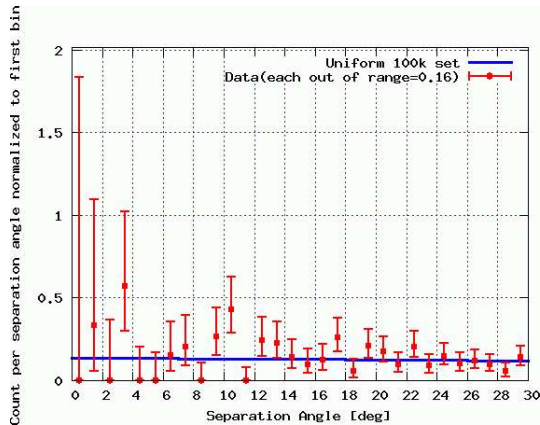


Fig. 14. The preliminary distribution of separation angles for any two cosmic rays with energies above 40 EeV normalized by solid angle. The points are the observed data and the blue line is the isotropic model. Error bars represent the Poisson upper and lower limits at 68% C.L.

Prospects

We will analyze the increasing TA data and measure energy spectrum, particle composition including UHE photons and UHE neutrinos, anisotropy of arrival directions more in detail and explore the origin of UHE cosmic rays and understand the extreme phenomena of the universe by using the characteristic features of the TA detector, the sampling of electromagnetic shower energy, the unique calibration of fluorescence generation, usage of HiRes-1 telescopes in the TA site, and the measurement in the northern hemisphere.

In the near future, we plan to determine energies of air showers within total uncertainty of about 10% and measure the spectrum of UHE cosmic rays precisely by using end-to-end absolute energy calibration of fluorescence telescopes with the ELS.

Towards large-scale UHECR observatory, wide attention has been raised to the detection of UHECR with radio techniques, either passive and active, in addition to the extension with the surface detectors and/or fluorescence detectors. An R/D study of the detection of radar echoes from extensive air showers (EAS) has started by installing a transmitter and receivers at the TA site. The R/D studies of the detection of bremsstrahlung from EAS are being discussed first by using the ELS.

A construction of TALE, a Low Energy extension of TA with the energy range down to 10^{17} eV is proposed to investigate the modulation of cosmic ray composition and spectrum expected by the galactic to extra-galactic transition of cosmic ray origins including “second knee” in the 10^{17} eV decade. By the TA+TALE project, comprehensive studies on UHE cosmic rays will be possible for wide energy range from $10^{16.5}$ to 10^{20} eV or above.

Bibliography

- [1] H. Kawai *et al.* (Telescope Array Collaboration), *Nucl. Phys. B Proc. Suppl.*, 2008, 175-176, 221-226; H. Kawai *et al.* (Telescope Array Collaboration), *J. Phys. Soc. Jpn. Suppl. A* **79** (2009), 108; H. Sagawa for the Telescope Array Collaboration, *Proc. 31st ICRC, Lodz, Poland* (2009).
- [2] T. Shibata *et al.*, *Nucl. Instr. and Meth. A* **597** (2008) 61-66.
- [3] S. Agostinelli *et al.*, *Nucl. Instr. and Meth. A* **506** (2003) 250.
- [4] R.U. Abbasi *et al.* (HiRes Collaboration), *Phys. Rev. Lett.* **100** (2008) 101101.
- [5] J. Abraham *et al.* (Pierre Auger Collaboration), *Phys. Rev. Lett.* **101** (2008) 061101.
- [6] D. Rodriguez, *Ph.D. thesis, University of Utah* (2011).
- [7] K. Kasahara and F. Cohen, *Proc. 30th ICRC, Merida, Mexico* 4 (2008) 581.
- [8] D. Ikeda, *Ph.D. thesis, University of Tokyo* (2010).
- [9] Heck, D. *et al.*, *Report FZKA* (1998) 6019.
- [10] K. Greisen, *Phys. Rev. Lett.* **16**, 748 (1966).
- [11] G.T. Zatsepin and V.A. Kuz'min, *JETP Lett.* **4**, 78 (1966) [*Pis'ma Zh. Eksp. Teor. Fiz.* **4**, 114 (1966)].
- [12] B. Stokes *et al.* (Telescope Array Collaboration), Proceedings of the International Symposium on the Recent Progress of Ultra-high Energy Cosmic Ray Observation (UHECR2010), 10-12 Dec 2010.
- [13] J. Abraham *et al.* (Pierre Auger Collaboration), *Phys. Rev. Lett.* **104** (2010) 09110.

- [14] R.U. Abbasi *et al.*, (HiRes Collaboration), *Phys. Rev. Lett.* **104** (2010) 161101.
- [15] Y. Tameda, *Ph.D. thesis, Tokyo Institute of Technology*, 2010; Y. Tameda *et al.*, Proceedings of UHECR2010, 10-12 Dec 2010.
- [16] G. Rubtsov *et al.* (Telescope Array Collaboration), Proceedings of UHECR2010 10-12 Dec. 2010.
- [17] T. Kashti and E. Waxman, *JCAP* **05** (2008) 006.
- [18] R.U. Abbasi *et al.* (HiRes Collaboration), *Astrophys. J. Lett.* **71B** (2010) 64.
- [19] T. Jarrett, arXiv:astro-ph/0405069.
- [20] P. Tinyakov *et al.* (Telescope Array Collaboration), Proceedings of UHECR2010, 10-12 Dec 2010.
- [21] E. Kido *et al.* (Telescope Array Collaboration), Proceedings of UHECR2010, 10-12 Dec 2010.
- [22] J. Abraham *et al.* (Pierre Auger Collaboration), *Science* **318** (2007) 939; J. Abraham *et al.* (Pierre Auger Collaboration), *Astropart. Phys.* **29** (2008).
- [23] R.U. Abbasi *et al.* (HiRes Collaboration), *Astropart. Phys.* **30** (2008) 175-179.
- [24] M.P. Véron-Cetty, P. Véron, and *Astron. Astrophys.* **455** (2006) 773.
- [25] N. Hayashida *et al.*, *Phys. Rev. Lett.* **77** (1996) 78.
- [26] M. Takeda *et al.*, *J. Phys. Soc. Jpn (Suppl.) B* **70** (2001) 15.
- [27] R.U. Abbasi *et al.*, *Astrophys. J.*, **610** (2004) 73.
- [28] T. Okuda *et al.* (Telescope Array Collaboration), Proceedings of UHECR2010, 10-12 Dec 2010.

Tibet AS γ Project

Experiment

The Tibet air shower experiment has been successfully operated at Yangbajing (90°31' E, 30°06' N; 4300 m above sea level) in Tibet, China since 1990. It has continuously made a wide field-of-view (approximately 2 steradian) observation of cosmic rays and gamma rays in the northern sky.

The Tibet I array was constructed in 1990 and it was gradually upgraded to the Tibet II by 1994 which consisted of 185 fast-timing (FT) scintillation counters placed on a 15 m square grid covering 36,900 m², and 36 density (D) counters around the FT-counter array. Each counter has a plastic scintillator plate of 0.5 m² in area and 3 cm in thickness. All the FT counters are equipped with a fast-timing 2-inch-diameter photomultiplier tube (FT-PMT), and 52 out of 185 FT counters are also equipped with a wide dynamic range 1.5-inch-diameter PMT (D-PMT) by which we measure up to 500 particles which saturates FT-PMT output, and all the D-counters

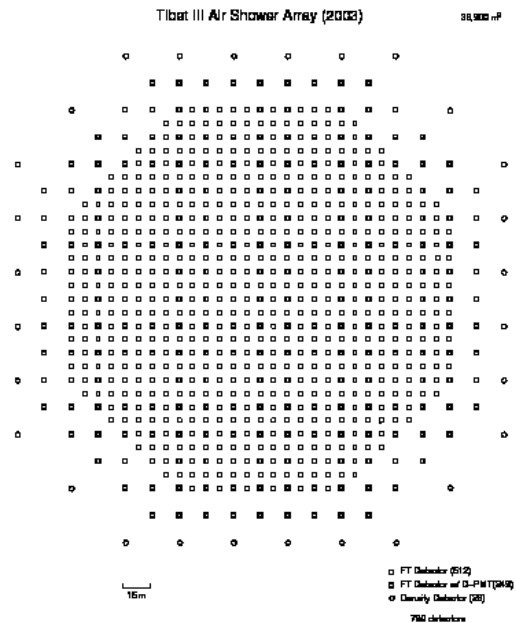


Fig. 1. Schematic view of the Tibet III array.

have a D-PMT. A 0.5 cm thick lead plate is put on the top of each counter in order to increase the counter sensitivity by converting gamma rays into electron-positron pairs in an electromagnetic shower. The mode energy of the triggered events in Tibet II is 10 TeV.

In 1996, we added 77 FT counters with a 7.5 m lattice interval to a 5,200 m² area inside the northern part of the Tibet II array. We called this high-density array Tibet HD. The mode energy of the triggered events in Tibet HD is a few TeV.

In the late fall of 1999, the array was further upgraded by adding 235 FT-counters so as to enlarge the high-density area from 5,200 m² to 22,050 m², and we call this array and further upgraded one Tibet III. In 2002, all of the 36,900 m² area was covered by the high-density array by adding 200 FT-counters more. Finally we set up 56 FT-counters around the 36,900 m² high density array and equipped 8 D-counters with FT-PMT in 2003. At present, the Tibet air shower array consists of 761 FT-counters (249 of which have a D-PMT) and 28 D-counters as in Fig. 1.

The performance of the Tibet air shower array has been well examined by observing the Moon's shadow (approximately 0.5 degrees in diameter) in cosmic rays. The deficit map of cosmic rays around the Moon demonstrates the angular resolution to be around 0.9° at a few TeV for the Tibet III array. The pointing error is estimated to be better than 0°.011, by displacement of the shadow's center from the apparent center in the north-south direction, as the east-west component of the geomagnetic field is very small at the experimental site. On the other hand, the shadow center displacement in the east-west direction due to the geomagnetic field enables us to spectroscopically estimate the energy scale uncertainty less than $\pm 12\%$.

Thanks to high statistics, the Tibet air shower experiment introduces a new method for energy scale calibration other than the conventional estimation by the difference between

the measured cosmic-ray flux by an air shower experiment and the higher-energy extrapolation of cosmic-ray flux measured by direct measurements by balloon-borne or satellite experiments.

Physics Results

Our current research theme is classified into 4 categories:

- (1) TeV celestial gamma-ray point/diffuse sources,
- (2) Chemical composition and energy spectrum of primary cosmic rays in the knee energy region [3],
- (3) Cosmic-ray anisotropy in the multi-TeV region with high precision[4],
- (4) Global 3-dimensional structure of the solar and interplanetary magnetic fields by observing the Sun's shadow in cosmic rays.

We will introduce a part of the results obtained in this fiscal year.

The first topic is on the knee-physics-related one.

We use the air shower array to measure the energy and arrival direction of each air shower. The primary energy of each event is determined by the shower size N_e , which is calculated by fitting the lateral particle density distribution to the modified NKG structure function. The energy resolution is less than 20% for the knee energy range. The arrival direction of an air shower is determined as follows. The direction cosine of the shower axis is determined using a least square method where the difference is minimized between the arrival time signals of each FT counter and the expected values on the assumed cone with a given direction cosine. This procedure determines the arrival angle with an accuracy smaller than 0.2° at energies above 10^{14} eV. The core detector was designed to detect the high-energy particles at the AS core by converting them into electromagnetic cascade showers (burst) using lead absorber of $160 \text{ cm} \times 50 \text{ cm}$ in area and 7 cm (in Phase I) or 3.5 cm (in Phase II) in thickness. The burst size under the lead plate was measured by scintillation counters of the same size as the lead plate in area and 2 cm in thickness. Four photo-diodes were mounted to the each corner of the scintillator whose attenuation length for the scintillation light was calibrated with electron beam. From the 4 photo-diode signals, we can estimate the burst size and the position of the burst center with spatial resolution of 10 cm. One hundred core detectors were used (total area is 80 m^2) to detect burst size greater than 5×10^4 . The study of the primary mass composition was made in two experimental phases. In the first phase, 6 layers of X-ray films were placed between lead plates with 1 cm depth interval to register the development of shower spots induced by high-energy γ and electrons (hereafter abbreviated as γ -rays) over a few TeV which are incident upon the detector, and detailed analysis on the structure of the high energy core has been made with use of image scanner in 2004 to obtain proton and helium spectra in 2006. The energy de-

termination of the individual γ -rays was made by comparing the transition curve of the optical density of the shower spots with electromagnetic shower theory. Such procedure of the energy determination using X-ray films was calibrated using 200 GeV electron beam at FNAL. A bundle of high energy γ -rays from successive nuclear interactions of the primary cosmic rays in the atmosphere is called γ -family, which can be detected by spatial reconstruction of the shower spots registered on X-ray films with angular resolution of 2.5° . They are reconstructed as groups of parallel tracks with typical lateral spread of at most several cm among uncorrelated single tracks, which are dropped off as background. The assignment of a γ family to an accompanied AS was made through the positional correlation between the X-ray film and the scintillator, and the correlation between the burst and air shower was made by their time stamps. The arrival directions obtained from air shower and the reconstruction of the shower spots were also used to uniquely determine the air shower candidate.

Such γ -family events are more efficiently generated by light primaries than the case of heavy primaries because of the penetrating nature in the atmosphere. Therefore, the AS core detectors can select the air showers of light primary origin naturally. The contamination of the events of heavy nuclei origin was estimated using Artificial Neural Network (ANN) based on extensive Monte Carlo simulation of air showers (MC) assuming interaction models and primary models using CORSIKA code. Two interaction models of QGSJET and SIBYLL are used in estimating the efficiency of the γ family generation, and also two mass composition models of proton dominant (PD) and heavy dominant (HD) are used to appreciate the contamination rate of heavy primaries. The efficiency of the family generation for various primary nuclei and its energy dependence is calculated by MC and used for obtaining the primary proton and helium fluxes. For example, the efficiencies by protons at the knee energy 4 PeV in phase I experiment are about 7 % and 10 % by QGSJET model and SIBYLL model, respectively. ANN is also used in procedures to obtain proton and helium spectra. Phase I experiment selected 177 γ family events with core energy $\sum E_\gamma > 20 \text{ TeV}$ and AS size $N_e > 2 \times 10^5$.

In the second phase experiment, X-ray films were not used and proton+helium (P+He) spectrum was studied without separating them but with higher statistics than that of phase I. The core detector was tuned to decrease the detection threshold energy of the AS core to have several times higher efficiency.

The energy spectrum of all particles was obtained as shown in Fig. 2 together with other data. The uncertainty of the absolute intensity due to the interaction models used in the analysis is shown by QGSJET and SIBYLL (10 % difference at most). The uncertainty due to the assumed primary mass composition is also shown by HD and PD. Although the composition is fairly different between HD and PD models at energies above 10^{15} eV, the difference of the absolute intensity is 20% at most between the two models and it decreases with increasing primary energy. Note that the shapes of the spectra from different models are almost the same and the position of the knee is clearly found at the energy around 4 PeV.

From the second phase experiment of air shower core observation, the energy spectrum of P+He was obtained with

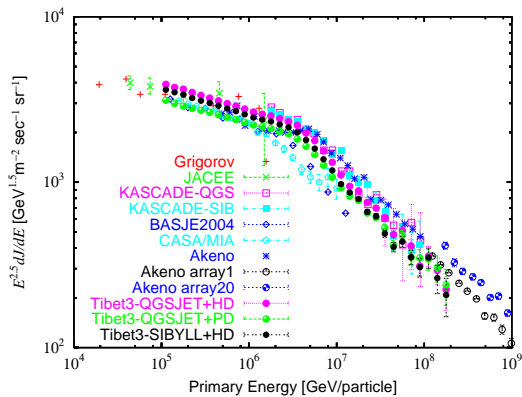


Fig. 2. All particle spectrum obtained by Tibet III. The results from three models of QGSJET+HD, QGSJET+PD, and SIBYLL+HD adopted in the analysis are shown.

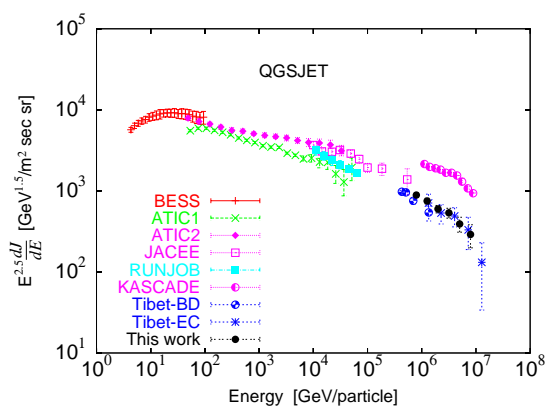


Fig. 3. P+He spectrum obtained by AS core observation (black closed circle).

high statistics and in good agreement with phase I as shown in Fig. 3, in which QGSJET model was used for the analysis. Use of SIBYLL model results in about 30 % lower intensity than that of the QGSJET analysis. There is a problem of discrepancy between Tibet and KASCADE data as shown in Fig.3, e.g., the flux of the light nuclei by KASCADE is higher than Tibet by more than a factor of 2. However, if SIBYLL model is used in the analysis of KASCADE, the difference between two data is much reduced. This fact does not necessarily mean that SIBYLL model is more preferable to explain the data at this energy range. KASCADE reported that QGSJET model explains high energy data better than SIBYLL, on the other hand, SIBYLL model is better at lower energies. This problem is related to the interaction model dependence of MC calculations and also to the different experimental methods used in two experiments. The Tibet experiment observes high energy part of the air showers, namely, the most forward region of the center of mass system (CMS) of interacting particles, while KASCADE experiment observes $N_e - N_\mu$ correlation, in which the muon component is sensitive to the central region of the CMS. The model dependence in forward region is about 30 % as studied by Tibet, but that of central region seems to be as large as a factor of 2.

Remarkable features of the energy spectrum of light com-

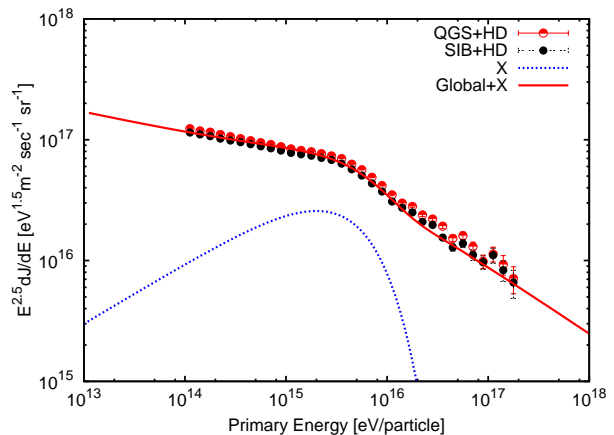


Fig. 4. Model A: Sharp knee is attributed to extra component (dashed line) from nearby source. Solid red line represents sum of the global component and the extra component.

ponent around 10^{15} eV are; (1) The power index is steeper than that of all-particle spectrum before the knee, suggesting that the light component has the break point at lower energy than the knee. (2) The fraction of the light component to the all-particles is less than 30 % which tells that the main component responsible for the knee structure is heavier than helium. The features of the energy spectrum and primary mass composition obtained by Tibet experiment can be interpreted by two scenarios of the origin of cosmic rays.

Model A : Sharp knee is caused by extra component from nearby source(s) as first pointed out by single source model. Figure 4 shows that the sharp knee of the all-particle spectrum can be reproduced by adding extra component around the knee over the global component which can be calculated as diffusive cosmic rays originating from multiple sources. The energy spectrum of the extra component can be approximated by $\propto E^{-2} \exp(-E/4PeV)$, which is close to the source spectrum expected from diffusive shock acceleration (DSA) mechanism of cosmic rays. A possible explanation of such extra component together with the knee composition is to assume nearby source(s) dominated by heavy elements such as type Ia SNRs or pulsars.

Model B : The knee is due to the characteristics of the DSA mechanism in which nonlinear effect plays an important role resulting in hard source spectrum of cosmic rays near acceleration limit energy. Figure 5 shows the primary mass composition calculated by nonlinear model in which it is assumed that heavy elements are more efficiently accelerated than light elements

This model predicts the rigidity-dependent hardening of the energy spectrum before the knee and heavy elements dominate at the knee and beyond. Recent direct observations of ATIC and CREAM reported hardening of the energy spectrum in $10^{12} - 10^{14}$ eV region and model B seems to be favorable to account for these data. It is also possible that both of models A and B contribute to the structure of the knee.

The second topic is related to cosmic-ray anisotropy.

Past cosmic-ray experiments that observed cosmic-ray anisotropy in the sidereal time frame consistently reported that

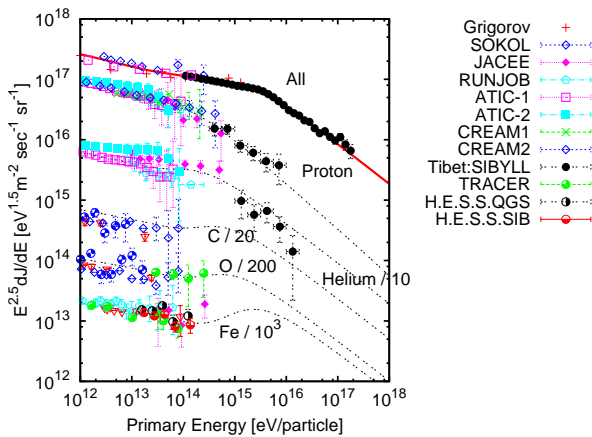


Fig. 5. Model B: Nonlinear effect in the DSA mechanism can explain the structure of the knee when high acceleration efficiency for heavy elements is assumed.

in the anisotropy there are two distinct broad structures with an amplitude of $\sim 0.1\%$; one is a deficit in the cosmic-ray flux called “loss-cone”, distributed around 150° to 240° in Right Ascension, and the other an excess called “tail-in”, distributed around 40° to 90° in Right Ascension. Recent underground muon and air-shower experiments are studying the anisotropy in great detail at multi-TeV energies. It is considered that the anisotropy of galactic cosmic rays at TeV energies reflects the structure of the local interstellar magnetic field surrounding the heliosphere, since the trajectories of charged cosmic rays are deflected and disturbed by the local interstellar magnetic field while they are traveling through the interstellar medium.

The air-shower events collected during the period from November 1999 through December 2008 (1916 live days) are used for analysis. After our standard data selections, 4.5×10^{10} events are left with a modal energy of 7 TeV.

The main systematic error to be accounted for is the amplitude of the anisotropy observed in the anti-sidereal time frame (364.2422 cycles/yr), because a possible seasonal change of the solar daily variation due to solar activities might produce a spurious variation in the sidereal time frame, which can be estimated by the daily variation observed in the anti-sidereal time frame. The root mean square of the anti-sidereal anisotropy in each declination band is calculated and added to the statistical error for the sidereal anisotropy in the corresponding declination band. Shown in Fig.1(a) is the relative intensity map obtained in $5^\circ \times 5^\circ$ pixels, which we model in terms of two components as:

$$I_{n,m} = I_{n,m}^{GA} + I_{n,m}^{MA}, \quad (2)$$

where $I_{n,m}^{GA}$ and $I_{n,m}^{MA}$, respectively, denote the intensities of the Global Anisotropy (GA) and the Midscale Anisotropy (MA) of the (n, m) pixel in the equatorial coordinate system. The GA component $I_{n,m}^{GA}$ is written as the combination of a uni-directional flow (UDF) and a bi-directional flow (BDF):

$$I_{n,m}^{GA} = a_{1\perp} \cos \chi_1(n, m : \alpha_1, \delta_1) + a_{1\parallel} \cos \chi_2(n, m : \alpha_2, \delta_2) + a_{2\parallel} \cos^2 \chi_2(n, m : \alpha_2, \delta_2). \quad (3)$$

In Eq.(3), the orientation (α_2, δ_2) denotes the reference axis of the BDF, and $a_{2\parallel}$ the amplitude of the BDF. The UDF is decomposed into two; one that is parallel to the BDF and has an amplitude of $a_{1\parallel}$, and the other that is perpendicular to the BDF, parallel to the axis (α_1, δ_1) , and has an amplitude of $a_{1\perp}$. The χ_1 denotes the angular distance of the center of the (n, m) pixel measured from the reference axis (α_1, δ_1) , and the χ_2 denotes that measured from the axis (α_2, δ_2) . Fig.6(b) shows the anisotropy map reproduced by attempting to fit Fig.6(a) with $I_{n,m}^{GA}$ alone. Although Fig.6(b) successfully reproduces the global “tail-in” and “loss-cone” structures, there remains the midscale anisotropy as can be seen in Fig.6(c). The $I_{n,m}^{MA}$, incorporated to model the residual midscale anisotropy, is expressed as:

$$I_{n,m}^{MA} = \left\{ b_1 \exp\left(-\frac{(\phi_{n,m} - \Phi)^2}{2\sigma_\phi^2}\right) + b_2 \exp\left(-\frac{(\phi_{n,m} + \Phi)^2}{2\sigma_\phi^2}\right) \right\} \exp\left(-\frac{\theta_{n,m}^2}{2\sigma_\theta^2}\right), \quad (4)$$

where b_1 and b_2 denote the amplitudes of the two excesses along the best-fit plane with the heliotail direction on it, both of which are symmetrically centered away from the heliotail direction by an angle Φ along the plane. The σ_ϕ and σ_θ denote the widths of the excesses parallel and perpendicular to the best-fit plane, respectively. The $\phi_{n,m}$ and $\theta_{n,m}$ denote the “longitude” of the center of the (n, m) pixel measured from the heliotail direction and its “latitude” measured from the best-fit plane, respectively. Fig.6(e) and (f) show the reproduced anisotropy and the residual anisotropy when we fit Fig.6(a) with $I_{n,m}^{GA} + I_{n,m}^{MA}$. The $I_{n,m}^{MA}$ extracted from Fig.6(e) is shown in Fig.6(d). Note that the obtained best-fit plane along which the MA is assumed is fairly consistent with the Hydrogen Deflection Plane (HDP) suggested by Gurnett et al. which contains the directions of the interstellar wind velocity and the interstellar magnetic field upstream the helionose; the angle difference between the direction normal to our best-fit plane and that to Gurnett’s HDP is only 2.1° . The best-fit parameters in Eq.(3) and Eq.(4) are listed in Table 1.

The GA can be interpreted as follows (for details). The local interstellar space of scale ~ 2 pc surrounding the heliosphere would be responsible for the GA. The BDF is produced by cosmic rays drifting parallel to the Local Interstellar Magnetic Field (LISMF) line into the heliosphere from outside the Local Interstellar Cloud surrounding the heliosphere. The UDF, perpendicular to the LISMF ($a_{1\perp} \gg a_{1\parallel}$) with an amplitude comparable to that of the BDF ($a_{1\perp} \simeq a_{2\parallel}$), can be produced by a diamagnetic drift arising from a spatial density gradient $(\nabla n/n)$ of galactic cosmic rays in the LISMF.

A sketch of a possible mechanism for the MA is shown in Fig.7(a). During the period of the data we analyzed, the orientation of the magnetic field in the heliotail B_{helio} is directed toward (away from) the Sun in the northern (southern) hemisphere. Suppose, for simplicity, that the B_{helio} surrounding the solar system is uniform within the spatial scale L toward the heliotail direction. Then the uniform B_{helio} bends the trajectories of cosmic rays propagating along the HDP from the heliotail direction, leading them to the solar system. A simple

geometrical consideration gives the following relation:

$$\begin{aligned} L [\text{AU}] &= R_L [\text{AU}] \sin \Phi \\ &= 206(E [\text{TeV}] / B_{\text{helio}} [\mu\text{G}]) \sin \Phi, \end{aligned} \quad (5)$$

where R_L is the Larmor radius of cosmic rays with energy E in B_{helio} . This equation implies that $\sin \Phi \propto 1/E$ if L is independent of energy. The observed energy dependence of $\sin \Phi$, shown in Fig.7(b), gives the following function:

$$\sin \Phi = (0.68 \pm 0.04) (E/10 [\text{TeV}])^{-0.20 \pm 0.08}, \quad (6)$$

suggesting $L \propto E^{0.8}$. This energy dependence of L might result from actual complex spatial structures of B_{helio} . These structures could be identified in the future by studies on the cosmic-ray transport in B_{helio} by means of Magneto-Hydrodynamic simulations. Substituting Eq.(6) into Eq.(5) and assuming $B_{\text{helio}} = 10\mu\text{G}$, the following equation holds:

$$L [\text{AU}] = (140 \pm 8) (E/10 [\text{TeV}])^{0.80 \pm 0.08}, \quad (7)$$

Eq.(7) implies that in the energy range of 4–30 TeV B_{helio} within ~ 70 AU to ~ 340 AU from the Sun is responsible for the MA. The MA being placed along the HDP suggests that it possibly originates from the modulation of galactic cosmic rays in B_{helio} . Another candidate for the heliospheric signature could be the excess region first reported as the ‘‘hot-spot’’ by the Milagro experiment. This region corresponds to the pixel in Fig.6(a) centered at $(72.5^\circ, 17.5^\circ)$, close to the heliotail, observed with the highest significance 9.06σ among all the pixels. The excess region is so collimated that it is difficult to construe it as a cosmic-ray inflow along the neutral sheet that separates B_{helio} between the northern and southern hemispheres. The Milagro experiment reported that the ‘‘hot-spot’’ has a localized spatial extension with a half-width of $2.6^\circ \pm 0.3^\circ$ and a half-length of $7.6^\circ \pm 1.1^\circ$. It should be noted here that the size of such a small-scale structure is greatly susceptible to the size and shape of the analysis window for background estimation to subtract the large-scale anisotropy superposed on the structure.

Other Activities

This group has developed and completed several automatic measuring systems that are powerful for analyzing cosmic ray tracks or air shower spots, that is, automatic microdensitometers, precise coordinate-measuring systems and image scanners controlled by a computer. Enormous data recorded on nuclear emulsion plates or X-ray films are rapidly and precisely measured by the use of these measuring systems.

The emulsion-pouring facilities can meet the demands for making any kind of nuclear emulsion plates which are used for cosmic ray or accelerator experiments. The thermostatic emulsion-processing facilities are operated in order to develop nuclear emulsion plates or X-ray films. Using these facilities, it is also possible to make and develop emulsion pellicles in $600\mu\text{m}$ thickness each. In this way, these facilities are open to all the qualified scientists who want to carry out joint research program successfully.

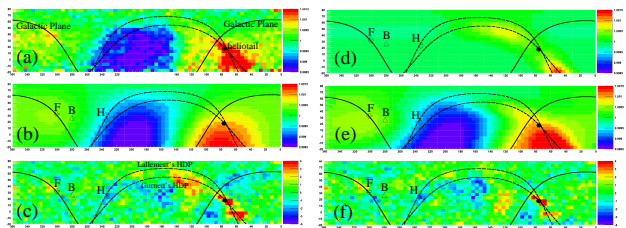


Fig. 6. Two-dimensional anisotropy maps of galactic cosmic rays observed and reproduced at the modal energy of 7 TeV. Each panel shows the relative intensity map or the significance map in $5^\circ \times 5^\circ$ pixels in the equatorial coordinate system.

(a): the observed cosmic-ray intensity ($I_{n,m}^{obs}$), (b): the best-fit Global Anisotropy (GA) component ($I_{n,m}^{GA}$), (c): the significance map of the residual anisotropy after subtracting $I_{n,m}^{GA}$ from $I_{n,m}^{obs}$, (d): the best-fit Midscale Anisotropy (MA) component ($I_{n,m}^{MA}$), (e): the best-fit GA+MA components ($I_{n,m}^{GA} + I_{n,m}^{MA}$), and (f): the significance map of the residual anisotropy after subtracting $I_{n,m}^{GA} + I_{n,m}^{MA}$ from $I_{n,m}^{obs}$. The solid black curves represent the galactic plane. The dashed black curves represent the Hydrogen Deflection Plane reported by Gurnett et al. and Lallement et al. The black filled circle represents the heliotail direction $(\alpha, \delta) = (75.9^\circ, 17.4^\circ)$ is indicated by the black filled circle. The open cross and the inverted star with the attached characters ‘‘F’’ and ‘‘H’’ represent the orientation of the local interstellar magnetic field (LISMf) by Frisch and by Heerikhuisen et al., respectively. The open triangle with ‘‘B’’ indicates the orientation of the best-fit bi-directional cosmic-ray flow (BDF) obtained in this analysis.

Future Plans

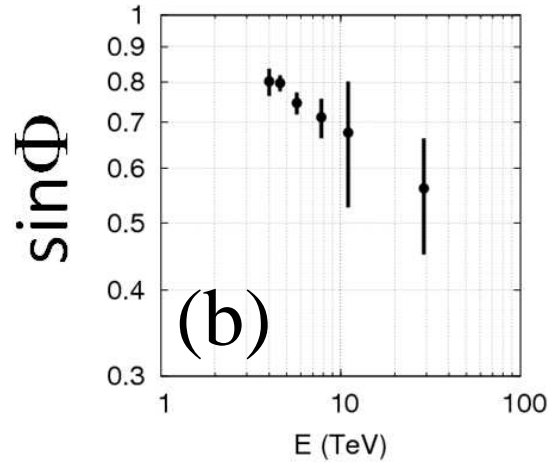
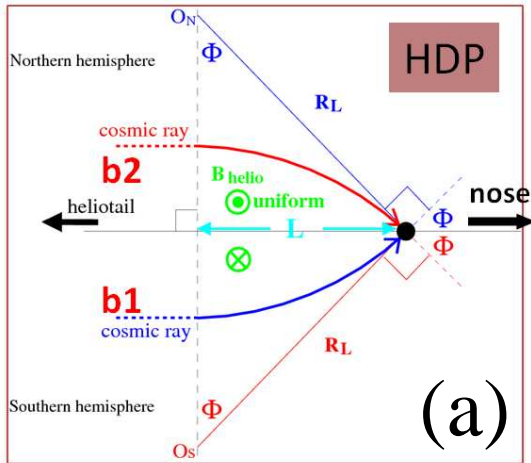
(1) Gamma-ray astronomy in the 100 TeV region

We have a plan to construct a large ($\sim 10,000 \text{ m}^2 \times 1.5 \text{ m}$ deep) underground (~ 2.5 m soil+concrete overburden) water Cherenkov muon detector array (Tibet MD) around an extended version (Tibet AS, $\sim 83,000 \text{ m}^2$) of Tibet III. By Tibet AS + MD, we aim at background-free detection of celestial point-source gamma rays in the 100 TeV region (10 TeV – 1000 TeV) with world-best sensitivity and at locating the origins of cosmic rays accelerated up to the knee energy region in the northern sky. The measurement of cut off energies in the energy spectra of such gamma rays in the 100 TeV region may contribute significantly to understanding of the cosmic-ray acceleration limit at SNRs. Search for extremely diffuse gamma-ray sources by Tibet AS + MD, for example, from the galactic plane or from the Cygnus region may be very intriguing as well. Above 100 TeV, the angular resolution of Tibet AS with 2-steradian wide field of view is 0.2° and the hadron rejection power of Tibet MD is 1/10000. The proposed Tibet AS + MD, demonstrated in Fig. 8, has the world-best sensitivity in the 100 TeV region, superior to HESS above 10-20 TeV and to CTA above 30-40 TeV.

Then, how many unknown/known sources do we expect to detect by Tibet AS + MD, assuming the energy spectra of the gamma-ray sources extend up to the 100 TeV region? Eleven of the HESS new 14 sources discovered by the galactic plane survey in the southern sky would be detected by Tibet AS + MD, if it were located at the HESS site. As no extensive search has been done by an apparatus with sensitivity comparable to HESS (1 % in unit of RX J1713.7-3946/50-hour observation) in the northern sky, we expect to discover some 10 new gamma-ray sources in the northern sky. In ad-

Table 1. Best-fit parameters in Eq.(3) and Eq.(4) for the 2D galactic-cosmic-ray anisotropy map observed at 7 TeV.

Global Anisotropy (GA)						
$a_{1\perp}$ (%)	$a_{1\parallel}$ (%)	$a_{2\parallel}$ (%)	α_1 (°)	δ_1 (°)	α_2 (°)	δ_2 (°)
0.139 ± 0.002	0.007 ± 0.002	0.131 ± 0.004	33.3 ± 1.1	38.4 ± 1.2	279.9 ± 0.9	-26.7 ± 2.0
Midscale Anisotropy (MA)						
b_1 (%)	b_2 (%)	σ_ϕ (°)	σ_θ (°)	Φ (°)		
0.154 ± 0.018	0.092 ± 0.006	24.5 ± 1.1	10.7 ± 0.8	49.2 ± 1.4		

Fig. 7. (a): a possible mechanism for the Midscale Anisotropy. (b): the observed energy dependence of $\sin\Phi$.

dition to unknown point-like sources, we expect to detect established sources in the 100 TeV region: TeV J2032+4130, HESS J1837-069, Crab, some new Milagro sources, Mrk421, Mrk501 are sufficiently detectable and Cas A, HESS J1834-087, LS I+63 303, IC443 and M87 are marginal.

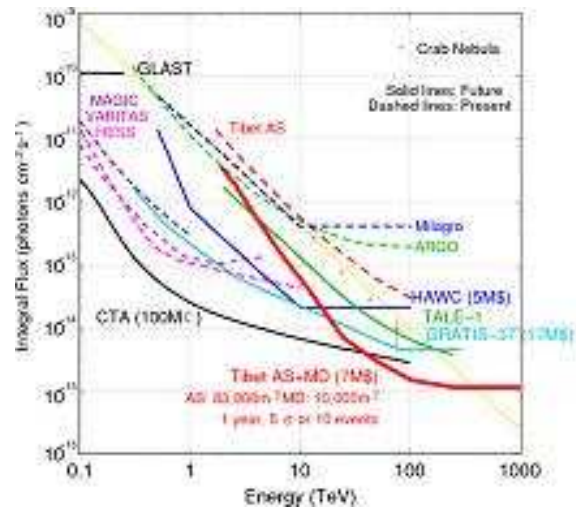
Furthermore, our integral flux sensitivity to diffuse gamma rays will be the world-best as well. The diffuse gamma rays from the Cygnus region reported by the Milagro group and also diffuse gamma-rays from the galactic plane will be clearly detected. Diffuse gamma-rays of extragalactic origin may be an interesting target as well.

In fall, 2007, a prototype underground muon detector, composed of two 52m² water pools, was successfully constructed in Tibet to demonstrate the technical feasibility, cost estimate, validity of our Monte Carlo simulation. Preliminary analysis indicates that our MC simulation reproduces real data quite reasonably.

In 2010, construction of roughly one-third of the full-scale MD started and the concrete-based water pools were successfully completed, as in Fig. 9. The data-taking of the Tibet III and the partial MD will be scheduled in 2011.

(2) Chemical composition of primary cosmic rays making the knee in the all-particle energy spectrum

We have measured the energy spectra of primary cosmic-ray protons, heliums, all particles around the knee energy region. The main component responsible for making the knee structure in the all particle energy spectrum is heavier nuclei

Fig. 8. Tibet AS + MD (red curve) integral flux sensitivity (5σ or 10 events/1yr) for a point source.

than helium. The next step is to identify the chemical component making the knee in the all particle energy spectrum. We have a plan to install an air shower core detector array (1000 to 5000 m² in area) around the center of Tibet III to distinguish the heavy component making the knee by measuring the difference in lateral distribution of energetic air shower cores. This will be the first experiment to selectively measure the energy spectrum of the heavy component in the knee en-



Fig. 9. Construction scene of underground muon detectors in 2010.

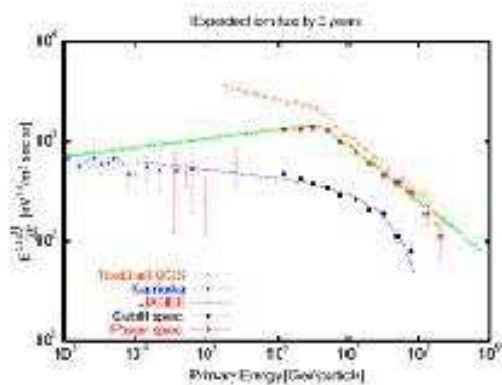


Fig. 10. Expected cosmic-ray iron energy spectra with Tibet AS + YAC.

ergy region and will demonstrate that the knee of the all particle energy spectrum is really composed of heavy nuclei. Figure 10 shows the expected energy spectra of cosmic-ray iron nuclei depending on theoretical models. Tibet AS + YAC has a strong model discrimination power. Sixteen YAC detectors were set up at Yangbajing in 2009 and preliminary analysis is under way.

Tibet AS γ collaboration

ICRR, Univ. of Tokyo, Kashiwa, Chiba 277-8582

In collaboration with the members of:

Hirosaki Univ., Hirosaki, Japan; Saitama Univ., Urawa, Japan; IHEP, Beijing, China; Yokohama National Univ., Yokohama, Japan; Hebei Normal Univ., Shijiazhuang, China; Tibet Univ., Lhasa, China; Shandong Univ., Jinan, China; South West Jiaotong Univ. Chengdu, China; Yunnan Univ., Kunming, China; Kanagawa Univ., Yokohama, Japan; Faculty of Education, Utsunomiya Univ., Utsunomiya, Japan; ICRR, Univ. of Tokyo, Kashiwa, Japan; Konan Univ., Kobe, Japan; Department of Physics, Shinshu Univ., Matsumoto, Japan; Center of Space Science and Application Research, Beijing, China; Tsinghua Univ., Beijing, China; Waseda Univ., Tokyo, Japan; NII, Tokyo, Japan; Sakushin Kakuin Univ., Utsunomiya, Japan; Tokyo Metropolitan Coll. of Industrial Technology, Tokyo,

Japan; Max-Planck Institute fuer Physik, Munich, Germany; Shonan Inst. of Technology, Fujisawa, Japan; RIKEN, Wako, Japan; School of General Education, Shinshu Univ. Matsumoto, Japan; Nihon University, Narashino, Japan; Institute of Disaster Prevention Science and Technology, Yanjiao, China.

Bibliography

Papers in refereed journals

- [1] “Observation of TeV Gamma Rays from the Fermi Bright Galactic Sources with the Tibet Air Shower Array”, M. Amenomori *et al.*, *ApJ* **709** L6–L10, (2010).
- [2] “On Temporal Variations of the Multi-TeV Cosmic Ray Anisotropy Using the Tibet III Air Shower Array”, M. Amenomori *et al.*, *ApJ*, **711** 119–124, (2010).
- [3] “Cosmic-ray energy spectrum around the knee observed with the Tibet air-shower experiment”, M. Amenomori *et al.*, *Astrophysics and Space Sciences Transactions*, **7** 15–20, (2011).

Papers in conference proceedings

- [4] “Heliospheric signatures seen in the sidereal anisotropy of high-energy galactic cosmic ray intensity”, M. Amenomori *et al.*, *AIP Conf. Proc.*, **1302** 285–290, (2010).

The Ashra Project

[Spokesperson: Makoto Sasaki]

ICRR, Univ. of Tokyo, Kashiwa, Chiba 277-8582

In collaboration with the members of:

ICRR, University of Tokyo, Kashiwa, Japan; Toho University, Funabashi, Japan; University of Hawaii at Manoa, Honolulu, USA; University of Hawaii at Hilo, Hilo, USA; Nagoya University, Nagoya, Japan; Kanagawa University, Yokohama, Japan

Overview

Ashra (*All-sky Survey High Resolution Air-shower detector*) [1, 2, 3, 4]. is a project to build an unconventional optical telescope complex that images very wide field of view, covering 77% of the sky, yet with the angle resolution of a few arcmin, sensitive to the blue to UV light with the use of image intensifier [5] and CMOS technology. The project primarily aims to observe Cherenkov and fluorescence lights from the lateral and longitudinal developments of very-high-energy (VHE) cosmic-ray air showers in the atmosphere. It can also be used to monitor optical transients in the wide field of sky. The observatory will firstly consist of one main station having 12 detector units and two sub-stations having 8 and 4 detector units. One detector unit has a few light collecting systems with segmented mirrors. The main station was constructed on Mauna Loa (3,300 m) on Hawaii Island in 2007.

We started observation of optical transients and commissioning observation of VHE tau neutrinos with some of

the light collectors in 2008. By analyzing the accumulated data from optical observations, we have already searched for early optical emissions in the field of GRB081203A [6] and GRB100906A [7] around the Swift/BAT-triggered GRB time. Furthermore, we reported [8] the first observational search for tau neutrinos (ν_τ) from gamma-ray bursts (GRBs) using the light collector facing Mauna Kea. The earth-skimming ν_τ technique of imaging Cherenkov τ showers was applied as a detection method in this search. We set stringent upper limits on the ν_τ fluence in PeV–EeV region for 3780 s (between 2.83 and 1.78 hr before) and another 3780 s (between 21.2 and 22.2 hr after) surrounding the *Swift* trigger time of GRB081203A. This first search for PeV–EeV ν_τ complements other experiments in energy range and detection method, and implies the prologue of “multi-particle astronomy” [9] with a precise determination of time and location.

Project

The observatory will firstly consist of one main station having 12 detector units and two sub-stations having 8 and 4 detector units. One detector unit has a few light collecting systems with segmented mirrors. The features of the system were studied with a prototype detector unit located on Haleakala. The main station was constructed on Mauna Loa (3,300 m) in 2007.

The key technical feature of the Ashra detector rests on the use of electrostatic lenses to generate convergent beams rather than optical lens systems. This enables us to realize a high resolution over a wide field of view. This electron optics requires:

- *image pipeline*; the image transportation from imaging tube (image intensifier) to a trigger device and image sensors of fine pixels (CCD+CMOS), with high gain and resolution, and
- *parallel self-trigger*: the systems that trigger separately for atmospheric Cherenkov and fluorescence lights.

Observational Objectives

optical transients; Ashra will acquire optical image every 6 s after 4-s exposure. This enables us to explore optical transients, possibly associated with gamma ray bursts (GRBs), flares of soft gamma-ray repeaters (SGRs), supernovae explosion, and so on, in so far as they are brighter than $B \simeq 13$ mag, for which we expect $3\text{-}\sigma$ signals. The unique advantage is the on-time detection of the events without resorting to usual satellite alerts. 10~20 events per year are expected in coincidence with the Swift gamma-ray events. The field of view that is wider than satellite instruments allows to detect more optical transients, including an interesting possibility for an optical flash, not visible with gamma rays.

TeV gamma rays; Atmospheric Cherenkov radiation will be imaged by Ashra. Requiring the signal-to-noise ratio (SNR) >5 , the system will allow to explore VHE gamma-ray sources with the energy threshold of several TeV at the limiting flux sensitivity of 5% Crab for 1-year observation.

EeV cosmic rays; For fluorescence lights from VHE cosmic rays the effective light gathering efficiency is comparable with that of the High Resolution Fly’s Eye detector (HiRes). The arcmin pixel resolution of Ashra provides finer images of longitudinal development profiles of EeV cosmic ray (EeV-CR) air showers. The resolution of arrival direction with the stereo reconstruction is thus significantly improved and it is better than one arcmin for the primary energy of EeV and higher [10]. This is useful to investigate events clustered around the galactic and/or extragalactic sources. This in turn would give us information as to the strength and coherence properties of the magnetic field.

PeV-EeV neutrinos; Ashra may detect Cherenkov and/or fluorescence signals generated from tau-particle induced air-showers that is generated from interactions of tau neutrinos with the mountain and/or the earth. This is identified by peculiar geometry of the air-shower axis. The 1-year detection sensitivity with the full configuration of Ashra is 5 and 2 times larger than the Waxman-Bahcall limit for mountain-produced event (Cherenkov) and earth-skimming event (fluorescence), respectively. The most sensitive energy of around 100 PeV is suitable for the GZK neutrino detection.

The expected performance for each observational object is summarized in Table 1. An example of a 42-degree FOV image taken by the Ashra light collector is shown in Figure 1.

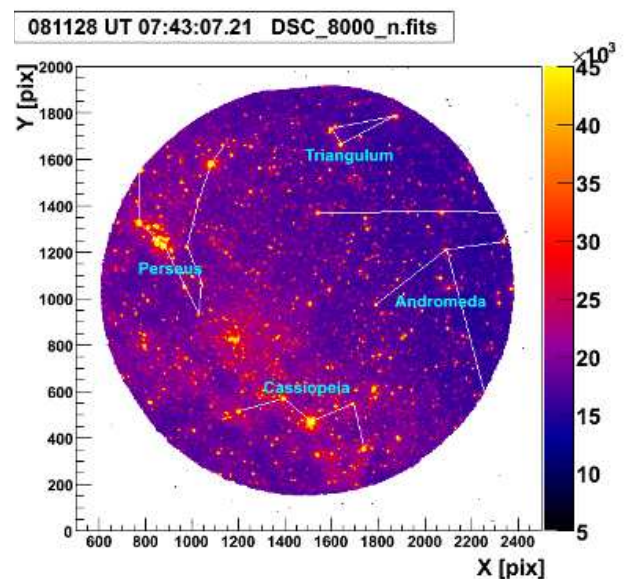


Fig. 1. Example of a 42-degree FOV image taken by the Ashra light collector. The solid lines are drawn to indicate constellations.

Site Preparation

After finishing the grading work for the area of 2,419 m² at the Mauna Loa site at the end of July 2005, installation of electrical power lines and transformers was performed until the beginning of September. We started the construction of the detector in October 2005 after receiving materials from

Opt. Transients	TeV- γ	Mountain- ν	Earth-skimming- ν	EeV-CR
B-UV	Cherenkov	Cherenkov	Fluorescence	Fluorescence
$\lambda=300\sim 420\text{nm}$	several TeV	a few 100 TeV	a few 10 PeV	a few 100 PeV
15 mag./4s @ 3σ	5% Crab/1yr@ 5σ	5 WB-limit/1yr	2 WB-limit/1yr	1600/1yr >10 EeV
2 arcmin	6 arcmin	unknown	3 arcmin @ 100 PeV	1 arcmin @ 10 EeV

Table 1. Summary of performance with the full configuration (Ashra-2) of three Ashra sites. Detected light, energy threshold, sensitivity limit, and angular resolution are listed from top down for each objective. For EeV-CRs, trigger requirement is two or more stations. Waxman and Bahcall have calculated a neutrino flux upper limit from astrophysical transparent source, here referred to as the WB-limit. For the observation time for objectives other than optical transients, the realistic detection efficiency is taken into account.

Japan. By the middle of December 2005, the first shelters having motorized rolling doors, acrylic plate windows to maintain air-tightness, and heat-insulating walls and floors have been constructed and positioned on eight construction piers of concrete blocks at the Mauna Loa site. In the shelters, the optical elements of the light collectors have been already installed. The optical performance were checked and adjusted to be optimum with star light images from the pilot observation.

In December 2005, we evaluated the night sky background flux on Mauna Loa using the Ashra light collector installed and aligned in a shelter. The result is fairly consistent with the background in La Palma and Namibia by the HESS group. From the star light observations, our understanding of the light correction efficiency to be accurate within 5% level.

The civil engineering construction of light collectors in shelters at the Mauna Loa site was completed in August 2007. Figure 2 shows a picture of the constructed Mauna Loa stations. In this Ashra-1 experiment, we are performing device installation and specific observation in a step-by-step way to enhance the scientific impacts.



Fig. 2. The Ashra main and sub stations at the Mauna Loa site.

Observation

As a first step, we have started the observation of optical transients. During observation, Optical images were constantly collected every 6 s after 4-s exposure. Figure 3 summarizes our observation statistics up to now. Maximum observable time is defined by the following condition:

- *Sun condition*; the altitude of the sun must be lower than -18 degree.
- *Moon condition*; the altitude of the moon is lower than 0 degree, or the moon fraction is less than 0.2.

We have accumulated more than 3500 hours of observation time in two years of observation. Good weather rate of 94% shows the superiority of our site and operation efficiency of 99% demonstrates the stability of our operation, where good weather rate is defined by observable time divided by maximum observation time and operation efficiency is defined by observed time divided by observable time.

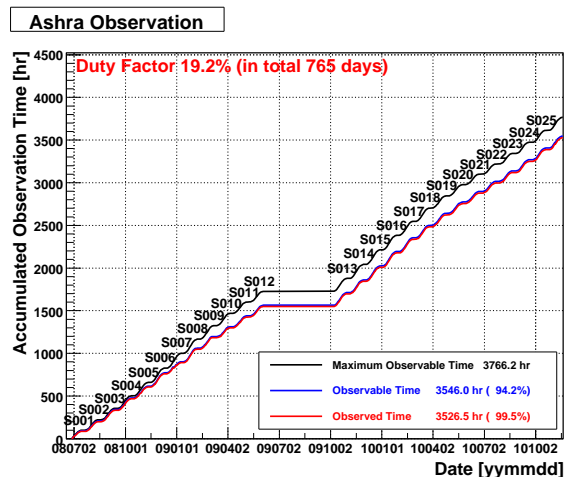


Fig. 3. Summary of Ashra optical transient observation time.

GRB100906A: Ashra-1 observation of early optical emission [7]

Our wide field observation covered the Swift-BAT error circle at the time of GRB100906A. We searched for optical emission in the field of GRB100906A around the BAT-triggered GRB time (T_0) with one of the light collector units in the Ashra-1 detector. The Ashra-1 light collector unit used in this analysis has the achieved resolution of a few arcmin, viewing 42 degree circle region of which center is located at $\text{Alt} = 60$ deg, $\text{Azi} = 0$ deg.

We quickly analyzed 200 images covering the field of GRB100906A every 6s with 4s exposure time respectively during the observation between T_0-600 s and T_0+600 s. We detected no new optical object within the PSF resolution around the GRB100906A determined by Swift-UVOT. As a result of our preliminary analysis, the 3-sigma limiting magnitudes were estimated in comparison with stars in Tycho-2 Catalog to be distributed between 12.0 and 12.2. Figure of limiting optical magnitudes vs time comparing with other measurements is shown in Fig.4.

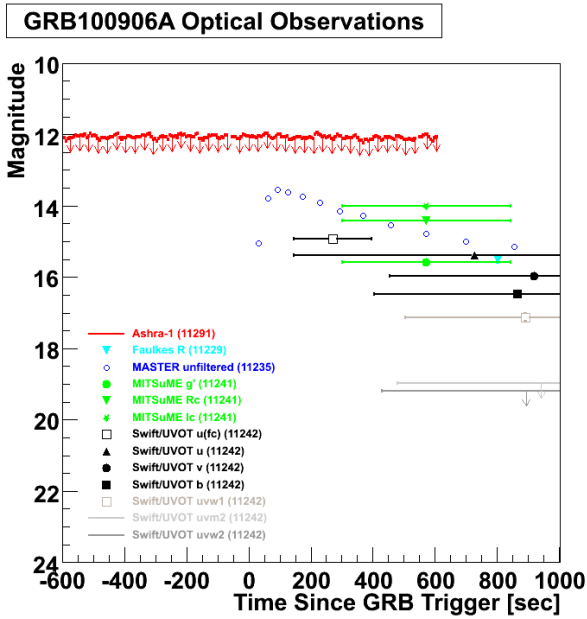


Fig. 4. Summarized lightcurve for GRB100906A around the trigger time. 3-sigma limiting magnitudes of our observation (labeled as Ashra-1) and other observations are compared as a function of time since GRB. The horizontal axis is in linear scale to show the limiting magnitudes in the precursor phase.

Performance of a 20-in. photoelectric lens image intensifier tube [5]

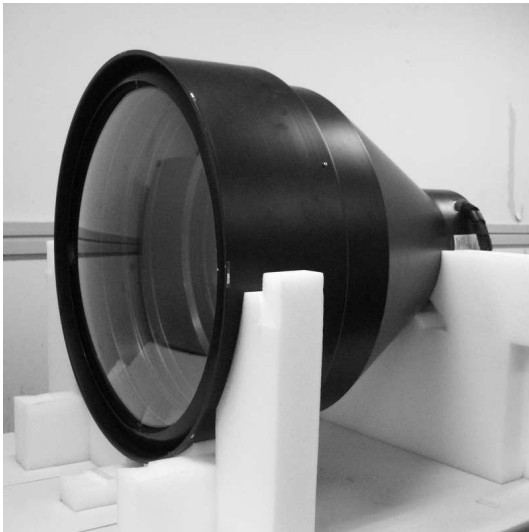


Fig. 5. A photograph of a 20-inch photoelectric lens image intensifier tube (PLI) [5].

We have evaluated a 20-in. photoelectric lens image intensifier tube (PLI) to be mounted on the spherical focal surface of the Ashra light collectors. The PLI, the worlds largest image intensifier, has a very large effective photocathode area of 20-in. diameter and reduces an image size to less than 1-in. diameter using the electric lens effect. This enables us to use a solid-state imager to take focal surface images in the Ashra light collector. Thus, PLI is a key technology for the Ashra experiment to realize a much lower pixel cost in comparison

with other experiments using photomultiplier arrays at the focal surface. Figure 5 shows a photograph of a 20-inch PLI. The design and performance of the 20-in. PLI in Ref. [5].

Observational search for PeV–EeV tau neutrino from GRB081203A [8]

First physics publication [8] from the Ashra-1 experiment was achieved by PeV–EeV tau neutrino search from GRB081203A. Here, we summarized our first published result.

The GRB standard model [11], which is based on internal/external shock acceleration, has been used to describe the general features of a GRB and the observed multi-wavelength afterglow. However, the standard model cannot well reproduce the complicated time evolution of GRBs and the high energy components in the prompt emission [12, 13, 14]. Although many authors have proposed theoretical models to reproduce these features, none of them are conclusive [15]. To better understand the ambiguous mechanisms of GRBs, observational probes of the optically thick region of the electromagnetic components, as well as hadron acceleration processes throughout the precursor, prompt, and afterglow phases are required. VHE ν_s can be used as direct observational probes, which are effective even in optically thick regions. A monitor search with sufficient time and spatial resolution and survey capability for VHEVs associated with GRBs is plausible.

The earth-skimming tau neutrino (ν_τ) technique [16], which detects extensive air showers, has the advantage of a large target mass, since it uses air showers produced by decay particles of tau leptons (τ_s) in the atmosphere as the observed signals. τ_s emerge out of the side of the mountain or the ground facing the detector; they are the product of interactions between VHE ν_τ and the earth matter they traverse. No air Cherenkov observation was made to date based on the earth-skimming ν_τ technique with air showers induced by τ decays (hereafter referred to as the Cherenkov τ shower method). However, it can achieve sufficient detection sensitivity in the PeV–EeV region to be useful in the search for ν_s originating from hadrons accelerated to EeV at astronomical objects. Additional advantages of the Cherenkov τ shower method are its perfect shielding of cosmic-ray secondary particles, highly precise arrival direction determination for primary ν_τ and negligible background contamination by atmospheric ν_s in the PeV–EeV energy range.

As shown in Fig. 6, one of the Ashra light collectors built on Mauna Loa has two geometrical advantages: (1) it faces Mauna Kea, allowing it to encompass the large target mass of Mauna Kea in the observational FOV, (2) it has an appropriate distance of ~ 30 km from Mauna Kea, yielding good observational efficiency when imaging air-shower Cherenkov lights which are directional with respect to the air-shower axis. Using the advanced features, we performed commissioning search for Cherenkov τ showers for 197.1 hr between October and December of 2008. We served limited 62 channels of photomultiplier tubes (PMTs) as trigger sensors prepared for the commissioning runs to cover the view of the surface area of Mauna Kea, maximizing the trigger efficiency for Cherenkov τ showers from Monte Carlo (MC) study. Adjacent-two logic was adopted to trigger the fine imaging, by judging discrim-

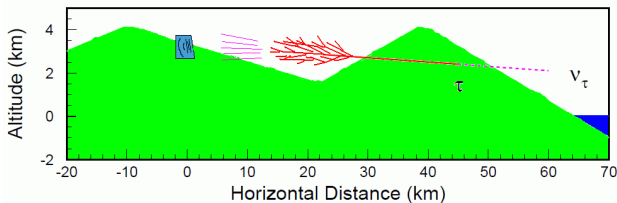


Fig. 6. Conceptual drawing of Cherenkov τ shower method. The right mountain is Mauna Kea and the left is Mauna Loa.

inated waveform signals from each pixel of the multi-PMT trigger sensor. During the search period, ~ 2 hr before the trigger of GRB081203A. GRB counterpart (R.A. 15:32:07.58, decl. +63:31:14.9) passed behind Mauna Kea, as viewed from the Ashra-1 observatory.

To investigate the features, selection criteria, detection efficiency, and background rate for the observation of Cherenkov τ shower images, intensive Monte Carlo (MC) studies were performed by utilizing CORSIKA, TAUOLA, and other relevant MC packages. The photometric and trigger sensitivity calibration of the Ashra light collector was based on a very stable YAP-light pulser. Non-uniformity in the detector gain due to the input light position was relatively corrected by mounting a spherical plate uniformly covered with luminous paint on the input window. To correct for the time variation of the photometric and trigger sensitivity because of variations in atmospheric optical thickness, we performed careful cross-calibration to compare the instrumental photoelectric response with the photometry of standard stars such as BD+75D325 of B-magnitude 9.2, for which the detected images passed through the same optical and photoelectric instruments except for the final trigger-controlled readout device.

To confirm the detection sensitivity and gain calibration for the Cherenkov τ shower, we detected and analyzed 140 events of normal cosmic-ray air-shower Cherenkov images for a total of 44.4 hr in 2008 December using the same instruments used in neutrino observation, but after rearranging the trigger pixel layout to view the sky field above Mauna Kea. In the cosmic-ray observation, the trigger pixel layout is centered at zenith angle of $\sim 65^\circ$. The observed and MC cosmic-ray flux spectra are shown in Fig. 7, in which the MC prediction used the typically observed cosmic-ray flux in the knee region [17, 18]. Since the primary cosmic-ray components are observationally undefined, we present the MC prediction of cosmic-ray flux spectra, assuming either only protons or irons as the primary cosmic rays in Fig. 7. Note that the same reconstruction procedure was applied to both of the observed and MC data to extract the observed energy. In both cases, the observed data and the MC prediction agreed well on the normalization and the shape of the distribution within the expected errors. The estimation of the detection sensitivity of the Ashra light collector and the validity of the reconstruction procedure were well demonstrated.

For the ν_τ search, we used image data acquired using the trigger for 197.1 hr in only case of the data status defined as good out of the total observation time of 215.8 hr. Detailed data analysis yielded a null ν_τ candidate [8]. Ef-

fective areas for Cherenkov τ showers induced by ν_τ s from the GRB081203A counterpart with changing ν_τ energy (E_{ν_τ}) were obtained from an MC study that assumed seven original positions on the GRB counterpart trajectory. On the basis of the above null result and the estimated effective areas, we placed 90% confidence level (CL) upper limits on the ν_τ fluence of precursor and afterglow emissions in the PeV–EeV region, for two 3780 s periods, the first between 2.83 and 1.78 hr before GRB081203A and the second between 21.2 and 22.2 hr after it, as shown in Fig. 8. As sources of systematic uncertainty in the MC estimates of the effective detection areas, we considered the ν_τ charged current interaction cross section, the energy loss by τ in the earth and the mountain, the geological model around the observation site, and the gain calibration of the light collector, which were evaluated to be 50%, 50%, 10%, and 30%, respectively. The conservatively combined systematic sensitivity error was obtained from the square sum of the above uncertainties as 77%, which affects the result of the 90% CL upper limit shown in Fig. 8, where we assumed a typical E_ν^{-2} flux to ensure unbiased constraints on observationally undefined physical mechanisms of a GRB.

For comparison, Fig. 8 shows other observational limits on the ν fluence from point sources [19, 20]. Our results are the most stringent in the PeV–EeV region and complementary to the IceCube results for the sub-PeV energy region, and indicate the advanced instantaneous sensitivity of the system even during this commissioning phase. Full-scale Ashra observations are expected to have 100 times better sensitivity, since the trigger pixel size is halved (1/4 the pixel area) and the trigger sensor will cover the entire FOV of the light collector. With this higher sensitivity, contamination of 0.55 clusters of air-shower secondary particles is expected in one year of observation data. The advanced angular determination of Ashra for Cherenkov τ showers to within $0^\circ.1$ will allow perfect rejection against contamination from air-shower secondary particles, and will provide a viable search method for earth-skimming ν_τ events, fully utilizing the zero background conditions. Our first search for PeV–EeV ν_τ reported in Ref. [8] complements other experiments in energy range and detection method, and implies the prologue of “multi-particle astronomy” [9] with a precise determination of time and location.

Bibliography

- [1] <http://www.icrr.u-tokyo.ac.jp/~ashra>
- [2] M. Sasaki, J. Phys. Soc. Japan **77SB**, 83 (2008).
- [3] Y. Aita *et al.*, in *Proc. of 30th ICRC (Mexico, 2007)*, Vol. 3, p. 1405 (2008).
- [4] M. Sasaki *et al.*, in *Proc. of 30th ICRC (Mexico, 2007)*, Vol. 3, p. 1559 (2008).
- [5] Y. Asaoka and M. Sasaki, Nucl. Instrum. Methods Phys. Res. A **647**, 34 (2011).
- [6] Y. Aita *et al.*, GCN Circ., 8632 (2008).
- [7] Y. Asaoka *et al.*, GCN Circ., 11291 (2010).

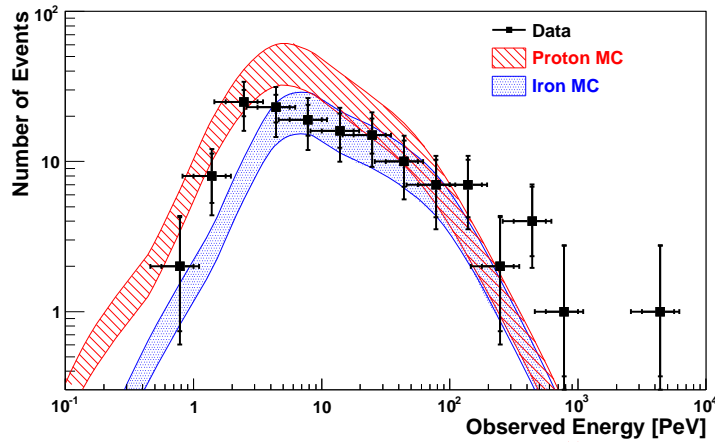


Fig. 7. Observed cosmic-ray flux spectrum (filled box) with bars indicating statistical and systematic errors and the MC predictions for proton primary (hatched band) and iron primary (shaded band) assumptions [8]. The width of the bands shows the evaluated systematic error of 30% of the MC prediction.

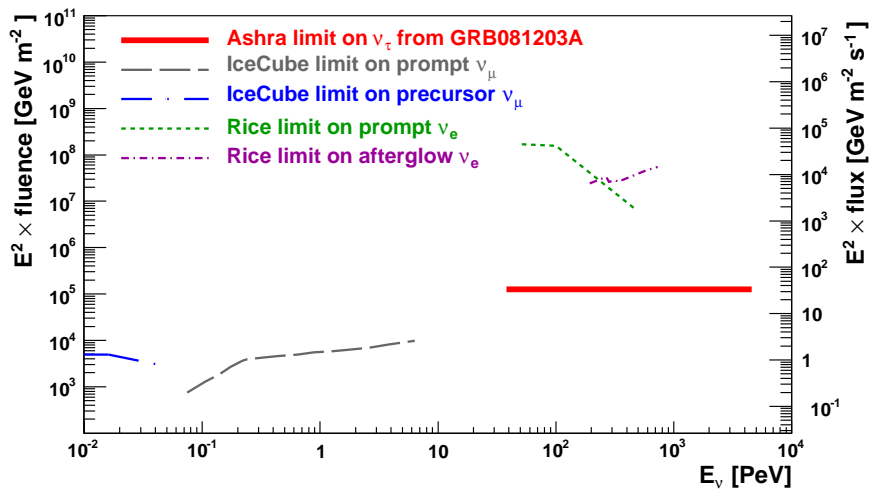


Fig. 8. Ashra 90% CL limit (thick continuous line (red)) on ν_τ fluence of precursor and afterglow emissions from the GRB081203A counterpart in the PeV–EeV region [8]. For comparison, IceCube limits [19] in the prompt (long dashed dotted (gray)) and precursor (long dashed dotted (blue)) phases and RICE limits [20] in the prompt (dashed (green)) and afterglow (dashed dotted (magenta)) phases are shown. The energy ranges were defined as containing 90%, 90%, and 80% of the expected signals from assumed spectrum for Ashra, IceCube, and RICE, respectively.

- [8] Y. Aita *et al.*, *ApJL* **736**, L12 (2011).
- [9] M. Sasaki, in *Proc. ICRR2000 Satellite Symposium: Workshop of Comprehensive Study of the High Energy Universe*, p. 110 (2000).
- [10] M. Sasaki, A. Kusaka and Y. Asaoka, *Nucl. Instrum. Methods Phys. Res. A* **492**, 49 (2002).
- [11] P. Mészáros, *Rep. Prog. Phys.* **69**, 2259 (2006), and references therein.
- [12] J. A. Nousek *et al.*, *ApJ* **642**, 389 (2006).
- [13] A. A. Abdo *et al.*, *ApJ* **706**, L138 (2009).
- [14] M. De Pasquale *et al.*, *ApJL* **709**, L146 (2010).
- [15] M. Ackermann *et al.*, *ApJ* **716**, 1178 (2010).
- [16] D. Fargion, *ApJ* **570**, 909 (2002).
- [17] T. Antoni *et al.*, *Astropart. Phys.* **24**, 1 (2005).
- [18] M. Amenomori *et al.*, *ApJ* **678**, 1165 (2008).
- [19] R. Abbasi *et al.*, *ApJ* **710**, 346 (2010).
- [20] D. Besson, S. Razzaque, J. Adams, and P. Harris, *Astropart. Phys.* **26**, 367 (2007).

High Energy Astrophysics Group

[Spokesperson: T. Terasawa]

ICRR, Univ. of Tokyo, Kashiwa, Chiba 277-8582

Overview

Since its creation in December 2009, the high energy astrophysics group has been making theoretical and observational studies of violent astrophysical phenomena in which

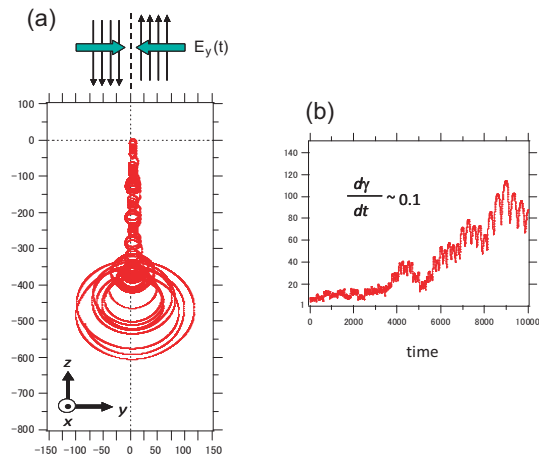


Fig. 1. Particle acceleration in a sheared flow, $V_z(y) = 0.3c \tanh(\frac{y}{c})$ (c : the velocity of light) with superposed time-dependent perturbations. The magnetic field is in the x direction. (a) An example of the particle trajectories in the y - z plane, where the spatial scale is normalized by a characteristic gyro radius, c/Ω_c (Ω_c : the non-relativistic cyclotron frequency). (b) An example of the energy history of accelerated particles.

nonthermal cosmic ray particles are being accelerated. Targets of the group's study include high energy astrophysical objects such as supernova explosions/pulsar magnetospheres, giant flares and repeating bursts of magnetars, jets from active galactic nuclei (AGN), star-burst galaxies, mysterious gamma ray bursts (GRB), as well as galaxy clusters. Research works on the origin of ultra high energy cosmic rays (UHECRs) are also within the coverage of the group.

In addition, studies have been made also for nonthermal phenomena within the heliosphere [5,11], such as interplanetary shocks and the earth's bow shock, magnetic reconnection, the interaction processes between the solar wind and the moon. While these heliospheric phenomena are limited in their energy coverage, their studies have proved to give a theoretical basis to interpret distant astrophysical high energy phenomena.

Research topics: 1. Reevaluation of acceleration processes

While the diffusive shock acceleration process has been accepted as the standard model of astrophysical particle acceleration, interests are being renewed on other processes such as second-order stochastic acceleration in relativistic turbulences. We have presented new results on the stochastic acceleration in time-dependent velocity-shear turbulence [6] (Figure 1) expected in relativistic jets in AGNs and GRBs.

Research topics: 2. Magnetars and pulsars

The magnetosphere around neutron stars are candidate sites for efficient particle acceleration. Magnetars, slowly-rotating neutron stars with strong magnetic field of 10^{13-15} G, occasionally show giant-flare (GF) activities with peak gamma-ray luminosities reaching to 10^{47} erg s^{-1} [1], which are as strong as the luminosities of AGNs. In addition to giant flares, magnetars also show burst activities, much weaker than GFs but repeating many times. Recently we have discovered ionospheric disturbances caused by repeating bursts of the magnetar SGR J1550-5418 in January 2009. Such iono-

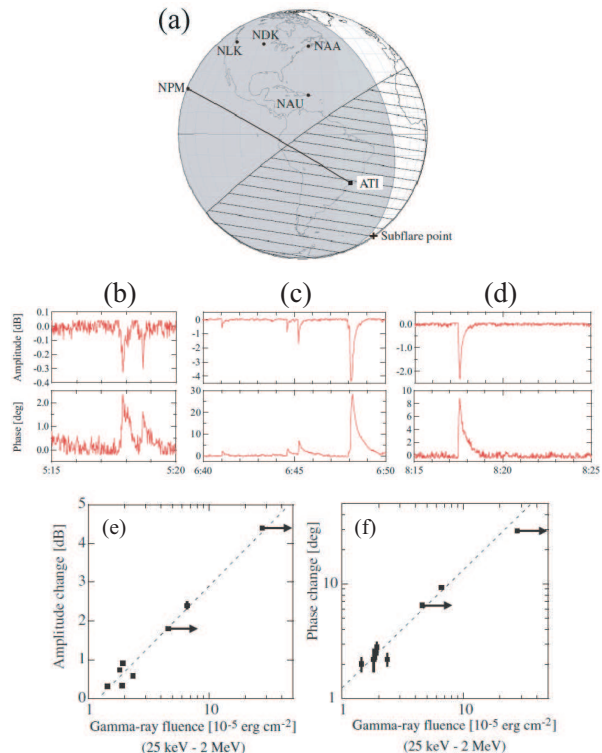


Fig. 2. (a) VLF (very low frequency) wave propagation path from the NPM transmitter in Hawaii to the ATI observing station in Brazil. The gray-shaded hemisphere indicates the nightside part of the Earth at 6:48 UT on 22 January 2009, when the largest burst occurred. The part of the Earth illuminated by gamma rays from the magnetar SGR J1550-5418 is shaded by lines. (b) Amplitude and phase variations of a VLF signal from the NPM transmitter (21.4kHz) observed at ATI from 5:15 UT to 5:20 UT, when repeated SGR bursts were detected at 05:17:51.7 UT and 05:18:39.5 UT. (c) The same as (b) but from 06:40 UT to 06:50 UT when repeated SGR bursts were detected at 06:41:02.1 UT, 06:44:36.4 UT, 06:45:13.9 UT, 06:47:57.1 UT, and 06:48:04.3 UT. (d) The same as (b) but from 08:15 UT to 08:25 UT when a repeated SGR burst was detected at 08:17:29.4 UT. (e) Relation between observed amplitude changes of VLF signals (NPM-ATI) and gamma-ray fluences (25 keV to 2 MeV) measured by the INTEGRAL satellite. (f) Same as (e) but for observed phase changes of the VLF signals.

spheric disturbance can be used as a new monitoring method for magnetars [4,10] (Figure 2).

Crab pulsar, the remnant of the supernova explosion in 1054 A.D., is one of the well-known neutron stars. While its physical properties have been studied for more than 40 years since its discovery, there remains an enigma about the origin of giant radio pulses (GRPs). While for a long time the GRPs had been regarded as a phenomenon limited to the radio frequency pulsar emission, a 3% enhancement of the optical emission at the GRP timing was discovered recently (Shearer et al., *Science*, 2003). Since only a very loose upper limit ($<250\%$) was obtained for the enhancement, if any, of the hard X-ray emission at the GRP timing (Lundgren et al., 1995), we have started a correlational study between the radio and hard X-ray observations collaborating with radio and X-ray astronomers at National Institute of Information and Communications Technology, Tokyo Institute of Technol-

Superposed epoch analysis

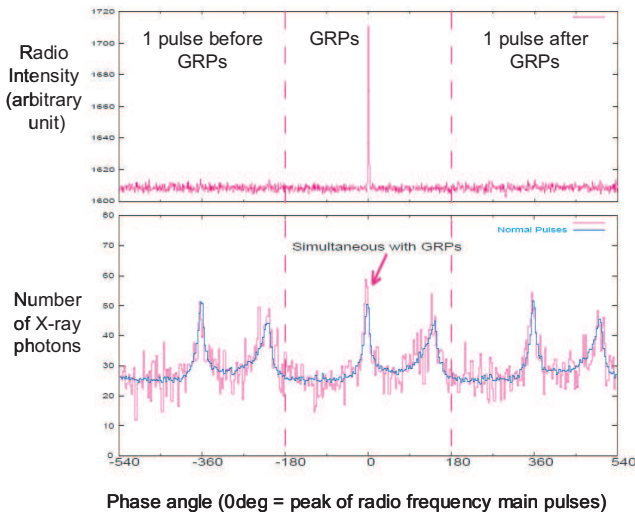


Fig. 3. (a) upper panel: Superposed intensity profile of the radio signal from the Crab pulsar in the interval of ± 1 pulse from the arrival of the GRPs. (b) lower panel: A blue curve shows the averaged X-ray intensity profile (SUZAKU/HXD, 15-75 keV) when the intensity of the radio pulses are normal (repeated 3 cycles). The red histogram shows the superposed X-ray intensity profile in the interval of ± 1 pulse from the arrival of the GRPs.

ogy, and Institute of Space and Astronautical Science in Japan Aerospace Exploration Agency.

Figure 3 [7] shows the preliminary result of our analysis: The average photon count rates around the main-pulse GRP peaks was $21.9 \pm 3.5 \text{ s}^{-1} \text{ bin}^{-1}$ while the average photon count rates at the same timing of normal radio pulses was $18.0 \pm 0.4 \text{ s}^{-1} \text{ bin}^{-1}$. Therefore while a weak enhancement of the photon count rates at the GRP peaks is seen, this is not statistically significant. We are continuing this correlational study to improve the photon statistics.

Research topics: 3. R/D study for radar detection of UHECRs and extraterrestrial grains

Wide attention has been attracted to the detection of ultra high energy cosmic rays (UHECRs) with radio techniques, either passive and active, towards future large-scale UHECR observatory on the ground. Collaborating with the TA group of ICRR, we have made a R/D study of the active method, namely, the detection of radar echoes from extensive air showers of UHECRs (UHECR echoes, hereafter). Parallel to the above R/D study, we have also joined a radar research project for extraterrestrial grains (meteors) collaborating with radar physicists and planetary physicists at National Institute for Polar Research, Research Institute for Sustainable Humanosphere in Kyoto University, and Department of Earth Planetary Sciences in the University of Tokyo. Despite more than three orders of magnitude difference in the echo duration between UHECR echoes ($< \sim \mu\text{s}$, expected but not yet identified) and meteor echoes (several - several tens of ms, observed), the know-how developed in the latter project provides a technical basis for the former (Figure 4, Yoshida et al., in preparation).

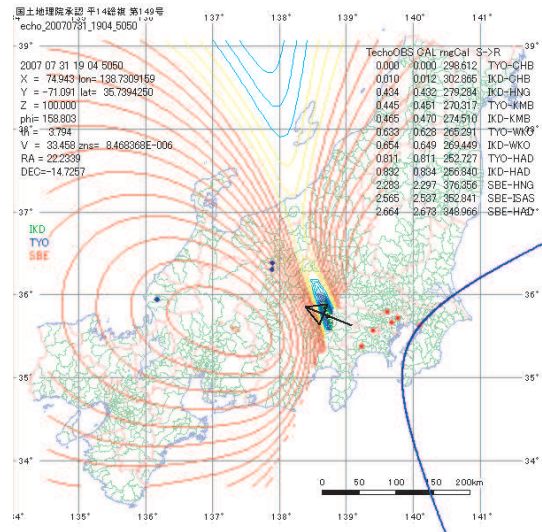


Fig. 4. A multi-static forward scattering radar system for the detection of extraterrestrial grains (meteors) was set over the Honshu island of Japan during the July-August season in 2007. Three amateur-radio beacon transmitters were at Sabae, Ikeda, and Toyoshina (blue dots), while a receiver array consisting of six stations (red dots) was deployed around the Tokyo bay. The impact geometry of an interplanetary grain at 19:04:50.5 JST (10:04:50.5 UT) on 31 July 2007 was successfully determined: It is found that this meteor had a radiant point (RA, DEC)=(22.2 hour, -14.7 deg) with the input velocity=33.5 km/s, and impacted against the atmosphere at the point (138.7°E, 35.8°N) (a black arrow in the center of the figure). Black-blue-yellow-red contours show the residual errors in the least-square fitting procedure for the impact point search. A blue hyperbola on the lower-right corner of the figure shows the footprint of the meteor radio echo at the timing of its first ground detection.

Research topics: 4. Interaction process between supersonic flow and solid objects

It is expected that the interactions between supersonic plasma flows and surfaces of solid bodies play important roles in many astrophysical environments.

The nearest example found recently is in the solar-wind-moon interaction [2,3,8,9], where detailed studies of kinetic properties of plasmas can be made. Figure 5 [2, 9] shows the time series data from SELENE, the Japanese lunar orbiter, between 12:00 and 18:00 UT on 4 April 2008, showing quiet (# 1) and active (# 3) conditions of the wake in the near-Moon space. From these observations, a new model of the near-Moon wake environment is proposed ([2], Figure 6), where the electromagnetic acceleration of the solar wind particles and the kinetic plasma instability (two stream instability) are playing the dominant role.

Bibliography

Papers in refereed journals

1. Masada, Y., S. Nagataki, K. Shibata, and T. Terasawa, "Solar-type magnetic reconnection model for magnetar giant flares", *Pub. Astron. Soc. Japan*, 104, 1093-1102, 2010.
2. Nishino, M. N., M. Fujimoto, Y. Saito, S. Yokota, Y. Kasahara, Y. Omura, Y. Goto, K. Hashimoto, A. Ku-

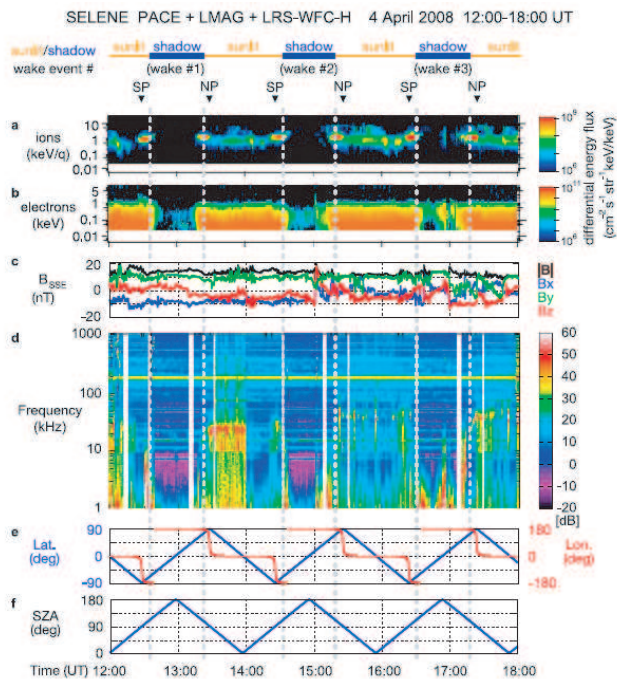


Fig. 5. Energy-time spectra of (a) protons and (b) electrons, (c) magnetic field in the SSE (Selenocentric Solar Ecliptic) coordinate, (d) frequency-time spectrogram of the plasma wave detector, and (e and f) spacecraft locations in the SSE coordinates and solar zenith angle (SZA) are shown [2]. Intervals of sunlit/shadow regions are indicated by orange/blue bars at the top of the figure, where the wake was observed within the shadow region.

mamoto, T. Ono, H. Tsunakawa, M. Matsushima, F. Takahashi, H. Shibuya, H. Shimizu, and T. Terasawa, “Effect of the solar wind proton entry into the deepest lunar wake”, *Geophys. Res. Lett.*, 37, L12106.1-4, 2010.

3. Saito, Y., S. Yokota, K. Asamura, T. Tanaka, M. N. Nishino, T. Yamamoto, Y. Terasawa, M. Fujimoto, H. Hasegawa, H. Hayakawa, M. Hirahara, T. Mukai, T. Nagai, T. Nagatsuma, T. Nakagawa, M. Nakamura, K.I. Oyama, E. Sagawa, S. Sasaki, K. Seki, I. Shinohara, T. Terasawa, H. Tsunakawa, H. Shibuya, M. Matsushima, H. Shimizu, F. Takahashi, “In-flight performance and initial results of plasma energy angle and composition experiment (PACE) on SELENE (Kaguya)”, *Space Sci. Rev.*, 154, 265-303, 2010.
4. Tanaka, Y. T., J.-P. Raulin, F. C. P. Bertoni, P. R. Fagundes, J. Chau, N. J. Schuch, M. Hayakawa, Y. Hobaru, T. Terasawa, and T. Takahashi, “First very low frequency detection of short repeated bursts from magnetar SGR J1550-5418”, *Astrophys. J.*, 721, L24-L27, 2010.

Books

5. Terasawa, T., “Shocks in the heliosphere”, Chapter 12, *IAGA Special Sopron Book Series vol. 4, “The Sun, the Solar Wind, and the Heliosphere”*, ed. by M. P. Miralles and J. S. Almeida, Springer, 2011.

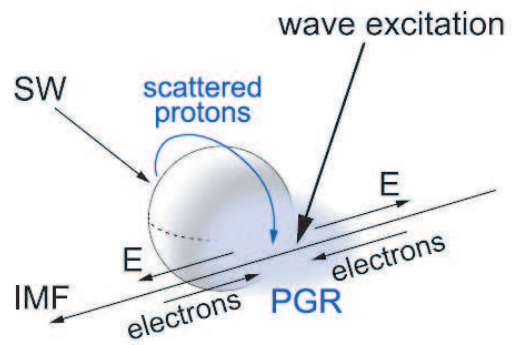


Fig. 6. A new model of the near-Moon wake environment where the protons of the solar wind origin scattered at the sunlit region of the Moon and accelerated by the $-V \times B$ electric field are penetrating deeply into the middle of the wake region and forming the proton governed region (PGR) [2]. Vectors in the figure, SW, E, and IMF, show directions of the solar wind flow, the ambipolar electric field, and the interplanetary magnetic field, respectively.

Thesis

6. Fujinuma, A., “Acceleration of UHECR in relativistic jets with velocity shear” (in Japanese), Master thesis, Department of Physics, Tokyo Institute of Technology, March 2011.
7. Nagata, K., “Study of giant radio pulses from the Crab pulsar” (in Japanese), Master thesis, Department of Physics, Tokyo Institute of Technology, March 2011.

Conference papers

8. Nishino, M. N., X. Wang, M. Fujimoto, H. Tsunakawa, Y. Saito, S. Yokota, W. Bian, C. Li, H. Shibuya, M. Matsushima, H. Shimizu, F. Takahashi, and T. Terasawa, “Anomalous deformation of the Earth’s bow shock in the lunar wake: Joint observations by Chang’E-1 and SELENE”, *Proceedings of American Geophysical Union Fall meeting*, Paper P54B-07, 2010.
9. Nishino, M. N., M. Fujimoto, Y. Saito, K. Yokota, Y. Kasahara, Y. Omura, Y. Goto, K. Hashimoto, A. Kumamoto, T. Ono, H. Tsunakawa, M. Matsushima, F. Takahashi, H. Shibuya, H. Shimizu, and T. Terasawa, “Effect of the solar-wind proton entry into the deepest lunar wake”, *Proceedings of EGU General Assembly*, vol. 5, EPSC2010-473, 2010.
10. Tanaka, Y, M. Hayakawa, T. Terasawa, T. Takahashi, “VLF detection of ionospheric disturbance caused by a magnetar giant gamma-ray flare”, *Proceedings of 38th COSPAR Scientific Assembly*, C11-0172-10, 2010.
11. Terasawa, T., “Collisionless shock and particle acceleration” in the IAU symposium 274, “*Advances in Plasma Astrophysics*”, 2010.

ASTROPHYSICS and GRAVITY DIVISION

Overview

Astrophysics and Gravity Division consists of Gravitational Wave Group, The Sloan Digital Sky Survey Group, Theory Group and Primary Cosmic Ray Group. The Gravitational Wave Group conducts experimental research of gravitational wave with researchers of gravitational wave experiment and theory in Japan. The main items are the construction of the large scale cryogenic interferometer(LCGT) at Kamioka underground and the operation of CLIO. The Sloan Digital Sky Survey Group has completed the planned imaging and spectroscopy observations, and it continues publishing papers in collaboration with worldwide researchers. This group has started a new optical deep survey project with the wide-field imager of Hyper Suprime-Cam mounted on the Subaru telescope. Theory Group conducts both theoretical study of the Universe and astroparticle physics. Primary Cosmic Ray Group reconstructs past cosmic ray changes and studies their impacts on climate change.

Gravitational Wave Group

Introduction

A gravitational wave is a physical entity in space-time predicted by Einstein's theory of general relativity. Its existence was proven by the observation of PSR1913+16 by Taylor and Hulse¹, who won the Nobel prize in 1993. However, nobody has succeeded to directly detect gravitational waves. The theory of gravitation can be tested by the detection of gravitational waves. A gravitational wave detector is the last tool of mankind to inspect the universe. In order to directly observe gravitational waves, we have started to construct the Large scale Cryogenic Gravitational wave Telescope (LCGT). In prior to the construction of LCGT, we developed a 300 m baseline interferometric gravitational wave detector, TAMA, at the Mitaka campus of the National Astronomical Observatory of Japan (NAOJ) and nine observation runs had been conducted. TAMA project started in April, 1995, as a five-year project and it was extended by two years after 1999. We acquired the interferometer technology and knowledge for the large scale interferometer by the experience of TAMA project, which was organized by researchers belonging to universities and national laboratories. We conducted the development of Seismic Attenuation System (SAS) installed for four main mirrors and tried to enhance the interferometer sensitivity. In regard with CLIO project, the construction of which was started in 2003 and ended in March, 2007, we have succeeded to break the room temperature limit by cryogenic mirror system that is operated at cryogenic temperature at first in the world.

^{*1} J. H. Taylor and J. M. Weisberg, *Astrophysical J.*, **345** (1989) 434.

LCGT Project

ICRR, Univ. of Tokyo, Kashiwa, Chiba 277-8582

In collaboration with the members of:

LCGT collaboration; National Astronomical Observatory (NAOJ), High Energy Accelerator Research Organization (KEK), Department of Physics (University of Tokyo, abbreviated as UT hereafter), Research Center for the Early Universe (UT), Institute for Laser Science (University of Electro-Communications), Photonic Innovation Center (University of Electro-Communications), Department of Advanced Materials Science (UT), Earthquake Research Institute (UT), Department of Astronomy (UT), Department of Physics (Osaka City University), Faculty of Engineering (Hosei University), Metrology and Measurement Science (National Institute of AIST), Space-Time Standards Group (National Institute of Information and Communication Technology), Department of Earth and Space Science (Osaka University), Department of Physics (Kyoto University), Yukawa Institute for Theoretical Physics (Kyoto University), Graduate School of Humanities and Sciences (Ochanomizu University), Advanced Research Institute for the Sciences and Humanities (Nihon University), Department of Advanced Physics (Hirosaki University), Astronomical Institute (Tohoku University), Department of Physics (Niigata University), Department of Physics (Rikkyo University), Department of Physics (Waseda University), College of Industrial Technology (Nihon University), Department of Humanities (Yamanashi Eiwa College), Department of Physical Science (Hiroshima University), Faculty of Science (University of the Ryukyus), Max Planck Institute for Gravitational physics (AEI), California Institute of Technology, Department of Physics (University of Western Australia), Department of Physics (Louisiana State University), Center for Computational Relativity and Gravitation (Rochester Institute of Technology), Department of Physics (Glasgow University), Columbia Astrophysics Laboratory (Columbia University in the city of New York), Department of Physics (Birmingham University), Department of Astronomy (Beijing Normal University), Inter University Center for Astronomy & Astrophysics (Pune University), Sternberg State Astronomical Institute (Moscow University), LATMOS (CNRS), Center for Astrophysics (University of Science and Technology of China), Center for Astrophysics (Tsinghua University), Institute of High Energy Physics (Chinese Academy of Sciences), Shanghai United Center for Astrophysics (Shanghai Normal University), Center for Measurement Standards (Industrial Technology Research Institute), Physics Department (Maryland University)

Objective of LCGT

After the discovery of the highly relativistic binary neutron star system², a new young binary pulsar was detected

^{*2} M. Burgay, *et al.*, *Nature*, **426** (2003) 531.

³. The former discovery increased the coalescence rate from 10^{-6} to 10^{-5} a year in a galaxy as big as our Galaxy ⁴ and the latter pushed up by another factor of six. Although it was good news for the detection of gravitational waves, we still need to wait for long time to detect by the presently existing detectors. This is the reason why we need to construct LCGT (Large-scale Cryogenic Gravitational wave Telescope). The objective of LCGT is to detect a few events of gravitational wave in a year. Since there are many other possible gravitational wave sources in the universe other than the coalescence of binary neutron stars, those sources are possible targets of LCGT project.

Status of LCGT Project

In order to fulfill the objective of LCGT, we designed the sensitivity of LCGT so as to observe binary neutron star coalescence events occurring at 250 Mpc with $S/N=8$ in its optimum configuration[1]. This is ten-times more sensitive than that of the LIGO (I), and by two orders more than that of TAMA at their most sensitive frequencies. This is achieved by the laser interferometer located underground, using three-kilometer length baseline, cooling mirrors at cryogenic temperature, and a high-power laser source employing 180 W output. The optical configuration is a power recycled Fabry-Perot-Michelson interferometer with the resonant-sideband-extraction (RSE) scheme (in Fig. 1). The detailed design of the control system was tested for the resonant sideband extraction scheme.[2] Table 1 lists the important parameters of LCGT. You may trace the history of the evolution of LCGT by references. [3] Ultimate sensitivity of a laser interferometer is determined by seismic noise at low frequencies (10-30 Hz) (which is reduced by improving the vibration isolation system), and it is limited by photon shot noise at higher frequencies (more than 300 Hz), which can be improved only by increasing the light power in the main cavities. The sensitivity of middle frequencies (30-300 Hz) is limited by the fluctuation of the photon recoil force noise. This requires that thermal noise is reduced both by decreasing the temperature and by decreasing the internal mechanical loss (*i.e.*, increasing the mechanical Q of vibration modes). The source of thermal noise comes from both mirror internal vibration, mechanical loss of the optical coating and swing noise of the pendulum suspending the mirror. The reduction of thermal noise is attained by cooling both the mirror, itself, and the suspension system that suspends the mirror.

Figure 2 compares the sensitivity curve of LCGT with those of TAMA, CLIO (a 100 m prototype cryogenic interferometer placed underground of Kamioka mine), LIGO (initial LIGO) and the design of TAMA. The sensitivity at low frequencies of LCGT is attained by SAS, which will be proven by the current SAS in TAMA. That of higher frequencies is attained by higher laser power, which has been basically shown by TAMA. The mid-frequency region is improved by cryogenic mirror and suspension system, which has been proven by CLIO (described in the next section*). The sensitivity improvement of two orders of magnitude at low frequencies is certainly realized by the completion of LCGT interferometer.

*³ D.R. Lorimer, *et al.*, *Astrophysical J.* **640**(2006) 428.

*⁴ C. Kim, V. Kalogera and D. R. Lorimer, *Astrophysical J.* **584** (2003) 985.

Table 1. LCGT design parameters to detect binary neutron-star coalescence events in 250 Mpc.

Item	Parameter
Baseline Length	3 km
Interferometer	One set
Optical Power	Power recycled Fabry-Perot-Michelson with RSE
	Laser: 180 W; Finesse: 1550
	Input power at BS: 825 W Cavity power 780 kW
Beam radius	3.4 cm(ITM)/4.5 cm(ETM)
Main Mirror	Sapphire 30 kg, 20 K Diameter 25 cm Mechanical Q: 10^8
Suspension	Frequency: 1 Hz; Q: 5×10^8
Pendulum	16 K
Vacuum	$\leq 10^{-7}$ Pa

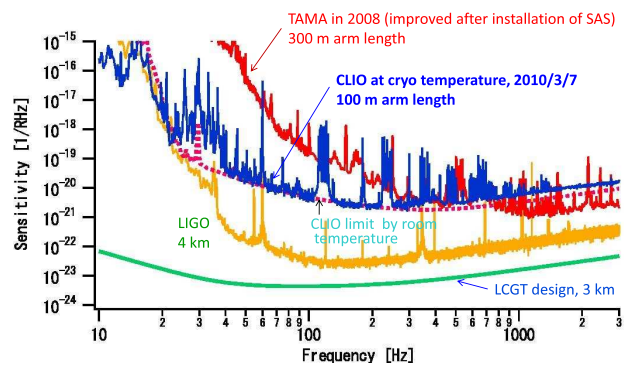


Fig. 2. LCGT design sensitivity compared with those of TAMA (red line), CLIO (a 100m prototype cryogenic interferometer placed underground of Kamioka mine, blue line), LIGO (initial LIGO, yellow line) and the CLIO limit at room temperature (red broken line). The horizontal axis is frequency [Hz] and the vertical axis represents sensitivity spectrum for gravitational waves $[1/\sqrt{\text{Hz}}]$.

Cryogenic Mirror development

The design of the cryogenic mirror system is shown in Fig. 3. The mirror is suspended by two loops of sapphire fibers connected to an auxiliary mirror that is a part of suspension point interferometer. This mirror is also suspended from an alignment control platform that is suspended with an insulator rod connected through the center holes of the radiation shields to an isolation table suspended by a low-frequency vibration isolator, which is placed at room temperature. The auxiliary mirror has a heat link to the platform and another heat link connects the platform and a heat anchor point (4 K) inside the vacuum located just above the platform. Both the cryogenic system and the vibration isolator are put inside a common high-vacuum chamber.

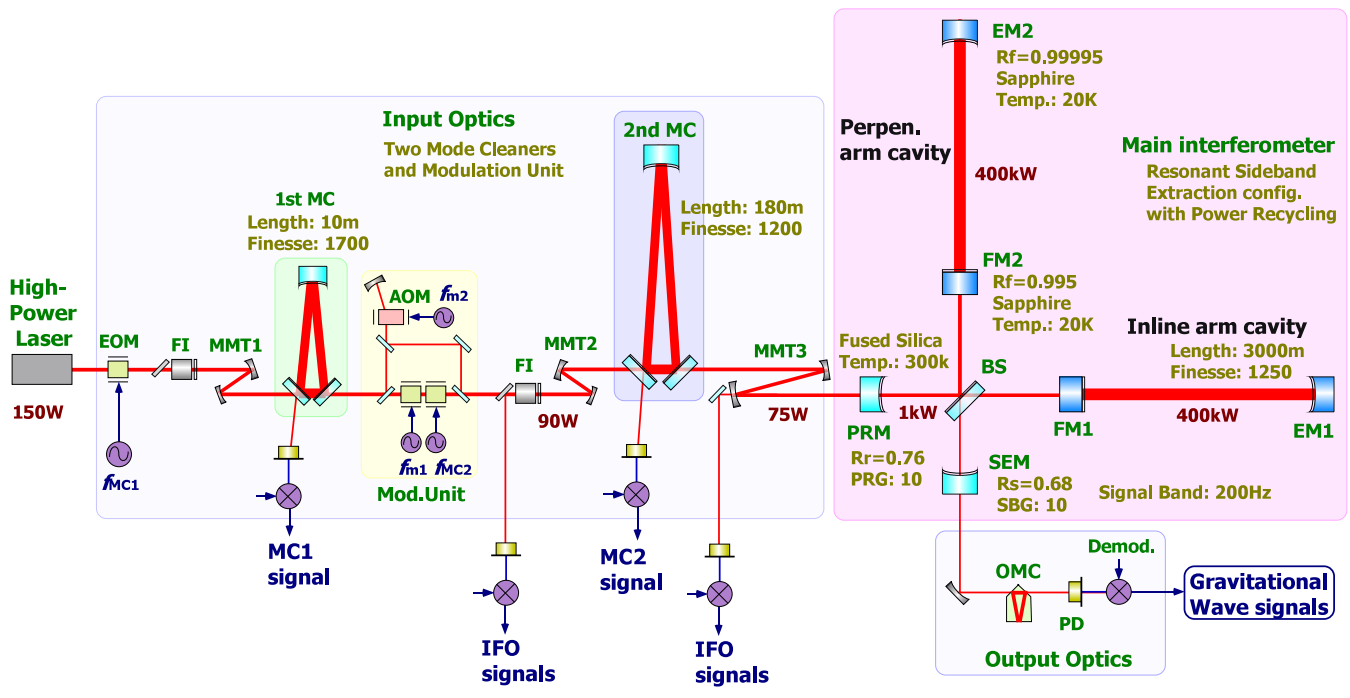


Fig. 1. Optical design of LCGT. The optical configuration is a power recycled Fabry-Perot-Michelson interferometer with the resonant-sideband-extraction (RSE) scheme.

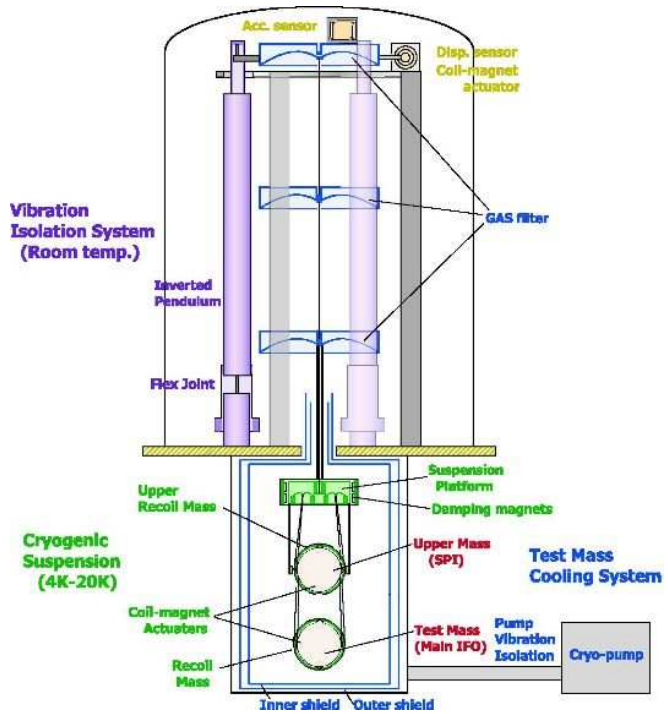


Fig. 3. Schematic design of the cryogenic suspension system. The mirror is suspended by sapphire fibers connected to an auxiliary mirror, which is suspended by metal wires from a platform that has a heat link to a 4 K heat anchor inside the vacuum. The platform is also suspended with an insulator rod connected through the holes of radiation shields to an isolation table suspended by a seismic attenuation system placed at room temperature in the common high vacuum.

To realize this concept, the following research subjects were conducted and reported:

1. Removal of heat produced by high-power laser illumination (annual report 1997-1998 and also in references [4])
2. Holding the high Qs of the mirror internal modes and suspension pendulum [5]
3. Reducing the contamination of mirror surfaces (annual report 2000-2001 and also in [6])
4. Estimating heat production by optical loss in the mirror [7]
5. Alignment control of mirrors in a cryogenic environment [8]
6. Low mechanical loss of the optical coating (annual report 2003-2004 and also in reference [9])

As for item 5, we confirmed that a superconducting film could be used for the receptor of the magnetic force in place of permanent bar magnets that are normally used in the existing detectors. The film can be easily sputtered on the mirror surface without harmfully degrading the mechanical Q of the mirror. With respect to the last item, we reported on a measurement of the bulk substrate of the mirror at cryogenic temperature in the annual report (2003–2004). We could correctly estimate the thermal vibration noise of the optical coating while considering the inhomogeneous loss that had been neglected at an early stage of interferometer development. The substrate of the cryogenic mirror is sapphire, which has a

large thermo-elastic thermal noise at room temperature. However, since the thermal-expansion ratio of sapphire at cryogenic temperature goes down to nearly 0 and the heat conductivity becomes greater, the thermo-elastic noise drastically reduces at the cryogenic temperature. Thermal noise estimated from the Q of the coating is well below the design sensitivity of LCGT, which means that this coating noise does not limit the sensitivity, whereas, the sensitivity of a room-temperature mirror is limited by this effect. Also thermal lens effect disappears at cryogenic temperature in the LCGT design. These are the significant merits of the cryogenic mirror system.

Study on the Bandwidth Optimization of LCGT

A broad band RSE (resonant-sideband extraction) configuration was selected as a default LCGT optical design since 2004. With recent progresses in technology, it appears that we have a chance to enhance the sensitivity of LCGT by selecting more suitable optical parameters. We obtained a recommendation by a working group to discuss and optimize the optical configuration including a possibility of the detuned RSE which has a narrower bandwidth but a better sensitivity in total (annual report 2009-2010). The purpose of this working group was to investigate and to make recommendations on the interferometer optical configuration design of LCGT and its observation band for gravitational waves.

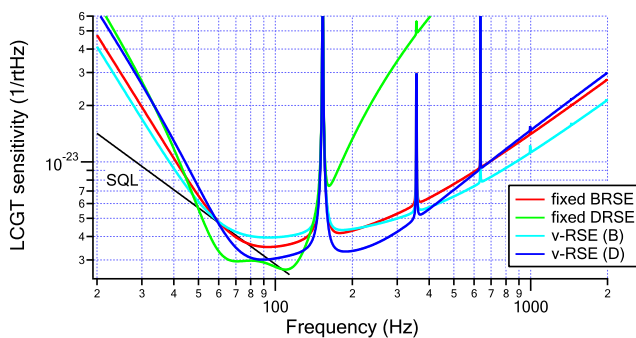


Fig. 4. Sensitivity curves of the candidate configurations: BRSE (red curve), DRSE (green curve), and VRSE (B/D) with sky-blue/blue curves.

It is possible to optimize and tune the observation frequency band for target gravitational-wave sources, by choosing suitable optical parameters. So as to determine the optical parameters, we define three candidate parameter sets: broadband RSE (BRSE), detuned RSE (DRSE), and variable RSE (VRSE) configurations. VRSE is designed to have good sensitivity both with tuned and detuned operation, and to switch observation bands depending on the observation purposes and targets. The detector sensitivity curves are estimated with the current best-estimated boundary conditions of LCGT: an input laser power, suspension and mirror thermal noises, seismic noise, and optical readout noises. The estimated sensitivity curves are shown in Fig. 4. and Table 2 shows brief summary of optical parameters.

The DRSE configuration (green curve) has the best floor-level sensitivity at around 100 Hz, and the best observable distance of 132 Mpc for neutron-star inspiral events (SNR=8, sky

averaged).⁵ The BRSE configuration (red curve) has wider observation band to cover various sources, and moderate observable range of 114 Mpc for neutron-star inspirals. The blue and sky-blue curves are for the VRSE configuration with a detuned mode VRSE (D) and with a broadband mode VRSE (B), respectively. They have slightly narrower and wider observation bands than the BRSE (red curve) configuration, respectively.

Scientific outcomes obtained from GW observation highly depend on the sensitivity and observation band of a detector. We surveyed possible GW sources which would be targets of LCGT, and discussed advantages and disadvantages of each candidate interferometer configurations.

The most important criteria in the comparison is to increase the possibility to achieve the minimum success of LCGT: detect at least a few GW events within one year operation. The primary target of LCGT is coalescences of neutron-star binaries. We estimated the observable range, expected event rates, required observation period for the first detection, and measurement accuracy of binary mass parameters for these sources. Figure 5 shows the expected detection rate as a function of sky average detection range. Then we surveyed scientific outcomes from the other GW sources: black-hole binaries, black-hole ringdown, supernovae with stellar-core collapses, pulsars. We also compare the candidate configurations from a viewpoint of international observation network. Here, we show Table 3 summarizing the range for black-hole binaries, etc.

The working group concluded the following interferometer design and observation strategy as a part of new default LCGT design.

- The optical configuration of LCGT should be VRSE: a RSE (resonant-sideband extraction) with variable observation band.
- In the first observation phase, LCGT interferometer should be operated with a detuned mode, VRSE (D), for earlier detection of gravitational-wave signals. After the first detections, the variable configuration provides the option to change the observation band to broadband, VRSE (B), so as to obtain more scientific information.

Construction of LCGT Organization

In order to conduct the construction of LCGT according to the budget under the program of the leading edge research facilities, the LCGT collaboration was reinforced by nominating the director of ICRR as the project integrator of LCGT and creating an executive committee controlling each sub-working group that was chaired by chief leader. The origin of each sub-working group was based on the team that functioned to establish the design of LCGT. The structure of the organization is represented in Fig. 6.

^{*5} Here, observable distance is defined as the range within which events are detected with higher signal-to-noise ratio than 8. Detector antenna pattern and wave polarizations are all-sky-averaged. Whereas, the horizon distance is the most remote distance under optimum configurations of the interferometer and the orbit.

Table 2. Setup parameters, inspiral range (IR), and strain sensitivity at 1 kHz of each configuration. The first number in each IR column is with the assumption that wave come from the optimal direction for LCGT, and each number in parenthesis is with the average over whole sky.

	T (Finesse)	T_s	ϕ [deg]	ζ [deg]	IR [Mpc]	Sensitivity [$\text{Hz}^{-1/2}$]
BRSE	0.004 (1550)	0.23	90	127.6	259 (114)	1.4×10^{-23}
DRSE	0.009 (690)	0.08	74.6	103.8	299 (132)	2.1×10^{-22}
VRSE (B)	0.004 (1550)	0.15	90	121.8	255 (112)	1.1×10^{-23}
VRSE (D)	0.004 (1550)	0.15	86.5	134.7	281 (123)	1.5×10^{-23}

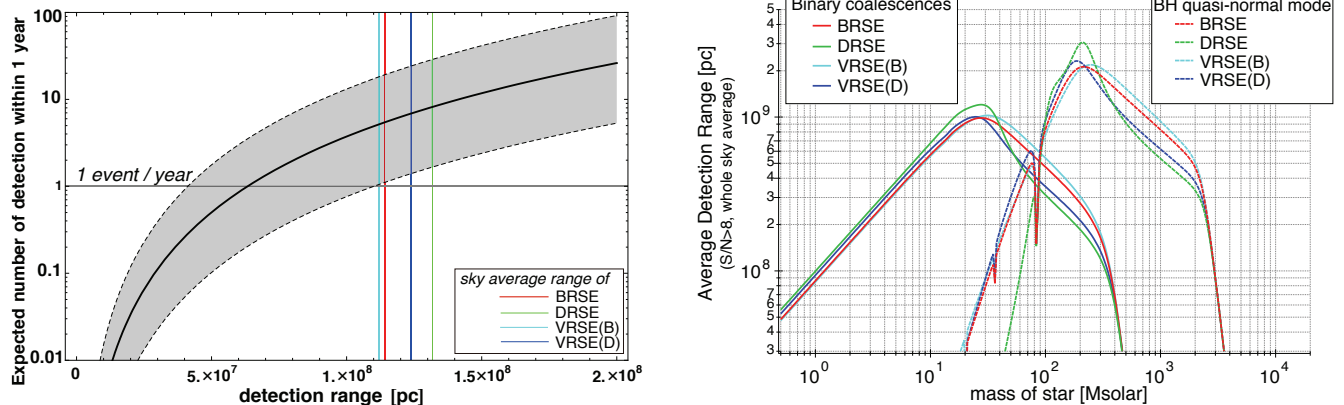


Fig. 5. *Left*: Solid thick black line is Expected event rate as a function of sky average detection range, and gray shaded zone is a confidence band of 95%. Solid thin lines show the range for binary coalescence. Colors are corresponding to the IFO configurations. *Right*: Sky-averaged detection ranges as a function of total mass of the source. Solid lines show the range for binary coalescence. Dashed lines show the range for ringdown GW from black-hole quasi-normal mode. Colors are corresponding to the IFO configurations.

Schedule

The funding was available for manufacturing the laser interferometer including its vacuum system for three years since FY 2010 and the excavation of the underground would start in FY 2011 for the period of two years. We planned to take the most efficient and most reliable way under these constraints. The present schedule is shown in Fig. 7. We note that the detail of the schedule would be flexibly changed due to the funding status in future.

Special working groups

We have established 14 sub-working groups under the executive committee. These groups shared the role of construction of LCGT. Along with activities of these groups we established several special working groups for solving on-going problems. They were

- Installation of two story floors for seismic attenuation system
- Cope with inclination of tunnel from horizontal level for drain water
- Shift to low frequency band
- Study of bandwidth design
- Roadmap to objective

The idea of two story floors came from the effective usage of rock structure of the underground, which guarantees the stable footing of the seismic attenuation system with lower cost

of excavation of the tunnel. The problem of the underground water forced us to design the inclined base floor of the tunnel, the effect of which was the increase of cross coupling between vertical vibration to horizontal. Without this inclination, we need to introduce drain water pumping system along the beam tubes, which might produce unexpected result on the seismic noise in low frequency. One of the recommendations by the review B (see the following sub-section*) was to lower the observational bandwidth from the present design of LCGT, which might reduce the laser power and ease the load of the heat extraction in the input test mass made of relatively higher optical absorption. We decided not to adopt this recommendation by fearing loss of objective range of observation. Both the results of last two items; study of the bandwidth and roadmap, will be presented in the report of the next year.

Topical R&Ds

Although we have confirmed the performances of new instruments applied to the interferometer of LCGT, some parts require the practical tests using the real models of those instruments. For example, the SAS (seismic attenuation system) was applied to TAMA interferometer and produced expected result. However, we have to technically know the difference between TAMA300 and LCGT with 3 km baseline. In prior to the installation of the real system, we plan to test the real model of SAS using TAMA interferometer at Mitaka campus. In respect with the cryogenic system, its prototype had been already applied to CLIO interferometer. However, the size and power of the refrigerator were increased and the cryo-

Table 3. BH observations. In this estimation, we assume the amplitude of ringdown GW corresponding to 3% of mass.

	IFO configurations			
	BRSE	VRSE (B)	VRSE (D)	DRSE
Binary coalescences NS-BH ($1.4-10M_{\odot}$)				
Detection range d_{avg} [Mpc]	240	235	261	278
Expected event rate [events/yr]		0.006 – 6		
Binary coalescences BH-BH ($10-10M_{\odot}$)				
Detection range d_{avg} [Mpc]	570	557	615	677
Expected event rate [events/yr]		0.07 – 7		
Quasi-normal mode :				
Detection range d_{avg} [Gpc] for $200M_{\odot}$	2.1	2.0	2.3	3.0
Survey mass region at 1 Gpc [M_{\odot}]	110 - 910	115 - 760	100 - 490	100 - 450

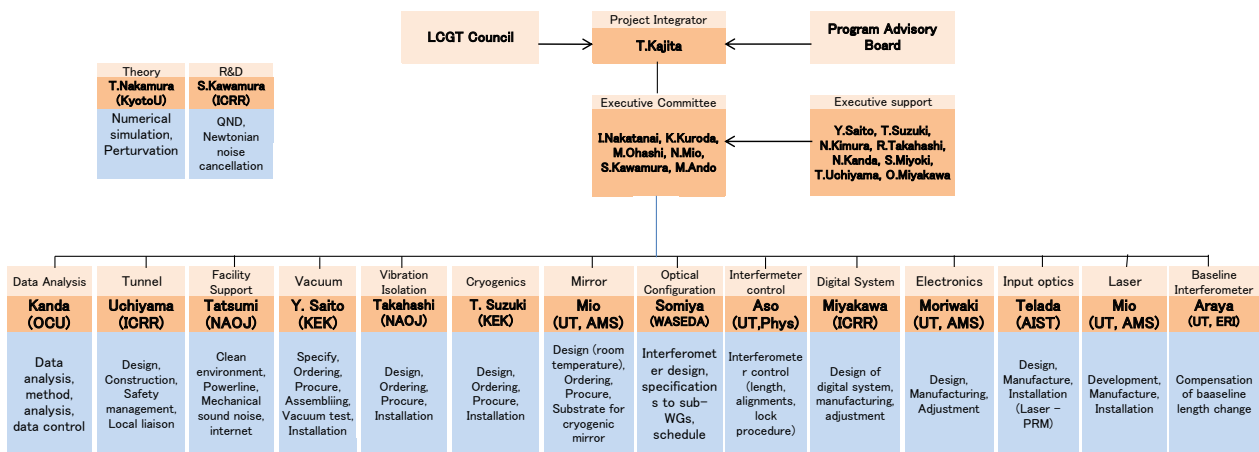


Fig. 6. LCGT organization for construction in the end of FY 2010.

genic payload completely changed from the prototype. It is natural to test in prior to the practical installation to LCGT. The test was planned to conduct in the next fiscal year.

Reviews

After finishing the design detail by sub-working groups, we conducted peer review on each sub-working group repeatedly since the November of 2010 and ended in January 2011. Summarizing these results, we organized the external review committee consisting of overseas specialists chaired by Dr. Mike Zucker in MIT (LIGO MIT), which was held for one week in the end of February and the beginning of March. The committee scrutinized the detailed design of LCGT except the facility and geophysical interferometer sub-working group. The report with recommendation was presented in March and we coped with the problems for solution. These series of reviews will be summarized by the review of the program advisory board in the next fiscal year.

Academic Agreements with overseas projects

In order to exchange technical information and support from overseas projects, we exchanged academic agreements with gravitational wave research projects in abroad. First, we made an attachment of collaborative research agreement be-

tween LIGO laboratory in Caltech and ICRR. The agreement was exchanged in prior fiscal year for introducing digital control system from LIGO to CLIO. Second, we exchanged the academic agreement of collaboration of gravity wave research between EGO/Virgo and ICRR. Third, the research agreement between Shanghai United Center of Astrophysics in Shanghai Normal University and ICRR was exchanged to promote R&D of LCGT and data analysis. Preparation of exchange of academic agreements was ongoing with GEO, Sannio University, and so on.

Public Relations

The nickname of LCGT was being searched by the naming committee chaired by Writer, Yoko Ogawa. The announcement of the recommendation of the committee was postponed to the next fiscal year due to the Eastern Japan disaster.

The current activity of LCGT was uploaded in the webpage: <http://gwcenter.icrr.u-tokyo.ac.jp/en/>

Bibliography

- [1] K. Kuroda *et al.*, “Status of LCGT”, *Class. Quantum Grav.* **27** (2010) 084004.

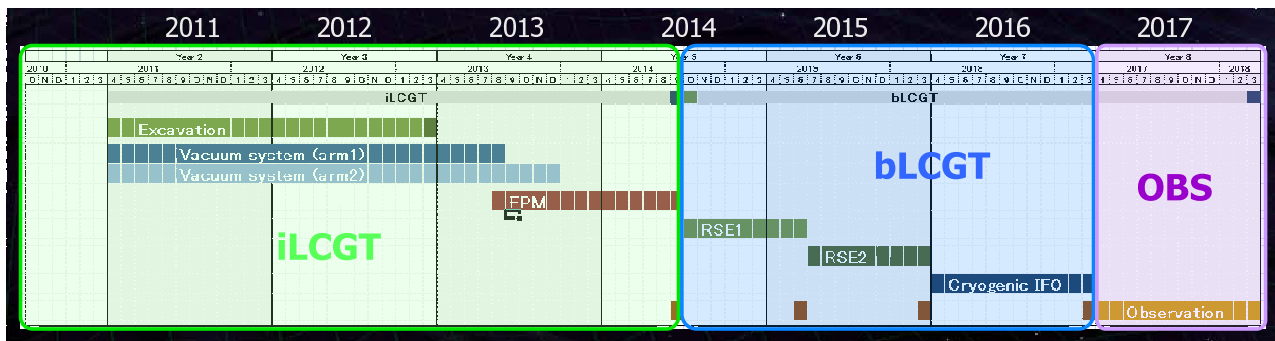


Fig. 7. Tentative schedule of LCGT for construction being discussed in the roadmap meeting.

- [2] F. Kawazoe *et al.*, J. Phys.: Conference Series **122** (2008) 012017.
- [3] K. Kuroda *et al.*, Int. J. Mod. Phys. **D 8** (1999) 557; K. Kuroda, *et al.*, Class. Quantum Grav. **19** (2002) 1237; T. Uchiyama, *et al.*, Class. Quantum Grav. **21** (2004) S1161.
- [4] T. Uchiyama, *et al.*, Phys. Lett. A **242** (1998) 211.
- [5] T. Uchiyama, *et al.*, Phys. Lett. A **261** (1999) 5; *ibid* **A273**(2000)310.
- [6] S. Miyoki, *et al.*, Cryogenics **40** (2000) 61; *ibid* **41** (2001) 415.
- [7] T. Tomaru, *et al.*, Phys. Lett. A **283** (2001) 80.
- [8] N. Sato, *et al.*, Cryogenics **43** (2003) 425.
- [9] K. Yamamoto, *et al.*, Class. Quantum Grav. **21** (2004) S1075.

CLIO Project

[Spokesperson : Masatake Ohashi]

ICRR, Univ. of Tokyo, Kashiwa, Chiba 277-8582

In collaboration with members of: KEK, Tsukuba; Kyoto-U, Kyoto; ERI of UT, Tokyo

Overview of CLIO

CLIO (Cryogenic Laser Interferometer Observatory) is a 100 m-baseline underground cryogenic interferometer at the Kamioka Mine. CLIO forms a bridge connecting the CLIK (7 m prototype cryogenic interferometer at Kashiwa campus) and the LCGT (3 km cryogenic interferometer at Kamioka). The site of CLIO, near the Super-Kamiokande neutrino detector, is shown in Fig. 8. The tunnel was dug in 2002, and a strain meter for geophysics was installed in 2003 [1]. The construction of CLIO began in late 2003, and installation of the mode cleaner vacuum system was reported in the annual report (2003–2004). Four sets of cryostats and whole vacuum system were installed (annual report 2004–2005). We started the operation of CLIO in 2006 (annual report 2006).

The prime purpose of CLIO is to demonstrate mirror thermal noise reduction with cryogenic mirrors. We achieved the



Fig. 9. Overview of the CLIO interferometer.

design sensitivity at the room temperature after noise hunting taken in 2008 (Annual report 2008) [2]. After then, we started out cooling the mirrors and noise hunting with the mirrors under 20K had been done. We firstly observed the sensitivity improvement due to the mirror thermal noise reduction.

CLIO sensitivity curve with cooled mirrors (cryogenic sensitivity) and without cooling (300K sensitivity) are shown in Fig. 12 with estimation curves of the mirror thermal noise. The 300K sensitivity and the cryogenic sensitivity were measured at 2008/11/5 and at 2010/03/20, respectively. When the cryogenic sensitivity was measured, two front mirrors were cooled and the rest of two end mirrors were at the room temperature. Temperature of the front mirrors were 17K and 18K. Modifications possibly affecting the sensitivity at the cryogenic sensitivity measurement are exchange of final suspension wires and addition of heat link wires to the suspension systems. Cooling the mirror took about 250 hours and vacuum pressure was better than 10^{-4} Pa for both sensitivity measurements.

The noise floor level of the cryogenic sensitivity from 90Hz to 240Hz is below the 300K sensitivity. Observation range for GWs from neutron star binary coalescence was also improved to 159kpc from 148kpc for the optimum direction. This is the first observation of sensitivity improvement by the cryogenic mirrors. The noise floor at 165Hz was reduced to 2.2×10^{-19} m/ $\sqrt{\text{Hz}}$ from 3.1×10^{-19} m/ $\sqrt{\text{Hz}}$ after cooling the front mirrors. Amount of this noise floor reduction is con-

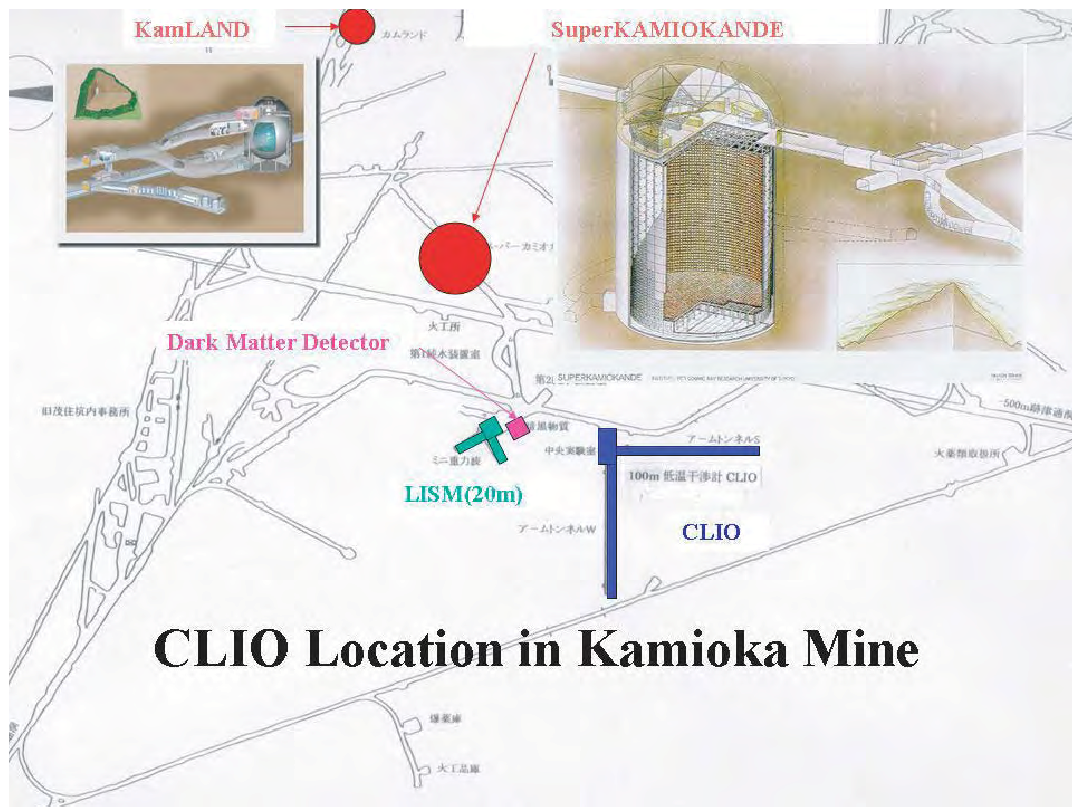


Fig. 8. Location of the CLIO interferometer.

sistent with the estimation of mirror thermal noise reduction due to cooling.

R&D: Local Suspension Point Interferometer

Local Suspension Point Interferometer (LSPI) is an active control system for a cryogenic mirror suspension system of CLIO. One set of LSPI has been installed in a cryostat of CLIO since 2010 and we successfully observed the damping effect in the room temperature as shown in Fig. 10. We found low effectiveness of a conventional magnet damping system for a cryogenic mirror suspension system, when the mirrors were at cryogenic temperature. Purpose of a damping system is to reduce amplitude of mirror motion. Without the damping system, it is impossible to keep a Fabry-Perot cavity on resonance. Thus, we have developed LSPI as a new damping system that is possible to use at cryogenic temperature. LSPI consists of a motion sensor using an interferometer and a feedback control system. The interferometer senses motion of a mass of the mirror suspension system. Feedback signal generated by the control system is converted to damping force by coil magnet actuators on the mass. Figure 10 shows transfer function of the mirror suspension system with and without LSPI in the room temperature. High Q factor resonances of 0.48Hz and 1.18Hz in the curve of without LSPI were clearly damped by LSPI.

Digital system in CLIO

The next generation interferometer for gravitational wave detection will have a very complicated control topology as called RSE (resonant sideband extraction) which has

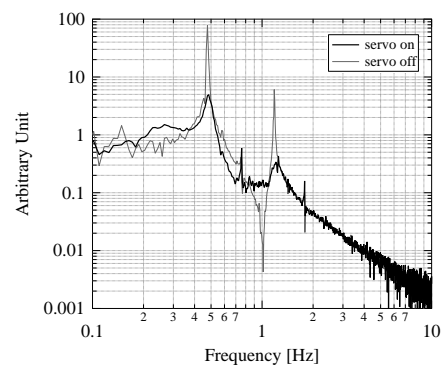


Fig. 10. Comparison with transfer function of a mirror suspension system with and without LSPI. There are two high Q resonances at 0.48Hz and 1.18Hz in the curve of without LSPI (servo off). Those resonances are damped by LSPI.

5 degrees of freedom for length control, ~ 40 degrees of freedom for alignment control, and ~ 100 degrees of freedom for local controls of damping suspensions. It is really important to implement a digital control system to deal with such a complicated interferometer since the digital system provides us a very flexible human interface. The flexibility leads a drastic reduction of time for noise hunting.

We developed a digital controls system for the gravitational wave detector by an international collaboration with LIGO group in the U.S and installed it into CLIO. This first system is a very simple standalone model to check the perfor-



Fig. 11. A sapphire mirror and cryogenic suspension system

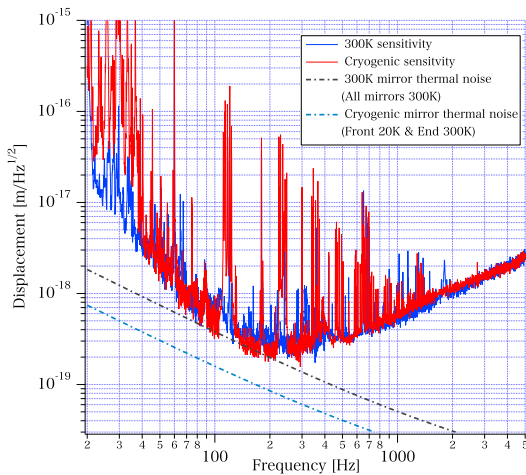


Fig. 12. Comparison of CLIO sensitivity curves. 300K sensitivity (solid blue line) and Cryogenic sensitivity (solid red line) show CLIO sensitivity curves without cooling mirrors measured at 2008/11/05 and with front mirrors under 20K measured at 2010/03/20, respectively. 300K mirror thermal noise (dot dash gray line) and Cryogenic mirror thermal noise (dot dash blue line) show estimation curve of mirror thermal noise corresponding to the each sensitivity measurements.

mance of digital system for noise, feasibility, flexibility and so on. This system consists of a computer, an I/O extension box, ADCs, DACs, and the related analog circuits like anti aliasing/imaging filters, whitening/dewhitening filters. The ADC has 32 differential channels and the DAC has 16 differential channels.

With this system we have established the lock acquisition of the single test mass control loop. The error signal of this arm motion is always monitored and calibrated into the sensitivity for gravitational waves. Using this ordinary sensitivity monitor, noise hunting has been performed very smoothly. It is known that the noise of ADC and DAC is typically 1000times higher than general analog circuits.

These noises have been effectively reduced using the whitening/dewhitening filterers. Finally we have shown the performance that the ADC and DAC noises are at least 10times lower than the best sensitivity of CLIO (See Fig. 13). Actually, the noise floor can be 10 times smaller if we use stronger whitening/dewhitening filters because we still can afford the dynamic range of whitening/dewhitening filters. We believe that this CLIO digital system showed an enough performance even for the km class interferometer like LCGT.

This digital control system has many number of input and output channels, so it can be used for many purposes, not only for the main arm length control. For example in CLIO, we implemented Mode Cleaner auto alignment, laser power controller injected into photo detector, local control system for LSPI which is used for the damping of mirror suspension, and so on. Currently we are planning to have an engineering observation run using this system to develop a data analysis environment including analysis software and data pipe line in this fiscal year.

This study at CLIO is a very good test bench for LCGT and it will lead not only a smooth installation of a full digital system into LCGT but also a smooth commissioning work for whole LCGT project.

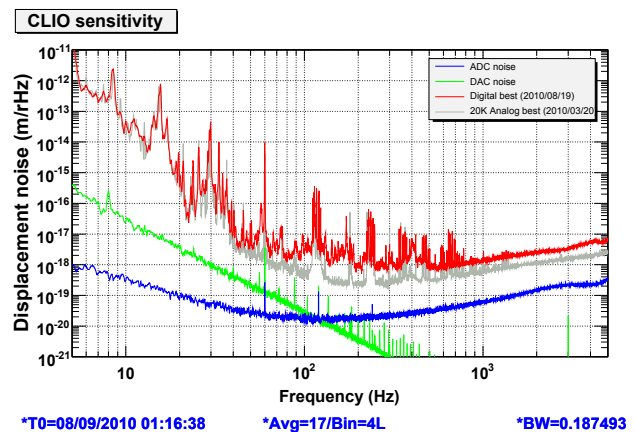


Fig. 13. Noise contribution of ADC and DAC noises. Green: DAC noise, blue: ADC noise, red: best sensitivity using digital servo, gray: best sensitivity of CLIO using analog servo. ADC and DAC noise is at least 10 times lower than CLIO best sensitivity.

Bibliography

- [1] S. Takemoto, *et al.*, Journal of Geodynamics **41** (2006) 23.
- [2] S. Miyoki, *et al.*, Journal of Physics: Conference Series **203** (2010) 012075.
- [3] R. W. P. Drever, *et al.*, Appl. Phys. B **31** (1983) 97-105.

Sloan Digital Sky Survey

Observational Cosmology

[Spokesperson : Masami Ouchi]

Statistics of 207 Ly α Emitters at a Redshift Near 7: Constraints on Reionization and Galaxy Formation Models

In collaboration with the members of Observatories of the Carnegie Institution of Washington, University of Tokyo, National Astronomical Observatory, IPMU, Tohoku University, ICRR, and Okayama Astrophysical Observatory

We have investigated Ly α luminosity function (LF), clustering, and Ly α line profiles based on the largest sample, to date, of 207 Ly α emitters (LAEs) at $z = 6.6$ on the 1-deg² sky of Subaru/XMM-Newton Deep Survey (SXDS) field (Fig. 1). Our $z = 6.6$ Ly α LF including cosmic variance estimates yields the best-fit Schechter parameters of $\phi^* = 8.5_{-2.2}^{+3.0} \times 10^{-4} \text{Mpc}^{-3}$ and $L_{\text{Ly}\alpha}^* = 4.4_{-0.6}^{+0.6} \times 10^{42} \text{erg s}^{-1}$ with a fixed $\alpha = -1.5$, and indicates a decrease from $z = 5.7$ at the $\gtrsim 90\%$ confidence level (Fig. 2). However, this decrease is not large, only $\simeq 30\%$ in Ly α luminosity, which is too small to be identified in the previous studies. A clustering signal of $z = 6.6$ LAEs is detected for the first time. We obtain the correlation length of $r_0 = 2 - 5 h_{100}^{-1} \text{Mpc}$ and bias of $b = 3 - 6$, and find no significant boost of clustering amplitude by reionization at $z = 6.6$. The average hosting dark halo mass inferred from clustering is $10^{10} - 10^{11} M_{\odot}$, and duty cycle of LAE population is roughly $\sim 1\%$ albeit with large uncertainties. The average of our high-quality Keck/DEIMOS spectra shows an FWHM velocity width of $251 \pm 16 \text{km s}^{-1}$. We find no large evolution of Ly α line profile from $z = 5.7$ to 6.6, and no anti-correlation between Ly α luminosity and line width at $z = 6.6$. The combination of various reionization models and our observational results about the LF, clustering, and line profile indicates that there would exist a small decrease of IGM's Ly α transmission owing to reionization, but that the hydrogen IGM is not highly neutral at $z = 6.6$ (Fig. 3). Our neutral-hydrogen fraction constraint implies that the major reionization process took place at $z \gtrsim 7$.

Bibliography

- [1] Ouchi, M., et al. 2010, *Astrophys. J.*, 723, 869
- [2] Ouchi, M., et al. 2008, *Astrophysical Journal Supplement*, 176, 301

The Subaru Ly α blob survey: A sample of 100 kpc Ly α blobs at $z = 3$

In collaboration with the members of Durham University, Tohoku University, Carnegie Institution of Washington, University of Tokyo, and University of Tsukuba.

We have conducted a survey for giant Ly α nebulae (LABs) at $z = 3$ with Subaru/Suprime-Cam. We obtained Ly α imaging at $z = 3.09 \pm 0.03$ around the SSA22 protocluster and

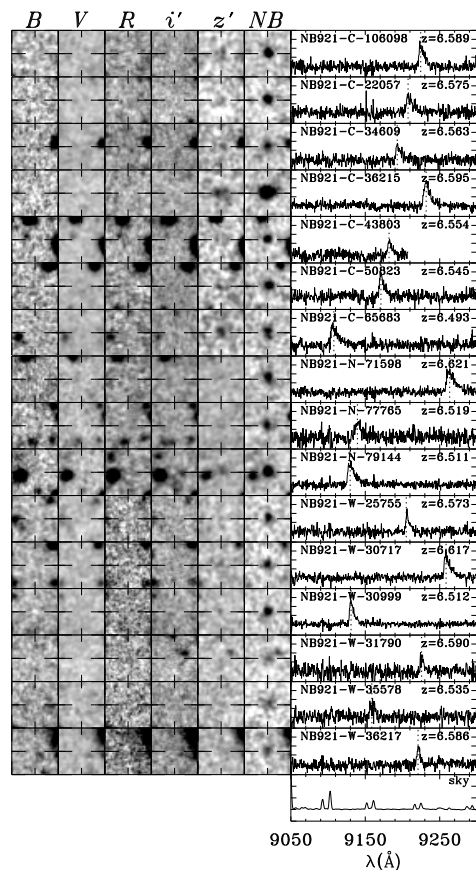


Fig. 1. Spectra and snapshots of some of our $z = 6.6$ LAEs confirmed with Keck/DEIMOS. Each object has a spectrum in the right panel and snapshots of B , V , R , i' , z' , and $NB921$ images in the left panels. Each snapshot is presented in a $6'' \times 6''$ box. The right bottom panel shows a typical DEIMOS spectrum of the sky background that is obtained in the process of sky subtraction. This figure is reproduced by permission of the AAS.

in several blank fields. The total survey area is 2.1 square degrees, corresponding to a comoving volume of $1.6 \times 10^6 \text{Mpc}^3$. Using a uniform detection threshold of $1.4 \times 10^{-18} \text{erg s}^{-1} \text{cm}^{-2} \text{arcsec}^{-2}$ for the Ly α images, we construct a sample of 14 LAB candidates with major-axis diameters larger than 100 kpc, including five previously known blobs and two known quasars. This survey triples the number of known LABs over 100 kpc. The giant LAB sample shows a possible "morphology-density relation": filamentary LABs reside in average density environments as derived from compact Ly α emitters, while circular LABs reside in both average density and overdense environments. Although it is hard to examine the formation mechanisms of LABs only from the Ly α morphologies, more filamentary LABs may relate to cold gas accretion from the surrounding inter-galactic medium (IGM) and more circular LABs may relate to large-scale gas outflows, which are driven by intense starbursts and/or by AGN activities. Our survey highlights the potential usefulness of giant LABs to investigate the interactions between galaxies and the surrounding IGM from the field to overdense environments at high-redshift.

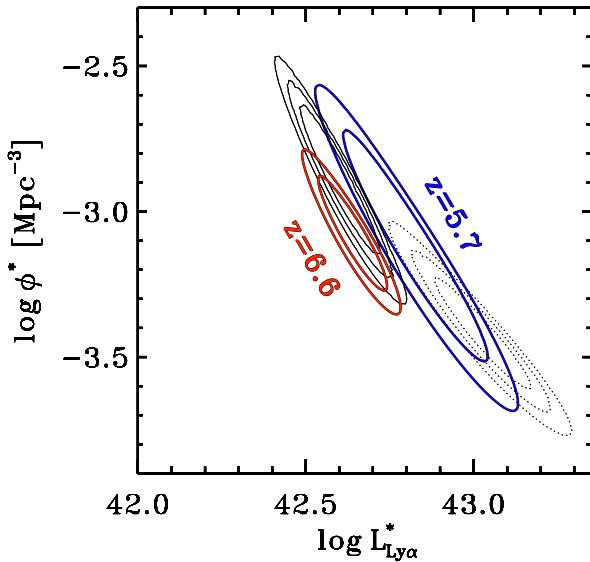


Fig. 2. Error ellipses of our Schechter parameters, $L_{\text{Ly}\alpha}^*$ and ϕ^* . Red contours represent the fit of $z = 6.6$ LF with the fixed slope of $\alpha = -1.5$ based on SXDS and SDF data. The inner and outer contours indicate 68% and 90% confidence levels, respectively, which include cosmic variance errors. Blue contours denote $z = 5.7$ LFs given by [2], which are similarly derived with cosmic variance errors. For a fair comparison with our $z = 6.6$ LF, we show error ellipses of the $z = 5.7$ LF derived by the classical method (see more details in [2]). The error ellipses of the $z = 5.7$ LF are larger than those of our $z = 6.6$ LF. This is because the data of $z = 5.7$ LF have more uncertainties of cosmic variance. Black solid and dotted lines indicate 1, 2, and 3 sigma confidence levels of $z = 6.6$ and $z = 5.7$ LFs with no cosmic variance errors previously derived solely with the smaller data of SDF. This figure is reproduced by permission of the AAS.

Bibliography

- [1] Matsuda, Y., et al. 2011, Monthly Notices of the Royal Astronomical Society, 410, L13

Keck Spectroscopy of Faint $3 < z < 7$ Lyman Break Galaxies:- II. A High Fraction of Line Emitters at Redshift Six

In collaboration with the members of University of Cambridge and California Institute of Technology.

As Lyman α photons are scattered by neutral hydrogen, a change with redshift in the Ly α equivalent width distribution of distant galaxies offers a promising probe of the degree of ionization in the intergalactic medium and hence when cosmic reionization ended. This simple test is complicated by the fact that Ly α emission can also be affected by the evolving astrophysical details of the host galaxies. In the first paper in this series, we demonstrated both a luminosity and redshift dependent trend in the fraction of Ly α emitters seen within color-selected ‘Lyman-break’ galaxies (LBGs) over the range $3 < z < 6$; lower luminosity galaxies and those at higher redshift show an increased likelihood of strong emission. We have studied the results from much deeper 12.5 hour exposures with the Keck DEIMOS spectrograph focused primarily on LBGs at $z \simeq 6$ which enable us to confirm the redshift de-

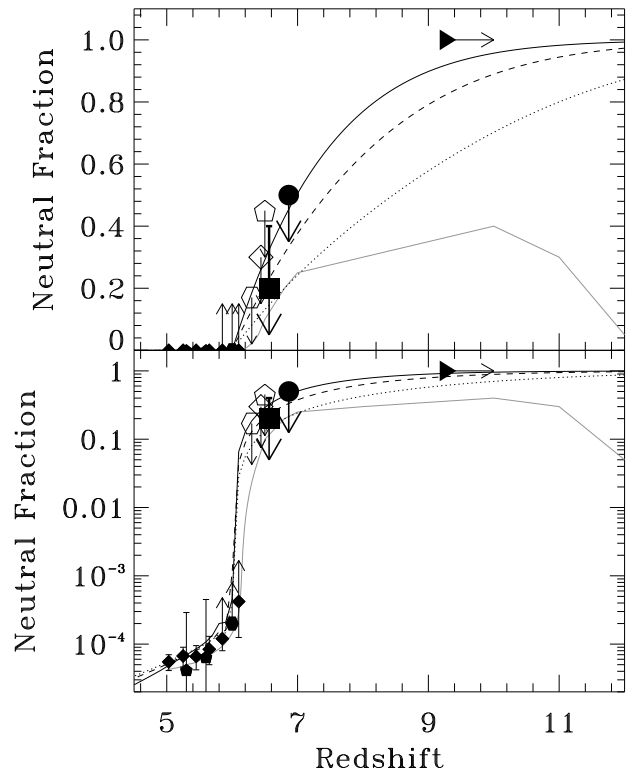


Fig. 3. Neutral hydrogen fraction, x_{HI} , of IGM as a function of redshift. Top and bottom panels are the same, but with a vertical axis of linear and log scales, respectively. Filled square and circle are the upper limits of x_{HI} that we obtain from the evolution of Ly α LF and clustering, respectively. Open symbols denote the upper limits from Ly α LF and Ly α damping wing of GRB given by the previous studies. Filled hexagon and pentagons indicate constraints given by GRB spectra and QSO dark gap statistics, respectively. Filled diamonds represent the measurements from GP optical depth of SDSS QSOs. Triangle plots the 1σ lower-limit of redshift of a neutral universe given by WMAP7 in the case of instantaneous reionization. Avoiding overlapping symbols, we give a small offset along redshift to the positions of the filled circle and the open diamond. Dotted, dashed, and solid lines show the evolution of x_{HI} for mini-halo, small, and large halo cases, respectively, predicted by the semi-analytic models. Gray solid line presents the prediction in the double reionization scenario suggested by the theoretical model. This figure is reproduced by permission of the AAS.

pendence of line emission more robustly and to higher redshift than was hitherto possible. We find $54 \pm 11\%$ of faint $z \simeq 6$ Lyman break galaxies show strong ($W_{\text{Ly}\alpha,0} > 25 \text{ \AA}$) emission, an increase of $1.6\times$ from a similar sample observed at $z \simeq 4$ (Fig. 4). With a total sample of 74 $z \simeq 6$ LBGs, we determine the luminosity-dependent Ly α equivalent width distribution. Assuming continuity in these trends to the new population of $z \simeq 7$ sources located with the Hubble WFC3/IR camera, we predict that unless the neutral fraction rises in the intervening 200 Myr, the success rate for spectroscopic confirmation using Ly α emission should be high.

Bibliography

- [1] Stark, D. P., Ellis, R. S., & Ouchi, M. 2011, Astrophys. J., 728, L2

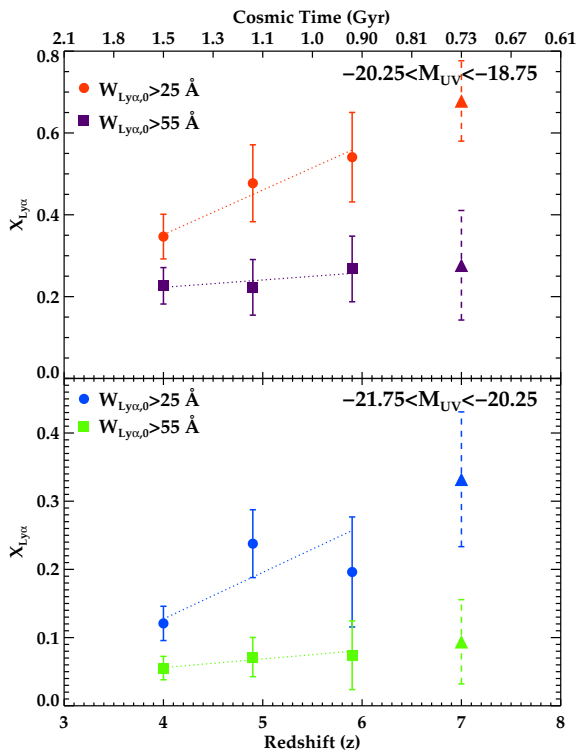


Fig. 4. Evolution in the overall fraction of Ly α emitters ($X_{Ly\alpha}$) in the LBG population over $4 < z < 6$. Luminous LBGs are considered in the bottom panel, and less luminous systems in the top panel. In each panel, we derive the Ly α fraction of LBGs with Ly α EWs larger than 25 Å (circles) and 55 Å (squares). Assuming a linear relationship between $X_{Ly\alpha}$ and z , we extrapolate these trends to $z \simeq 7$ (triangles with dashed-line error bars). This figure is reproduced by permission of the AAS.

Lyman- α Emitters and Lyman-break Galaxies at $z = 3 - 6$ in Cosmological SPH Simulations

In collaboration with the members of IPMU, University of Nevada Las Vegas, Observatories of the Carnegie Institution of Washington, Max-Planck-Institut für Astrophysik, and Harvard University.

We study the properties of Lyman- α emitters (LAEs) and Lyman-break galaxies (LBGs) at $z = 3 - 6$ using cosmological SPH simulations. We investigate two simple scenarios for explaining the observed Ly α and rest-frame UV luminosity functions (LFs) of LAEs: (i) the “*escape fraction*” scenario, in which the *effective* escape fraction (including the IGM attenuation) of Ly α photons is $f_{Ly\alpha} \approx 0.1$ (0.15) at $z = 3$ (6), and (ii) the “*stochastic*” scenario, in which the fraction of LAEs that are turned on at $z = 3$ (6) is $C_{stoc} \approx 0.07$ (0.2) after correcting for the IGM attenuation. Our comparisons with a number of different observations suggest that the stochastic scenario is preferred over the escape fraction scenario. We find that the mean values of stellar mass, metallicity and black hole mass hosted by LAEs are all smaller in the stochastic scenario than in the escape fraction scenario. In our simulations, the galaxy stellar mass function evolves rapidly, as expected in hierarchical structure formation. However, its evolution is largely compensated by a beginning decline in the specific star formation

rate, resulting in little evolution of the rest-frame UV LF from $z = 6$ to 3. The rest-frame UV LF of both LAEs and LBGs at $z = 3$ & 6 can be described well by the stochastic scenario provided the extinction is moderate, $E(B - V) \approx 0.15$, for both populations, although our simulation might be overpredicting the number of bright LBGs at $z = 6$. We also discuss the correlation function and bias of LAEs. The Ly α LFs at $z = 6$ in a field-of-view of 0.2 deg^2 show a significantly larger scatter owing to cosmic variance relative to that in a 1 deg^2 field, and the scatter seen in the current observational estimates of the Ly α LF can be accounted for by cosmic variance.

Bibliography

- [1] Nagamine, K., Ouchi, M., Springel, V., & Hernquist, L. 2010, Publications of the Astronomical Society of Japan, 62, 1455

Primary Cosmic Ray Group

[Spokesperson : H. Miyahara]

ICRR, Univ. of Tokyo, Kashiwa, Chiba 277-8582

Reconstruction of solar cycles at the grand solar minima

In collaboration with the members of Univ. of Tokyo, Yamagata Univ. Hirosaki Univ. and Australian National Univ.

Our group has been conducting the reconstruction of solar cycles during the prolonged sunspot absence such as the Maunder Minimum and the transitional periods, by measuring the cosmogenic nuclide in tree rings with annual resolution using the Accelerator Mass Spectrometer. It will provide a clue for understanding the mechanism of long-term changes in solar activity and constructing a methodology of forecasting near future solar activity. For this study, trees from Yaku Island, Nara prefecture, Aomori prefecture and Shizuoka Prefecture have been used. We use the Accelerator Mass Spectrometers at the University of Tokyo, Yamagata University and The Australian National University. We have detected the deviations of solar cycle lengths from 11 years around the two preceding cycles of grand solar minima, although the characteristics may be different by the duration of event (Miyahara et al., 2010).

Bibliography

- [1] H. Miyahara, K. Kitazawa, K. Nagaya, Y. Yokoyama, H. Matsuzaki, K. Masuda, T. Nakamura, and Y. Muraki, Journal of Cosmology, 8 (2010) 1970.

Long-term changes in solar modulation of galactic cosmic rays in the heliosphere and their influence on climate change

In collaboration with the members of Univ. of Tokyo, Nagoya Univ. Hirosaki Univ. and National Institute of Polar Research.

We have investigated solar modulation of galactic cosmic rays around the Maunder Minimum based on beryllium-10

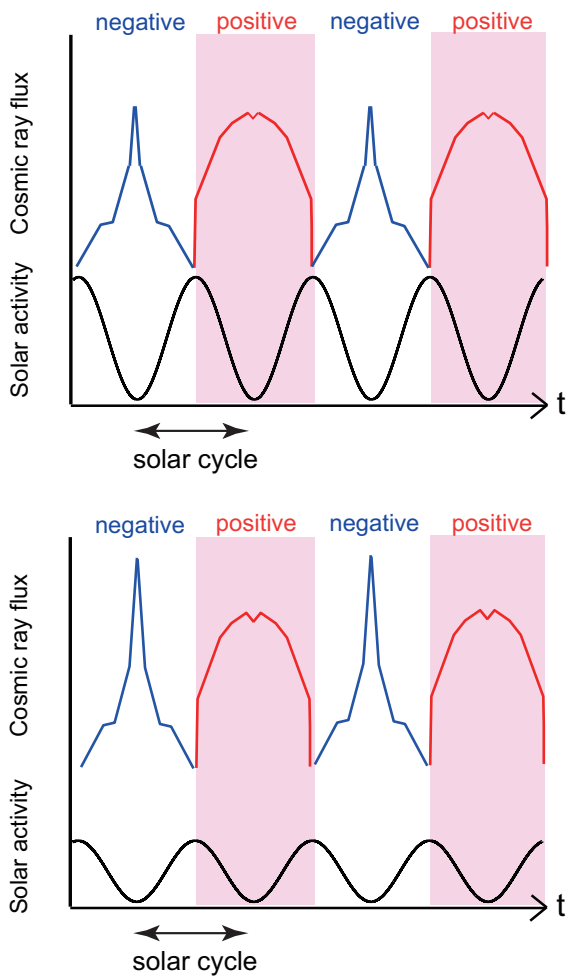


Fig. 1. Model of cosmic ray variations at present (above) and at the Maunder Minimum (below) (Miyahara et al., 2009) estimated based on the results of numerical simulation of solar modulation by Kota and Jokipii (2001). For the Maunder Minimum, the range of the tilt angle is assumed to be 0-75 degrees. For this case, the variability of cosmic rays at negative solar polarity get anomalously increased, resulting in the amplification of the 22-year cosmic-ray cycles.

records from ice cores. Variation of beryllium-10 content provides the information on the state of solar modulation of cosmic rays at sunspot absence, and thus the state of solar magnetic field and the heliosphere. We find that the variation of cosmic rays associated with solar polarity reversals were unique at the Maunder Minimum. About 30-50

Bibliography

- [1] H. Miyahara, Y. Yokoyama, and Y. T. Yamaguchi, Proceedings of the IAU symposium No. 264, (2009) 427.
- [2] Y. T. Yamaguchi, Y. Yokoyama, H. Miyahara, K. Sho and T. Nakatsuka, Synchronized Northern Hemisphere Climate Change and Solar Magnetic Cycles during the Maunder Minimum, Proceedings of the National Academy of Sciences, (2010) doi: 10.1073/pnas.1000113107.

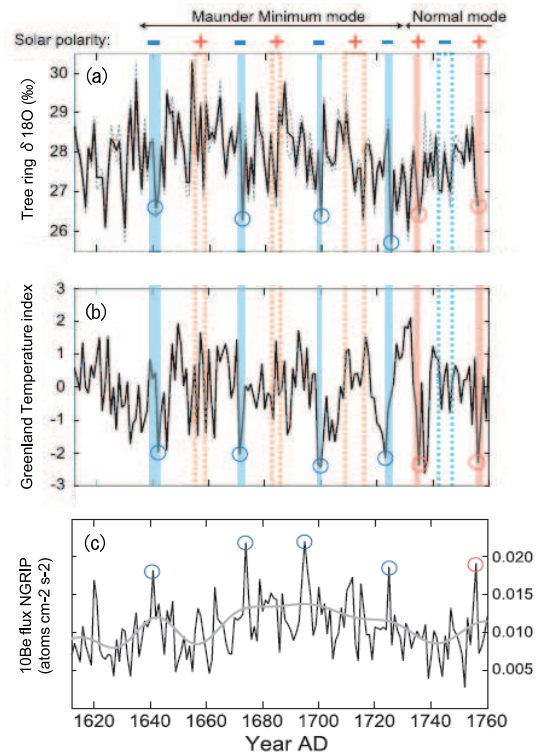


Fig. 2. Comparison of cosmic rays and reconstructed climate around the Maunder Minimum (Yamaguchi et al., 2010). (a) Reconstructed relative humidity in Japan around June. (b) Reconstructed temperature based on oxygen-18/oxygen-16 ratio in the Greenland ice core by Vinther et al. (2003). (c) Beryllium-10 record from Greenland ice core by Berggren et al. (2009). The blue shaded areas correspond to the solar cycle minima of polarity negative determined by carbon-14 record.

Influence of solar rotation on the tropical convective clouds

In collaboration with the members of Univ. of Tokyo and Hokkaido Univ.

We have examined the influence of the 27-day rotation of the Sun on cloud formation. Total solar Irradiance (TSI), solar ultraviolet (UV), and galactic cosmic rays change in association with the 27-day rotation of the Sun. The variability of solar-related parameters at a range of 27-day period tends to be larger at solar maximal periods. We have found that the 27-day solar rotational period affect cloud activity around the Western Pacific Warm Pool (WPWP) and Indian Ocean. The generation of 30-60 day period in cloud activity called as Madden-Julian Oscillation (MJO) in tropics has not been well understood. We suggest that its rhythm is under the control of periodic variation of solar related parameters. Our study also suggests that the areas 27-day variations are detected are influenced by the two phases of Quasi-Biennial Oscillation (QBO) in the stratosphere (Fig. 3).

Bibliography

- [1] Y. Takahashi, Y. Okazaki, M. Sato, H. Miyahara, K. Sakanoi, and P. K. Hong, Atmospheric Chemistry and Physics **10** (2010), 290.

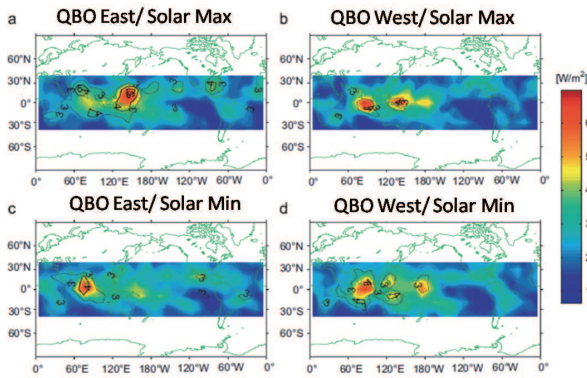


Fig. 3. Power of the 27-day periodicity in cloud activity for solar maxima/solar minima and for QBO easterly/westerly phases.

- [2] P. K. Hong, H. Miyahara, Y. Yokoyama, Y. Takahashi, M. Sato, Implications for the low latitude cloud formations from solar activity and the Quasi-Biennial Oscillation, *Journal of Atmospheric and Solar-Terrestrial Physics* (2011), doi:10.1016/j.jastp.2010.11.026.

Reconstruction of climate change based on stable isotopes in tree rings

In collaboration with the members of Univ. of Tokyo, Nagoya Univ. and Tokyo Institute of Technology.

We are now conducting the measurements of multiple stable isotopes in tree rings from Japan in order to reconstruct the climate changes during the past two millenia in Japan. We have mainly conducting measurements using the 1850-year old cedar tree from Yakushima (Fig. 4) as well as the recent 150-year trees from the same area for the calibration.



Fig. 4. Japanese cedar tree used in this study. The tree has been obtained from the Yaku Island.

Deriving Historical Total Solar Irradiance from Lunar Borehole Temperatures

In collaboration with the members of JAXA and NASA/Goddard Space Flight Center.

As the Moon lacks atmosphere as well as any influence of human activities, lunar borehole temperatures are primarily driven by changes in solar irradiance. Variations of total solar irradiance (TSI), directly measured by radiometers flown onboard several satellites in recent decades, have provided a

reliable short-term record of variations since 1978. However, this instrumental record has not yet led to a consensus result for solar variations on multi-decadal and longer timescales. It is important to clarify the actual variability of TSI in terms of distinguishing the contribution of change in TSI to the Little Ice Age. We have conducted the re-analysis of thermal properties of lunar regolith obtained by the Apollo Heat Flow Experiments, and conducted numerical simulations of heat flow in the regolith. We have shown that the historical changes in Total Solar Irradiance can be distinguished by small but potentially detectable differences in temperature, on the order of 0.01 K and larger depending on latitude, within 10 m depth of the Moon's surface (Fig. 5). In order to accomplish this experiment, we are now conducting discussions on the possible future missions. We are now discussing the potential preliminary mission for shallower depth at the next Japanese lunar landing mission.

Bibliography

- [1] H. Miyahara, G. Web, and R. F. Cahalan, *Geophysical Research Letters* **35** (2008), L02716.

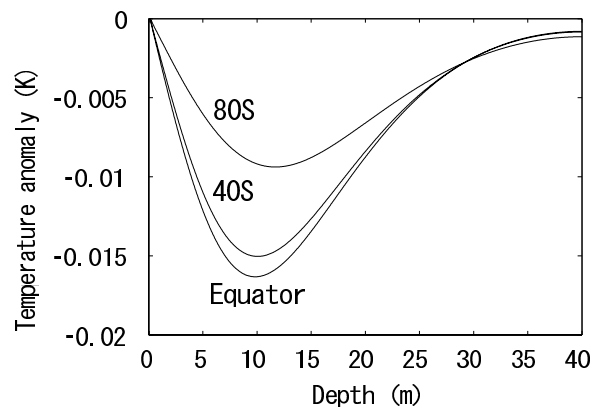


Fig. 5. Temperature anomalies in lunar regolith as response to 2 W/m² difference in total solar irradiance at the Maunder Minimum, at the equator, mid-latitude (40S) and near the south pole (80S) (Miyahara et al., 2008).

Theory Group

We have studied particle physics (mainly particle physics phenomenology) and astroparticle physics (mainly particle cosmology).

The supersymmetric (SUSY) extension of the standard model (SM) in the particle physics is considered to be one of the most promising models beyond the standard model. It solves the naturalness problem for the Higgs boson mass term in the standard model, and it is also compatible with the grand unified theories (GUTs). Our group has been studying phenomenological and cosmological aspects of the SUSY models.

Recent cosmological observations determine precisely the mean densities of matter and baryon in the Universe, and existence of non-baryonic dark matter is established. Weakly interacting massive particles (WIMPs) are considered to be

good candidates of the dark matter. They act as the cold dark matter in the structure formation of the universe. Our group has been studying model building for dark matter and detectability in direct and indirect search experiments.

For understanding of the early universe, a role of the elementary particle physics is crucial. Recent progress in the particle physics such as grand unification theories and supersymmetry leads us to a more deeper insight into the fundamental aspects of the early universe. In the inflationary universe, the quantum fluctuations of the scalar field which drives the inflation become the density fluctuations and lead to formation of the structure observed in the present universe. On the other hand cosmology and astrophysics are used to test new theories in particle physics. Such particle cosmology is one of main subjects of our group.

Big Bang Nucleosynthesis (BBN) is one of the most important subjects in modern cosmology. Predicted abundances of the light elements are very sensitive to the cosmological scenario. On the other hand, physics beyond the standard model predicts the new particles which would have existed at the BBN epoch. Such particles may spoil the success of BBN, which leads to constraints on the new particles and the particle physics models.

The grand unified theories (GUT) predict that our universe undergoes several vacuum phase transitions. In the course of phase transitions topological defects (monopoles, cosmic strings and domain walls) are generally produced depending on symmetries of the vacua. Our group has studied evolution of various topological defects.

Particle Phenomenology

[Spokesperson : J. Hisano]

Gluon contribution to dark matter direct detection

In collaboration with the members of ICRR, Nagoya University, IPMU, California Institute of Technology, University of Tokyo, and MISC .

We calculate the nucleon-dark matter elastic scattering cross section at the leading order of the strong coupling constant α_s , which is relevant to the dark matter direct detection experiments. Our approach based on the effective field theory reveals that the interaction of dark matter with gluon as well as quarks yields sizable contribution to the scattering cross section, though the gluon contribution is induced at loop level. In the evaluation of the contribution, we treat separately the loop diagrams whose typical loop momentum scales are the masses of quarks and other heavier particles. Then, we have properly taken into account each contribution and completed formulae for the cross section. As an application of our formulae, we study the direct detection of pure bino[1] and wino dark matter[1, 2] in the supersymmetric model, and the first Kaluza-Klein photon dark matter in the minimal universal extra dimension model[3]. It is found that there is a substantial difference between all of the results and those in the previous works. In the wino dark matter scenario we find the cross sec-

tion is smaller than the previous results by more than an order of magnitude, while the cross section of the first Kaluza-Klein photon dark matter turns out to be larger by up to a factor of ten.

Bibliography

- [1] J. Hisano, K. Ishiwata and N. Nagata, Phys. Rev. D **82** (2010) 115007 [arXiv:1007.2601 [hep-ph]].
- [2] J. Hisano, K. Ishiwata and N. Nagata, Phys. Lett. B **690** (2010) 311 [arXiv:1004.4090 [hep-ph]].
- [3] J. Hisano, K. Ishiwata, N. Nagata and M. Yamanaka, arXiv:1012.5455 [hep-ph].

Direct Detection of Electroweak-Interacting Dark Matter

In collaboration with the members of ICRR .

Assuming that the lightest neutral component in an $SU(2)_L$ gauge multiplet is the main ingredient of dark matter in the universe, we calculate the elastic scattering cross section of the dark matter with nucleon, which is an important quantity for the direct detection experiments. When the dark matter is a real scalar or a Majorana fermion which has only electroweak gauge interactions, the scattering with quarks and gluon are induced through one- and two-loop quantum processes, respectively, and both of them give rise to comparable contributions to the elastic scattering cross section. We evaluate all of the contributions at the leading order and find that there is an accidental cancellation among them. As a result, the spin-independent cross section is found to be $\mathcal{O}(10^{-(46-48)}) \text{ cm}^2$, which is far below the current experimental bounds.

Bibliography

- [1] J. Hisano, K. Ishiwata, N. Nagata, T. Takesako, [arXiv:1104.0228 [hep-ph]].

Astrophysics and Cosmology

[Spokesperson : M. Kawasaki]

Kahler moduli double inflation

In collaboration with the members of ICRR.

We show that double inflation is naturally realized in Kähler moduli inflation, which is caused by moduli associated with string compactification. We find that there is a small coupling between the two inflatons which leads to amplification of perturbations through parametric resonance in the intermediate stage of double inflation. This results in the appearance of a peak in the power spectrum of the primordial curvature perturbation. We numerically calculate the power spectrum and show that the power spectrum can have a peak on observationally interesting scales. We also compute the TT-spectrum of CMB based on the power spectrum with a peak and see that it better fits WMAP 7-years data.

Bibliography

- [1] M. Kawasaki and K. Miyamoto, JCAP **1102**, 004 (2011) [arXiv:1010.3095 [astro-ph.CO]].

Inflation from a Supersymmetric Axion Model

In collaboration with the members of ICRR and Tohoku Univ.

We show that a supersymmetric axion model naturally induces a hybrid inflation with the waterfall field identified as a Peccei-Quinn scalar. The Peccei-Quinn scale is predicted to be around 10^{15} GeV for reproducing the large-scale density perturbation of the Universe. After the built-in late-time entropy-production process, the axion becomes a dark matter candidate. Several cosmological implications are discussed.

Bibliography

- [1] M. Kawasaki, N. Kitajima and K. Nakayama, Phys. Rev. D **82**, 123531 (2010) [arXiv:1008.5013 [hep-ph]].

Prospects for Direct Detection of Inflationary Gravitational Waves by Next Generation Interferometric Detectors

In collaboration with the member of ICRR, Nihon Univ. and Nagoya Univ.

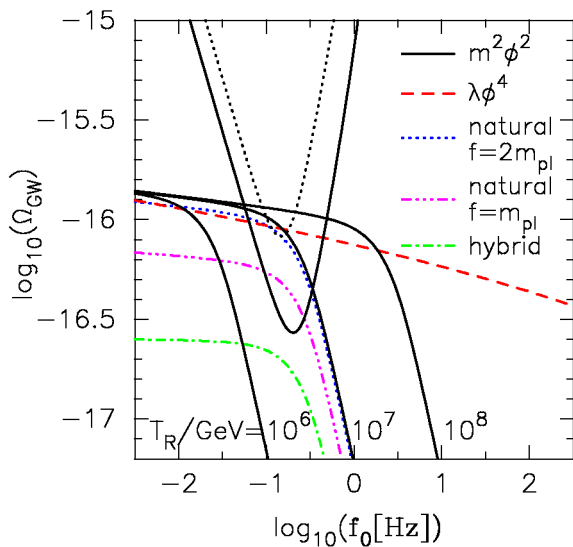


Fig. 1. Spectra of the gravitational wave background for different inflation models and different reheating temperatures $T_{RH} = 10^6, 10^7, 10^8$ GeV, shown with the sensitivity curves of DECIGO (dotted) and BBO (solid).

We study the potential impact of detecting the inflationary gravitational wave background by the future space-based gravitational wave detectors, such as DECIGO and BBO. The signal-to-noise ratio of each experiment is calculated for chaotic/natural/hybrid inflation models by using the precise predictions of the gravitational wave spectrum based on numerical calculations. We investigate the dependence of each

inflation model on the reheating temperature which influences the amplitude and shape of the spectrum, and find that the gravitational waves could be detected for chaotic/natural inflation models with high reheating temperature. From the detection of the gravitational waves, a lower bound on the reheating temperature could be obtained. The implications of this lower bound on the reheating temperature for particle physics are also discussed.

Bibliography

- [1] S. Kuroyanagi, T. Chiba and N. Sugiyama, Phys. Rev. D **83**, 043514 (2011) [arXiv:1010.5246 [astro-ph.CO]].

Effects of Light Fields During Inflation

In collaboration with the member of IPMU.

In the inflationary universe, there can be light fields other than the inflaton. We explore a possibility that such light fields source the primordial perturbations, while minimally affecting the inflaton dynamics. We show that during inflation, fluctuations of the light fields can be converted to adiabatic curvature perturbations, which accumulate and become significant by the end of the inflationary era. An additional goal of this work is to distinguish between light fields which can/cannot be ignored during inflation. Such criteria become useful for examining cosmological scenarios with multiple fields. As concrete examples, our results are applied to D-brane inflation models. We consider effects from KK modes (oscillation modes) of wrapped branes in monodromy-driven large-field models, and angular directions of throat geometries in warped D-brane inflation.

Bibliography

- [1] T. Kobayashi and S. Mukohyama, Phys. Rev. D **81**, 103504 (2010) [arXiv:1003.0076 [astro-ph.CO]].

Non-Gaussianity from Lifshitz Scalar

In collaboration with the members of IPMU.

A Lifshitz scalar with the dynamical critical exponent $z = 3$ obtains scale-invariant, super-horizon field fluctuations without the need of an inflationary era. Since this mechanism is due to the special scaling of the Lifshitz scalar and persists in the presence of unsuppressed self-couplings, the resulting fluctuation spectrum can deviate from a Gaussian distribution. We study the non-Gaussian nature of the Lifshitz scalar's intrinsic field fluctuations, and show that primordial curvature perturbations sourced from such field fluctuations can have large non-Gaussianity of order $f_N L = O(100)$, which will be detected by upcoming CMB observations. We compute the bispectrum and trispectrum of the fluctuations, and discuss their configurations in momentum space. In particular, the bispectrum is found to take various shapes, including the local, equilateral, and orthogonal shapes. Intriguingly, all integrals in the in-in formalism can be performed analytically.

Bibliography

- [1] K. Izumi, T. Kobayashi and S. Mukohyama, JCAP **1010**, 031 (2010) [arXiv:1008.1406 [hep-th]].

Running Spectral Index from Inflation with Modulations

In collaboration with the member of IPMU.

We argue that a large negative running spectral index, if confirmed, might suggest that there are abundant structures in the inflaton potential, which result in a fairly large (both positive and negative) running of the spectral index at all scales. It is shown that the center value of the running spectral index suggested by the recent CMB data can be easily explained by an inflaton potential with superimposed periodic oscillations. In contrast to cases with constant running, the perturbation spectrum is enhanced at small scales, due to the repeated modulations. We mention that such features at small scales may be seen by 21 cm observations in the future.

Bibliography

- [1] T. Kobayashi and F. Takahashi, JCAP **1101**, 026 (2011) [arXiv:1011.3988 [astro-ph.CO]].

Destruction of ${}^7\text{Be}$ in big bang nucleosynthesis via long-lived sub-strongly interacting massive particles as a solution to the Li problem

In collaboration with the members of ICRR.

We identify reactions which destroy $\text{Be}7$ and $\text{Li}7$ during big bang nucleosynthesis (BBN) in the scenario of BBN catalyzed by a long-lived sub-strongly-interacting massive particle (sub-SIMP or X particle). The destruction associated with nonradiative X captures of the nuclei can be realized only if the interaction strength between an X particle and a nucleon is properly weaker than that between two nucleons to a degree depending on the mass of X. Binding energies of nuclei to an X particle are estimated taking the mass and the interaction strength to nuclei of the X as input parameters. Nuclear reaction rates associated with the X are estimated naively and adopted in calculating evolutions of nuclear abundances. We suggest that the $\text{Li}7$ problem, which might be associated with as-yet-unrecognized particle processes operating during BBN, can be solved if the X particle interacts with nuclei strongly enough to drive $\text{Be}7$ destruction but not strongly enough to form a bound state with $\text{He}4$ of relative angular momentum $L=1$. Justifications of this scenario by rigorous calculations of reaction rates using quantum mechanical many-body models are highly desirable since this result involves many significant uncertainties.

Bibliography

- [1] M. Kawasaki and M. Kusakabe, Phys. Rev. D **83**, 055011 (2011) [arXiv:1012.0435 [hep-ph]].

Quantum Statistical Corrections to Astrophysical Photodisintegration Rates

In collaboration with the members of Univ. Notre Dame, Mimar Sinan Fine Arts Univ. Besiktas, NAOJ, Univ. Tokyo, Univ. Wisconsin, Madison and ICRR.

Tabulated rates for astrophysical photodisintegration reactions make use of Boltzmann statistics for the photons involved as well as the interacting nuclei. We derive analytic corrections for the Planck-spectrum quantum statistics of the photon energy distribution. We show that these corrections affect not only the photodisintegration rates but also modify the conditions of nuclear statistical equilibrium as represented in the Saha equation. We deduce new analytic corrections to the classical Maxwell-Boltzmann statistics which can easily be added to the reverse reaction rates of existing reaction network tabulations. We show that the effects of quantum statistics, though generally quite small, always tend to speed up photodisintegration rates and are largest for nuclei and environments for which $Q/kT \ll 1$. As an illustration, we examine possible effects of these corrections on the r-process, the rp-process, explosive silicon burning, the α -process, and big bang nucleosynthesis. We find that in most cases one is quite justified in neglecting these corrections. The correction is largest for reactions near the drip line for an r-process with very high neutron density, or an rp-process at high temperature.

Bibliography

- [1] G. J. Mathews, Y. Pehlivan, T. Kajino, A. B. Balantekin and M. Kusakabe, Astrophys. J. **727**, 10 (2011) [arXiv:1012.0519 [astro-ph.SR]].

Cosmological constraints on dark matter models with velocity-dependent annihilation cross section

In collaboration with the member of ICRR, Nagoya Univ. KEK, and Tokyo Univ.

We derive cosmological constraints on the annihilation cross section of dark matter with velocity-dependent structure, motivated by annihilating dark matter models through Sommerfeld or Breit-Wigner enhancement mechanisms. In models with annihilation cross section increasing with decreasing dark matter velocity, big-bang nucleosynthesis and cosmic microwave background give stringent constraints.

Bibliography

- [1] J. Hisano, M. Kawasaki, K. Kohri, T. Moroi, K. Nakayama and T. Sekiguchi, Phys. Rev. D **83**, 123511 (2011) [arXiv:1102.4658 [hep-ph]].

Improved estimation of radiated axions from cosmological axionic strings

In collaboration with the member of ICRR, Kyoto Univ. Tokyo Inst. Tech. and Tokyo Univ.

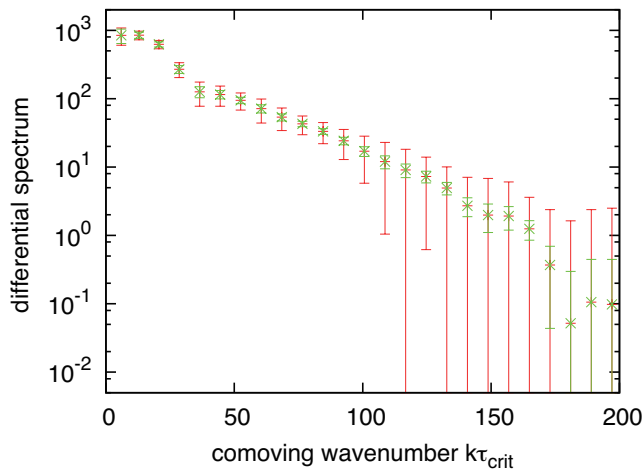


Fig. 2. Differential energy spectrum of radiated axions. Green (red) bars correspond to statistical errors alone (statistical and systematic errors). τ_{crit} is the conformal time at the phase transition. The scale in y -axis is arbitrary.

Cosmological evolution of axionic string network is analyzed in terms of field-theoretic simulations in a box of 512^3 grids, which are the largest ever, using a new and more efficient identification scheme of global strings. The scaling parameter is found to be $\xi = 0.87 \pm 0.14$ in agreement with previous results. The energy spectrum is calculated precisely using a pseudo power spectrum estimator which significantly reduces the error in the mean reciprocal comoving momentum. The resultant constraint on the axion decay constant leads to $f_a \leq 3 \times 10^{11}$ GeV. We also discuss implications for the early Universe.

Bibliography

- [1] T. Hiramatsu, M. Kawasaki, T. Sekiguchi, M. Yamaguchi and J. Yokoyama, arXiv:1012.5502 [hep-ph].

Evolution of string-wall networks and axionic domain wall problem

In collaboration with the members of ICRR and Tohoku Univ.

We study the cosmological evolution of domain walls bounded by strings which arise naturally in axion models. If we introduce a bias in the potential, walls become metastable and finally disappear. We perform two dimensional lattice simulations of domain wall networks and estimate the decay rate of domain walls. By using the numerical results, we give a constraint for the bias parameter and the Peccei-Quinn scale. We also discuss the possibility to probe axion models by direct detection of gravitational waves produced by domain walls.

Bibliography

- [1] T. Hiramatsu, M. Kawasaki and K. Saikawa, [arXiv:1012.4558 [astro-ph.CO]].

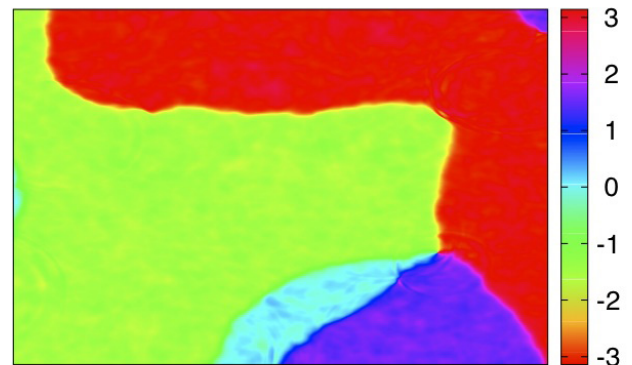
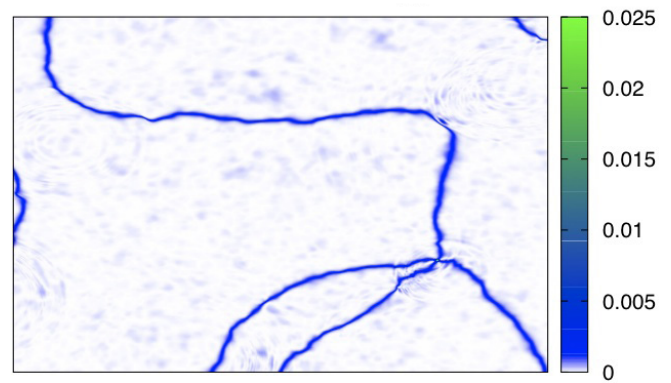


Fig. 3. The distribution of the potential energy and the phase of the PQ field.

Study of gravitational radiation from cosmic domain walls

In collaboration with the members of ICRR and Tohoku Univ.

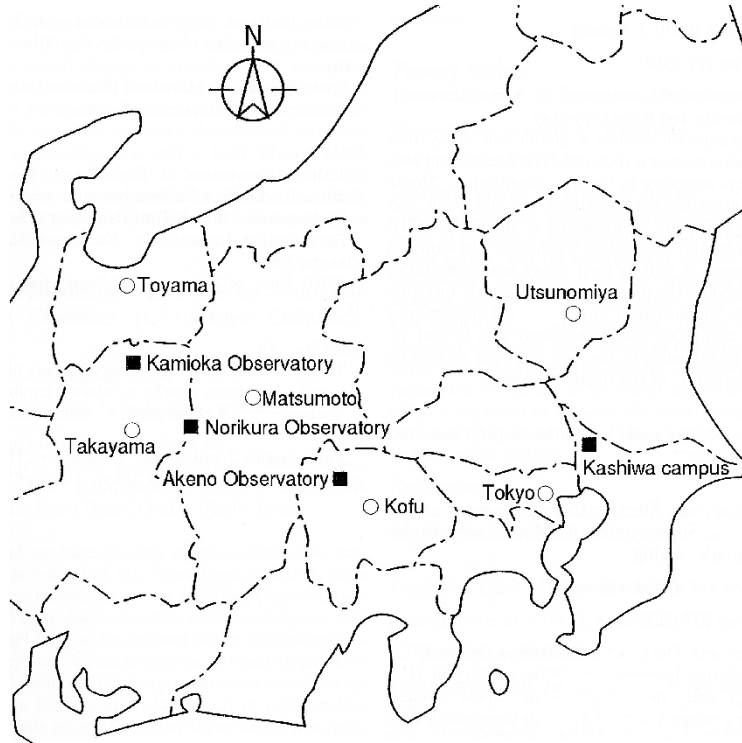
In this work, following the previous study, we evaluate the spectrum of gravitational wave background generated by domain walls which are produced if some discrete symmetry is spontaneously broken in the early universe. We apply two methods to calculate the gravitational wave spectrum: One is to calculate the gravitational wave spectrum directly from numerical simulations, and another is to calculate it indirectly by estimating the unequal time anisotropic stress power spectrum of the scalar field. Both analyses indicate that the slope of the spectrum changes at two characteristic frequencies corresponding to the Hubble radius at the decay of domain walls and the width of domain walls, and that the spectrum between these two characteristic frequencies becomes flat or slightly red tilted. The second method enables us to evaluate the GW spectrum for the frequencies which can not be resolved in the finite box lattice simulations, but relies on the assumptions for the unequal time correlations of the source.

Bibliography

- [1] M. Kawasaki and K. Saikawa, [arXiv:1102.5628 [astro-ph.CO]].

OBSERVATORIES and A RESEARCH CENTER

Location of the Institute and the Observatories in Japan



Norikura Observatory

Location: Iwaitani, Nyukawa-cho, Takayama-shi, Gifu Prefecture 506-2254
 N $36^{\circ}06'$, E $137^{\circ}33'$, 2770 m a.s.l.
 Telephone (Fax): +263-33-7456
 Telephone (satellite): 090-7721-5674
 Telephone (car): 090-7408-6224

Akeno Observatory

Location: 5259 Asao, Akeno-machi, Hokuto-shi, Yamanashi Prefecture 407-0201
 N $35^{\circ}47'$, E $138^{\circ}30'$, 900 m a.s.l.
 Telephone / Fax: +551-25-2301 / +551-25-2303

Kamioka Observatory

Location: 456 Higashi-mozumi, Kamioka-cho, Hida-shi, Gifu Prefecture 506-1205
 N $36^{\circ}25'26''$, E $137^{\circ}19'11''$, 357.5 m a.s.l.
 Telephone / Fax: +578-85-2116 / +578-85-2121

Research Center for Cosmic Neutrinos

Location: 5-1-5 Kashiwanoha, Kashiwa, Chiba Prefecture 277-8582
 Telephone / Fax: +4-7136-3138 / +4-7136-3115

NORIKURA OBSERVATORY

Introduction

Norikura Observatory (36.10°N and 137.55°E) was founded in 1953 and attached to ICRR in 1976. It is located at 2770 m above sea level, and is the highest altitude manned laboratory in Japan. Experimental facilities of the laboratory are made available to all the qualified scientists in the field of cosmic ray research and associated subjects. The AC electric power is generated by the dynamo and supplied throughout the observatory. In 1996, two dynamos of 70 KVA each were replaced with the new ones. The observatory can be accessed easily by car and public bus in summer (July-September). The 50th anniversary of Norikura Observatory was celebrated in 2003.

The feasibility of the automatic operation of Norikura Observatory during winter period has been tested since winter 2004 in order to study the possibilities to reduce maintenance and labor costs without seriously damaging to the use of researches. A long-distance (~40km) wireless LAN system (11M bps) was set up in 2003. Two new easy-to-handle and easy-to-maintain dynamos of 115 KVA each were installed in 2004 as well. The unmanned operation of Norikura Observatory was successful in the first winter, during which the battery backed-up solar panels and/or wind power generators kept supplying the electricity to the wireless LAN and on-going cosmic-ray experiments.

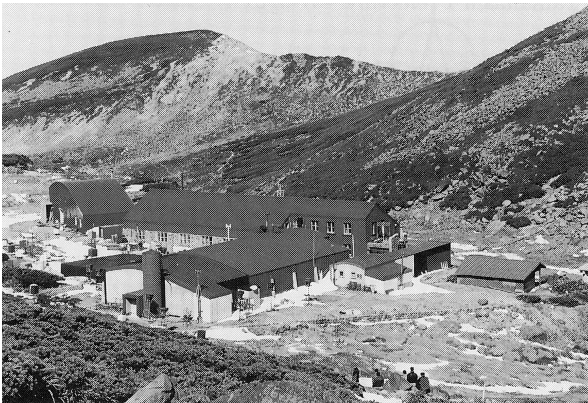


Fig. 1. Norikura Observatory.

Present major scientific interests of the laboratory is focused on the modulation of high energy cosmic rays in the interplanetary space associated with the solar activity and the generation of energetic particles by the solar flares, both of which require long-term monitoring. This research has been carried out by the group of universities, where ICRR provides them with laboratory facility. A part of the facility has been open for the environmental study at high altitude such as the aerosol removal mechanism in the atmosphere or for the botanical study of the high altitude environment.

Cosmic Ray Physics

For the modulation study[2], two small experiments have been operated continuously for a long time. One is a neutron monitor operated to study the correlation of solar activity and the cosmic ray flux. The other is a high counting muon telescope consisting of 36 m² scintillation counters to study the time variation of cosmic rays with energies of 10–100 TeV over 20 years. The neutron monitor data are open to researchers worldwide as a world observation network point (WDC). The 5 years from 2000 corresponded to the solar maximum (2000) to a declining phase in the solar cycle 23. The sun spot number in 2004 is approximately one fourth of the those at maximum. Nonetheless, there occurred active cosmic-ray phenomena associated with Coronal Mass Ejection (CME). As regards solar cosmic rays, although many ground level enhancement (GLE) phenomena took place every year, such GLEs were observed only by neutron monitors in Japan, as the maximum cosmic-ray energy was several GeV in the GLEs and the magnetic rigidity cutoff in Japan is approximately 10 GeV for charged particles initiating secondary muons. The sunspot numbers in the solar cycle 23 was smaller than those in the previous cycle 22, indicating less solar activities of cycle 23. Although the GLEs above 10 GeV were not observed in cycle 23, the total number of GLEs were greater in cycle 23 than in cycle 22. This suggests that the charged particle acceleration associated with CME was less frequent in the cycle 23 than in the cycle 22. On the other hand, Forbush decreases in galactic cosmic rays caused by CME in the Sun were observed frequently in cycle 23, though the solar activities have been in a declining phase since 2000. The worldwide observation of Forbush decreases may contribute significantly to space weather study.

In addition, space weather observation is actively made by a 25 m² muon hodoscope at Norikura Observatory[1], [2],[3],[4],[5], [6],[7],[8]. A loss cone anisotropy is observed by a ground-based muon hodoscope in operation at Norikura Observatory in Japan for 7 hours preceding the arrival of an interplanetary shock at Earth on October 28, 2003. Best fitting a model to the observed anisotropy suggests that the loss cone in this event has a rather broad pitch-angle distribution with a half-width about 50° from the interplanetary magnetic field (IMF). According to numerical simulations of high-energy particle transport across the shock, this implies that the shock is a "quasi-parallel" shock in which the angle between the magnetic field and the shock normal is only 6°. It is also suggested that the leadtime of this precursor is almost independent of the rigidity and about 4 hour at both 30 GV for muon detectors and 10 GV for neutron monitors (see paper [7]).

The Sun is the nearest site to the Earth capable of accelerating particles up to high energies. When the Sun becomes active, flares are frequently observed on its surface. The flare accelerates the proton and ion to high energy and they are de-

tected on the Earth soon after the flare. Among the particles generated by the flare, high energy neutrons provide the most direct information about the acceleration mechanism as they come straight from the flare position to the Earth without deflected by the magnetic field.

In 1990, Nagoya group constructed a solar neutron telescope consisting of scintillators and lead plates, which measures the kinetic energy of incoming neutrons up to several hundred MeV. This telescope observed high energy neutrons associated with a large flare occurred on the 4th of June, 1991. The same event was simultaneously detected by the neutron monitor and the high counting muon telescope of Norikura Observatory. This is the most clear observation of solar neutrons at the ground level in almost ten years since the first observation at Jungfraujoch in 1982.

A new type of the large solar neutron telescope (64 m² sensitive area) was constructed by Nagoya group in 1996. It consists of scintillators, proportional counters and wood absorbers piled up alternately. This takes a pivotal role among a worldwide network of ground based solar neutron telescopes of the same type in Yangbajing in Tibet, Aragatz in Armenia, Gornergrat in Switzerland, Chacaltaya in Bolivia and Mauna Kea in Hawaii. The Sun is being watched for 24 hours using this network.



Fig. 2. New Solar-Neutron Telescope of Nagoya Group.

The Sun reached the maximum activity in 2000 and the active phase continued for the next few years. All the telescopes in Norikura Observatory, neutron telescope, neutron monitor, muon telescope and muon hodoscope, have been operated almost continuously through the solar cycle 23 in order to obtain comprehensive information on the solar flare phenomena. Important hints for understanding the mechanism of cosmic-ray acceleration near the solar surface will be obtained by these measurements, especially by energy spectra measured by the timing information of arriving neutrons and muons.

Furthermore, the relation between the electric fields induced by thunderclouds is studied recently[10]. The electric fields with thunderclouds change the intensity of secondary cosmic rays observed on the ground. This effect has been investigated using several detectors located at Norikura Observatory where excesses of 1 % and more of the average counting rate are observed when the observatory is covered with thunderclouds. A frequency analysis of the time series

of days with such excesses for the period 26 October 1990 to 15 January shows the expected summer maximum in the rate of occurrence and, surprisingly, a 26-day variation. An electric field mill was installed to help determine the relationship between the intensity variations and the strength and direction of the field near the detector system: the excess is usually observed when a negative electric field (accelerating negative charges downward) greater than 10 kV/m is present in the atmosphere above the observatory. Based on Monte Carlo simulations, it is predicted that excess counting rates measured without charge discrimination will be expected as a consequence of the excess of positive muons among the secondary cosmic rays.

Subsequently, during thunderstorms on 2008 September 20, an intense radiation burst, comprising γ rays and electrons, was detected [11] by at the Norikura observatory. Outside the observatory, a radiation detection system was set up on 2008 September 4, and operated it until 2008 October 2. The system has a radiation monitor and environmental sensors. The radiation monitor consists of a spherical NaI scintillator with a diameter of 7.62 cm, and a 5 mm thick plastic scintillator with an area of 45 × 40 cm². The plastic scintillator is enclosed in an aluminum box with the top and bottom being 1 mm and 3 mm thick, respectively. Each scintillator has a photomultiplier (HAMAMATSU R878) of its own, and each output signal is fed to a self-triggering electronics system, incorporating a 12 bit ADC. The burst, lasting 90 seconds, was associated with thunderclouds rather than lightning. The photon spectrum, extending to 10 MeV, can be interpreted as consisting of bremsstrahlung γ rays arriving from a source which is 60 - 130 m in distance at 90% confidence level. The observed electrons are likely to be dominated by a primary population escaping from an acceleration region in the source.

In addition to the long-term cosmic-ray observations mentioned above, various kinds of short-dated experiments are carried out every year taking an advantage of the high altitude of the observatory. A few examples include a search for super heavy particles with plastic plates, a precise measurement of atmospheric gamma rays and muons, collection of cosmic dusts contained in the snow, measurement of air fluorescence light yield for ultra high-energy cosmic-ray observation and the performance study of the balloon borne cosmic ray experiments.

Environmental Study

One of the interesting topics is atmospheric environment especially relating with atmospheric aerosol particles and water soluble gases. Because of its height, AC power supply, accommodation facility, and accessibility of cargos, the cosmic ray observatory at Mt. Norikura provides a very unique opportunity for atmospheric observation, especially for free-tropospheric conditions. (The atmosphere lower than a few kilometer is highly affected by the ground. This height level is named as 'atmospheric boundary layer'. The height of the boundary layer is about 4 km in daytime and about 2 km in nighttime around Norikura area. The atmosphere higher than this atmospheric boundary layer is called 'free troposphere'.)

Originally, atmospheric observation at the cosmic ray observatory was initiated to study cosmogenic radionuclides with Prof. Suzuki at Shizuoka University. During early stage of the research at Mt. Norikura, a local effect of air contamination was recognized. To reduce air contamination from diesel exhausts and other activities around the observatory, an atmospheric observation hut (6 m²) was installed at the west end (windward) of the observatory in September 1999. From year 2000, continuous monitoring (mostly mid-May to mid-October) of meteorology was started, number-size distribution of aerosols, dew point, aerosol chemical composition, ozone and radon concentrations, and column amount of aerosols from sky radiometer and ceilometer. Monitoring of ozone and radon concentrations was extended during 2 winters from 2001 to 2003. During summer season, also collected were rain, fog, water-condensed aerosol samples. These samples combined with other parameters were used in several thesis (master) works and provided useful information about future seeds of hygroscopic study of aerosols. During the past 5 years, the following results [12],[13],[14] were obtained at Mt. Norikura.

(1) Polluted air pumping effects over central Japanese Alps in summer

Under the clear sky conditions in summer, polluted air from mountain valley area is lifted up about 4km of altitude (1km above the mountain top) over Mt. Norikura. The height of observatory is within the atmospheric boundary layer in the daytime, and is out of (higher than) the atmospheric boundary layer in nighttime. The ratio of aerosol volume concentration for daytime (polluted valley wind) to nighttime (clean free-tropospheric) conditions was about 10. The air pumping effects over central Japanese Alps carry about 10 time higher concentration of aerosols to the free-troposphere over Japan in summer. Under the high-pressure system centered over the northwest Pacific in typical summer condition, backward air trajectories were originated from the northwest Pacific to Mt. Norikura and forward trajectories returned to the north Pacific with some deviations to east Russia and the Kurile Islands. The air pumping effects over mountain area provide a strong pollution source mechanism to the free-troposphere over the western Pacific region including East Asia.

(2) Seasonal variation of aerosol chemistry in free troposphere

An automated aerosol sampler was installed at the site in September 2000 to obtain seasonal aerosol samples. The sampler collected aerosols from mid-May to mid-October in 2001 and 2002. Results of its analysis showed seasonal changes in major and minor constituents of aerosols associating with changes of dominant air mass type over Japan.

(3) Vertical profiles of aerosols and clouds near the top of the atmospheric boundary layer

Ceilometer (lidar with small output energy) was installed in summer 2002, and was operated in 4 summer seasons. The aerosol and cloud profiles near the top of the atmospheric boundary layer have been observed. Some events of Asian

dust, and of smoke from Siberian forest fire at lower free troposphere have been detected.

Botanical Study

It is predicted that ecosystems in high-latitudes and alpine regions are sensitive to global climatic warming. The significant increasing trends in air temperature are found in the Hida Mountains, where Mt. Norikura is located. Thus, effects of climatic change caused by global warming on alpine ecosystems must be urgently studied in the alpine region of central Japan. The Hida Mountains, strongly influenced by cold-air masses from Siberia in winter, receive some of the heaviest snowfall in the world. Due to heavy snowfall, dynamics of alpine ecosystems may be peculiar to the Hida Mountains. However, few studies have been made because of difficulty in approach to the alpine study site. The inter-university research program of ICR, gave an opportunity to make an intensive study all year around in the alpine region on Mt. Norikura [15],[16].

(1) Tree line dynamics

The tree form of evergreen sub-alpine fir (*Abies mariesii*) is studied at the upper distribution limit (2500m above sea level)

on Mt. Norikura. Leader stems degenerate above the maximum snowpack line (3-4m high), whereas branches below the snowpack line grow densely. In winter, leaves above snowpack line were severely damaged by environmental stresses, such as abrasion by wind-blown snow particles, desiccation, photoinhibition. Longevity of leaves was shortened to 4-5 years due to high mortality rate in winter. In contrast, leaves below snowpack line were protected from environmental stresses and their longevity was 11 years. As a result, biomass below the snowpack line takes more than 80% with climate change should have unfavorable effects on tree line *Abies mariesii*.

(2) Alpine region

Pinus pumila, an alpine prostrated pine, is dominant in the alpine regions (2500~3000m above sea level). At wind-protected sites, *Pinus pumila* grows vigorously with the tree height of 1-2m. They were buried in snowpack throughout the winter. At the wind-exposed ridge, growth is suppressed with the tree height of 0.2-0.5m. Throughout the winter, the surface of the pine community was exposed due to strong wind at the ridge. Leeward leaves were sound, because pine stems with high elasticity were prostrated and buried in snow. Thus, alpine pine can catch and accumulate snow to protect itself. This feature may be advantageous to alpine trees in comparison with sub-alpine trees (*Abies mariesii*). On the other hand, at the windward side (western), cuticular layer covering epidermal cells of leaf was abraded probably due to wind-blown snow and ice particles. By spring, abraded leaves at the windward side were dead caused by desiccation and photoinhibition. Even *Pinus pumila* community could reduce its habitat in small snowfall condition caused by global warming.

Impact of global warming due to so-called greenhouse gases like CO₂, CH₄ and others on vegetation ecology is among the most serious environmental issues. To investigate how plants response to global warming, an experiment of greenhouse effect on vegetation has been continued at a high mountain, Mt. Norikura (3,025 m a.s.l.), central Japan, since 1997. Five open-top chambers which are small greenhouses with a size of maximum open-top diameter, the maximum basal diameter and the height of the chamber were 47 cm, 85 cm and 30 cm, respectively, were set over alpine plant communities consisting of small woody plants and herbaceous vegetation. At places inside and outside of the chambers, seasonal changes in vegetation growth and phenology were observed every month. Using automatic data-recorders, some climate elements such as air and ground temperatures, humidity and rainfall have been observed every hour. Some results through the experiment were quite remarkable. Due to the temperature enhancement of about 0.8 °C for air temperature and about 0.3 °C for ground temperature, plant growth rates and phenological changes showed notable differences between inside and outside of the chambers. The responses to warming, however, were different by different plant species. The results suggest [17],[18] that dominant species in plant community should be replaced by the species with a high physiological response to warming and with a growing form extending tree crown.

Bibliography

- [1] "Precursors of geomagnetic storms observed by the muon detector network", K. Munakata, J. W. Bieber, S. Yasue, C. Kato, M. Koyama, S. Akahane, K. Fujimoto, Z. Fujii, J. E. Humble, and M. L. Duldig, *J. Geophys. Res.*, Vol. 105, No.A12, pp. 27,457-27,468 (2000).
- [2] "Solar cycle variations of modulation parameters of galactic cosmic- rays in the heliosphere", K. Munakata, H. Miyasaka, I. Sakurai, S. Yasue, C. Kato, S. Akahane, M. Koyama, D. L. Hall, Z. Fujii, K. Fujimoto, S. Sakakibara, J. E. Humble, and M. L. Duldig, *Adv. Space Res.*, Vol.29, No.10, pp.1527-1532 (2002).
- [3] "A 1.7 year quasi-periodicity in cosmic ray intensity variation observed in the outer heliosphere", C. Kato, K. Munakata, S. Yasue, K. Inoue, and F. B. McDonald, *J. Geophys. Res.*, Vol.18, No.A10, p.1367, doi:10.1029/2003JA009897 (2003).
- [4] "Exploration of the heliosphere by cosmic rays", K. Munakata, published as the chapter 2 of *Advances in Solar-Terrestrial Physics*, pp.101-116, edited by H. Oya, published by TERRAPUB, Tokyo (2004).
- [5] "Cosmic-ray modulation in the heliosphere: global and near-earth measurements and modeling", K. Munakata, Rapporteur paper in 28th *International Cosmic Ray Conference*, Vol.8, edited by T. Kajita et al., pp.251-276, Univ. Acad. Press, Tokyo (2004).
- [6] "Geometry of an interplanetary CME on October 29, 2003 deduced from cosmic rays", T. Kuwabara, K. Munakata, S. Yasue, C. Kato, S. Akahane, M. Koyama, J. W. Bieber, P. Evenson, R. Pyle, Z. Fujii, M. Tokumaru, M. Kojima, K. Marubashi, M. L. Duldig, J. E. Humble, M. Silva, N. Trivedi, W. Gonzalez and N. J. Schuch, *Geophys. Res. Lett.*, Vol.31, L19803, doi:10.1029/2004GL020803 (2004).
- [7] "A "loss-cone" precursor of an approaching shock observed by a cosmic-ray muon hodoscope on October 28, 2003", K. Munakata, T. Kuwabara, S. Yasue, C. Kato, S. Akahane, M. Koyama, Y. Ohashi, A. Okada, T. Aoki, H. Kojima and J. W. Bieber, *Geophys. Res. Lett.*, Vol.32, L03S04, doi:10.1029/2004GL021469, 2005.
- [8] "CME-geometry and cosmic-ray anisotropy observed by a prototype muon detector network", K. Munakata, T. Kuwabara, J. W. Bieber, P. Evenson, R. Pyle, S. Yasue, C. Kato, Z. Fujii, M. L. Duldig, J. E. Humble, M. R. Silva, N. B. Trivedi, W. D. Gonzalez and N. J. Schuch, *Adv. Space Res.*, doi:10.1016/j.asr.2003.05.064, 2005, in press.
- [9] "Acceleration below Thunder Clouds at Mount Norikura", by the Tibet hybrid experiment", Y. Muraki *et al.*, Proceedings in the 28th International Cosmic Ray Conference, (31 July - 7 August 2003, Tsukuba, Japan), Vol.7, pp 4177-4180.
- [10] "Effects of atmospheric electric fields on cosmic rays", Y. Muraki *et al.*, *Phys. Rev. D*, **69**, 123010–1-13 (2004).
- [11] "Observation of an energetic radiation burst from mountain-top thunderclouds", H. Tsuchiya *et al.*, *Phys. Rev. Lett.*, **102**, 255003 (2009).
- [12] K. Osada, M. Kido, C. Nishita, K. Matsunaga, Y. Iwasaka, M. Nagatani, H. Nakada, Changes in ionic constituents of free tropospheric aerosol particles obtained at Mt. Norikura (2770 m a. s. l.), central Japan, during the Shurin period in 2000, *Atmos. Environ.*, **36**, 5469-5477, 2002.
- [13] "Atmospheric diffusion process based on time change of ²²²Rn vertical profile", K. Yoshioka, *Journal of Aerosol Research, Japan*, **17**, 267-275, 2002 (in Japanese).
- [14] "Free-tropospheric aerosols based on airplane and mountain observations", K. Osada, *Journal of Aerosol Research, Japan*, **15**, 335-342, 2000 (in Japanese).
- [15] "Diurnal changes in needle gas exchange in alpine *Pinus pumila* during snow-melting and summer seasons", A. Ishida, T. Nakano, S. Sekikawa, E. Maruta, T. Masuzawa, *Ecological Research* **16**, 107-116 (2001).
- [16] "Effects of high light and low temperature during harsh winter on needle photodamage of *Abies Mariesii* growing at the forest limit on Mt. Norikura in Central Japan", J. Yamazaki, A. Ohashi, Y. Hashimoto, E. Negishi, S. Kumagai, T. Kubo, T. Oikawa, E. Maruta, *Plant Science* **165**, 257-264, (2003).

- [17] "Chemistry of surface water at a volcanic summit area, Norikura, central Japan: Multivariate statistical approach", K. Anazawa and H. Ohmori, *Chemosphere*, 45, 807-816, (2001).
- [18] "Experimental research on vegetation response to artificial warming on a mid-latitude high mountain, central Japan", H. Ohmori, J.H. Iguchi, T. Ohta, A. Terazono and K. Hikita, *Geogr. Rev. Japan*, 77, 301-320, (2004).

AKENO OBSERVATORY

The Observatory is in Akeno town of Hokuto-city situated 20 km west of Kofu and 130 km west of metropolitan Tokyo. The location is at the longitude of 138.5°E and the latitude of 35.5°N. The altitude is ~ 900 m above sea level (Fig.1).

The Observatory was established in 1977 as a research center for air shower studies in the very high energy region. It has been administered by the ICRR as a facility of joint-university-use.

The Akeno Air Shower Experiment started in 1979 with an array covering 1 km² area (1 km² array). The array was enlarged to 20 km² in 1985 and was gradually expanded to Akeno Giant Air Shower Array (AGASA) of approximately 100 km² area by 1990.



Fig. 1. Aerial View of Akeno Observatory and 1 km² array area

One of the distinctive features of Akeno experiments is that the measurement was made over five decades of energies well covering 10¹⁵ eV - 10²⁰ eV by using both the surface detector (for electromagnetic component) and the shielded detector (for muon component). The wide energy coverage was accomplished by the arrays of scintillation detectors of various inter-detector spacings from 3 m to 1 km and with different triggering conditions.

The AGASA was an air shower array composed of 111 scintillation detectors and 27 muon detectors. Each component was placed by about 1 km separation and covered the ground area of 100 km² in the neighboring villages of the observatory. All detectors were interconnected by optical fibers for the precise timing determination and the data transmission (Fig.2). The AGASA was the largest air shower array in the world. Its operation was ceased in January of 2004 after the construction of Telescope Array (TA) had been funded in 2003.

The AGASA observed a total of 11 events with energies exceeding 10²⁰eV in 13 years of operation, and heralded rich physics of ultra-high energy cosmic rays now being explored by the Pierre Auger Observatory in Argentina and the Telescope Array (TA) in Utah, USA.

The observatory currently supports two experiments by

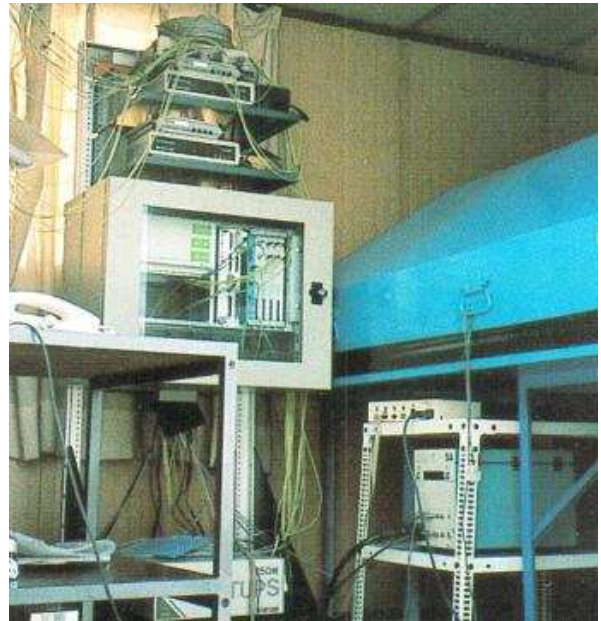


Fig. 2. AGASA scintillation detector and data acquisition system.

the university users; one for the observation of galactic cosmic ray modulation by the muon telescope and another for the rapid follow-up observation of gamma ray bursts by the multi-color robotic telescope. It is also used for supporting the operation of TA and various research and development works related to the measurement of very high energy cosmic rays.

KAMIOKA OBSERVATORY

Kamioka observatory is located at 1000 m underground (2700 m water equivalent) in the Kamioka Mine, Gifu prefecture, about 200 km west of Tokyo. The observatory was established in 1995 in order to operate Super-Kamiokande. The underground laboratories are located under Mt. Ikeno-yama and accessible to the experimental site through a 1.7 km horizontal tunnel. The observatory also has surface research buildings and a dormitory located at the distance of 15 minutes drive from the entrance of the mine. The Super-Kamiokande experiment had discovered neutrino oscillations through the observations of atmospheric and solar neutrinos (see the section for Neutrino and Astroparticle Division). The atmospheric neutrino oscillation was confirmed by the K2K accelerator neutrino experiment, which was conducted between 1999 and 2004. A new long baseline neutrino oscillation experiment (the T2K experiment) using a high intensity beam, 50 times of the K2K neutrino beam, by the J-PARC proton accelerator has started in 2009.

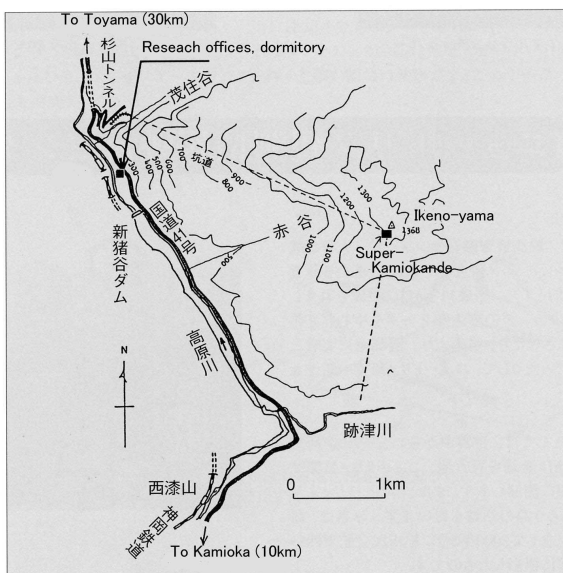


Fig. 1. Map of Kamioka observatory.

The low cosmic ray flux and low seismic noise environment in the underground site enables us to conduct various researches. There is a 100 m long laser interferometer, which is a proto-type of the planned 3 km gravitational wave antenna called LCGT, aiming to detect gravitational waves from extraterrestrial sources (see section of Astrophysics Gravity Division). Using the low radioactive background environment in the Kamioka Mine, A dark matter experiment, called XMASS is being prepared. The XMASS group has performed R&D study using a small proto-type detector and subsequently, the construction of the 800kg liquid xenon detector was started in 2007 and will be ready for data taking by the summer in 2010. The R&D study of a tracking type detector for dark matter search by the Kyoto University group (the NEWAGE experi-

ment) has also been performed in an underground laboratory. The construction of the CANDLE experiment (Osaka Univ.), a double beta decay experiment in the Kamioka Underground Observatory, has started in 2009. The study to improve the neutrino detection sensitivity by adding gadolinium to Super-Kamiokande is on going. Especially in 2009, a new cavern dedicated for the R&D study of the gadolinium project was excavated. In order to support those experiments and also related R&D works, the Observatory is equipped with low background Germanium detector, ICP-MS and so on to measure extremely low radioactive backgrounds.

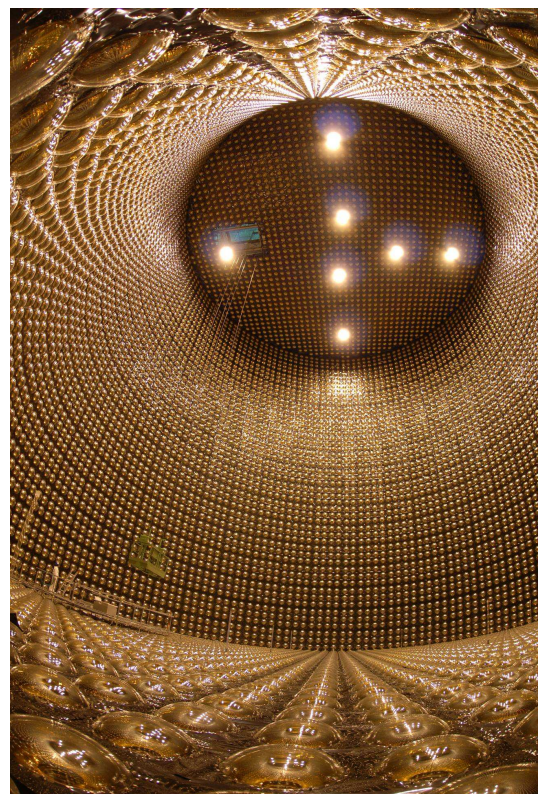


Fig. 2. Super-Kamiokande detector.



Fig. 3. 100 m baseline laser interferometers for gravitational wave and geophysics in Kamioka mine.

RESEARCH CENTER FOR COSMIC NEUTRINOS

The Research Center for Cosmic Neutrinos (RCCN) was established in April, 1999. The main objective of this center is to study neutrinos based on data from various observations and experiments. In order to promote studies of neutrino physics, it is important to provide the occasion to discuss theoretical ideas and experimental results on neutrino physics. Therefore, one of the most important practical jobs of this center is the organization of neutrino-related meetings. On March 9, 2011, we hosted one domestic neutrino workshop on high-energy cosmic neutrinos. About 30 physicists participated in this meeting.

Members of this center have been involved in the Super-Kamiokande and T2K experiments, carrying out researches in neutrino physics. Atmospheric neutrino data from Super-Kamiokande give one of the most precise pieces of information on neutrino oscillations. With increased data, it is more important to have better predictions of the neutrino flux. Therefore, in addition to data analysis of the data from these experiments, we work on calculating the atmospheric neutrino flux.

It is important that the general public knows about the achievements of the present science. For this reason, we hold public lectures every year. From FY2009, two public lectures per year are co-sponsored by this Institute and the Institute for the Physics and Mathematics of the Universe. The spring lecture is co-organized by RCCN and the Public Relation Office of ICRR. The public lecture was held on April 17 (Sat), 2010 at Kashiwa Library. About 100 people heard the lecture.

background underground facility in the Kashiwa campus. The facility is currently equipped with 4 Ge detectors mainly for the measurements of cosmic radioactive isotopes. The scientific activities that are related to this facility is described elsewhere.



Fig. 1. Public lecture held in Kashiwa in April 18, 2009.

RCCN, together with the computer committee of ICRR, is in charge of operating the central computer system in ICRR. It had been highly utilized for the analyses and simulations of various cosmic-ray physics. In 2010, the total disk size was increased by more than a factor of 2, allowing more data to be studied by each research group. RCCN also supported the users of the computer system, including physicists working outside ICRR.

Since 2004, RCCN has been acting as a body for accepting the ICRR inter-university programs related to the low-

APPENDICES

A. ICRR Workshops and Ceremonies

B. ICRR Seminars

C. List of Publications

- (a) **Papers Published in Journals**
- (b) **Conference Papers**
- (c) **ICRR Reports**

D. Doctoral Theses

E. Public Relations

- (a) **ICRR News**
- (b) **Public Lectures**
- (c) **Visitors**

F. Inter-University Researches

G. List of Committee Members

- (a) **Board of Councillors**
- (b) **Advisory Committee**
- (c) **Inter-University Research Advisory Committee**

H. List of Personnel

A. ICRR Workshops and Ceremonies

GWADW2010 (Gravitational Wave Advanced Detector Workshop 2010) –Future directions for Laser Gravitational Wave Detectors–

Date: May 16–21, 2010

Place: Hearton Hotel Kyoto, Kyoto, Japan

Outline: The workshop was organized for experimentalists of gravitational wave detection in the world. Originally it used to be held in annual base at Elba island in Italy. Since 2009, the workshop place becomes to be in rotation among Europe, America and Japan. This was the first time in Japan. In this workshop, we laid the groundwork for future detectors of gravitational waves. Leading the way would be lessons learned at CLIO, in particular, how to work underground and at cryogenic temperatures. The ongoing operations at Enhanced LIGO, Virgo+, TAMA and GEO600 gave us an understanding of some of the problems to be faced in building and operating second generation Advanced Detectors (Advanced LIGO, Advanced Virgo, LCGT, AIGO and GEO-HF) and in planned third generation detectors like ET. They might also impact plans for space based antennae such as LISA and DECIGO. The organizers hoped that young scientists and students would find the means to attend and this was finally satisfied by the attendance of many young scientists.

Participants: 40 from Japan, 19 from USA, 15 from UK, 10 from Italy, 8 from France, 7 from Germany, 3 from Australia, 3 from Netherlands, 1 from Russia, and 1 from Taiwan.

International Symposium on the Recent Progress of Ultra-High Energy Cosmic Ray Observation

Date: Dec 10–12, 2010

Place: Nagoya Congress Center, Aichi, Japan

Outline: In this Symposium, recent progress of Ultra-High Energy Cosmic Ray (UHECR) observation was reviewed. Such topics as the energy spectrum, mass composition, hadronic interactions at extremely high energy, anisotropy and arrival directions of UHECRs were reported and discussed. Future large scale ground experiments and space observatories were reviewed.

Participants: 59 from Japan, 19 from USA, 8 from Italy, 8 from Korea, 6 from Germany, 5 from France, 3 from Russia, 2 from Belgium, 1 from China, 1 from Ireland, 1 from Mexico, and 1 from Spain.

B. ICRR Seminars

1. Apr 1, 2010: Akira Tonomura (HITACHI), "Physics Explored by Electron Microscope"
2. Apr 5, 2010: Kaoru Yokoya (KEK), "Current Status of Linear Collider Technology"
3. Apr 16, 2010: Akira Ukawa (Tsukuba University), "Current Status and Future of Lattice QCD"
4. May 12, 2010: David Tanner (University of Florida), "Seeking the unseen: gravitational waves with LIGO and axion dark matter with ADMX"
5. May 14, 2010: Hironari Miyazawa (Univ. of Tokyo), "Discovery of the muon by Yoshio Nishina"
6. May 21, 2010: Kota Murase (Tokyo Institute of Technology), "Gamma-Ray Signals from Ultrahigh-Energy Cosmic-Ray Sources and Implications of Ultrahigh-Energy Nuclei Production in the Sources"
7. May 28, 2010: Enrico Barausse (University of Maryland), "Hamiltonian of a Spinning Test-particle in Curved Space-time"

8. Jun 4, 2010: Kazuo Makishima (University of Tokyo), "SUZAKU observation of magnetars—neutron stars with ultra-strong magnetic field"
9. Jun 25, 2010: Kazuoki Munakata (Shinshu University), "Sidereal anisotropy of galactic cosmic ray intensity: Latest results of two hemisphere observations by Tibet & IceCube"
10. Jul 16, 2010: Hideo Matsuhara (JAXA/ISAS), "From AKARI to SPICA: Present and future of Space Infrared Astronomy"
11. Jul 23, 2010: Shigehiro Nagataki (Kyoto University), "Numerical High-Energy Cosmic Rays and Astrophysics"
12. Jul 30, 2010: Hiroyuki Sagawa (ICRR), "Recent results from the Telescope Array experiment"
13. Dec 15, 2010: Shuhei Okubo (Earthquake Research Institute, U. Tokyo), "Solid State Earth Science and Cosmic-Ray/Gravitational-wave Research"
14. Dec 28, 2010: Martin A. Lee (ICRR/U. New Hampshire), "The Interaction of the Heliosphere with the Local Interstellar Medium: Interstellar Gas, Pickup Ions, Anomalous Cosmic Rays and the Solar Wind Termination Shock"
15. Jan 24, 2011: Ichiro Nakatani (ICRR/Aichi University of Technology), "Space Robot"
16. Feb 2, 2011: Jun Kataoka (Waseda University), "Recent progress on high energy emission from AGN jets"

C. List of Publications

(a) Papers Published in Journals

1. "Measurement of K^+ production cross section by 8 GeV protons using high energy neutrino interactions in the SciBooNE detector", SciBooNE Collaboration (G. Cheng et al.), to be published in Phys.Rev.D, [arXiv:1105.2871 [hep-ex]].
2. "Measurement of inclusive charged current interactions on carbon in a few-GeV neutrino beam", SciBooNE Collaboration (Y. Nakajima et al.), Phys.Rev.D83:012005 2011, [arXiv:1011.2131 [hep-ex]].
3. "Improved measurement of neutral current coherent π^0 production on carbon in a few-GeV neutrino beam", SciBooNE Collaboration (Y. Kurimoto et al.), Phys.Rev.D81:111102 2010, [arXiv:1005.0059 [hep-ex]].
4. "Measurement of inclusive π^0 production in the Charged-Current Interactions of Neutrinos in a 1.3-GeV wide band beam", K2K Collaboration (C. Mariani et al.), Phys.Rev. D83:054023, 2011, [arXiv:1012.1794 [hep-ex]].
5. "Solar neutrino results in Super-Kamiokande-III", Super-Kamiokande Collaboration (K. Abe et al.), Phys. Rev. D83:052010, 2011, [arXiv:1010.0118 [hep-ex]].
6. "Atmospheric neutrino oscillation analysis with sub-leading effects in Super-Kamiokande I, II and III", Super-Kamiokande Collaboration (R. Wendell and C. Ishihara et al.), Phys. Rev. D81:092004, 2010, [arXiv:1002.3471 [hep-ex]].
7. "Improvement of low energy atmospheric neutrino flux calculation using the JAM nuclear interaction model", M. Honda, T. Kajita, K. Kasahara and S. Midorikawa, to be published in Phys. Rev. D, [arXiv:1102.2688 [astro-ph.HE]].
8. "Atmospheric Neutrinos And Discovery Of Neutrino Oscillations", T. Kajita, Proc. Japan Acad. B86, 303-321, 2010.
9. "Further study of neutrino oscillation with two detectors in Kamioka and Korea", F. Dofour, T. Kajita, E. Kearns and K. Okumura, Phys. Rev. D81: 093001, 2010, [arXiv:1001.5165 [hep-ph]].
10. "Status of Very High Energy Gamma Ray Astronomy and Future Prospects", M.Teshima, Tenmmon Geppou, Vol 104-7, 2011 333.
11. "A search for very-high energy gamma-ray emission from Scorpius X-1 with the MAGIC telescopes", MAGIC Collaboration (J. Aleksy and M. Teshima et al.), Astrophys. J. Letters 735, 2011 L5, [arXiv:1103.5677].
12. "MAGIC discovery of VHE Emission from the FSRQ PKS 1222+21", MAGIC Collaboration (J. Aleksy and M. Teshima et al.), Astrophys. J. Letters 730, 2011, L8, [arXiv:1101.4645].

13. "MAGIC observations and multiwavelength properties of the quasar 3C279 in 2007 and 2009", MAGIC Collaboration (J. Aleksí and M. Teshima et al.), *Astron. Astrophys.* 530, 2011, A4, [arXiv:1101.2522].
14. "Observations of the Blazar 3C 66A with the MAGIC Telescopes in Stereoscopic Mode", MAGIC Collaboration (J. Aleksí and M. Teshima et al.), *Astrophys. J. Lett.* 726, 2010, 58, [arXiv:1010.0550].
15. "Detection of very high energy γ -ray emission from the Perseus cluster head-tail galaxy IC 310 by the MAGIC Telescopes", MAGIC Collaboration (J. Aleksí and M. Teshima et al.), *Astrophys. J. Lett.* 723, 2010, L207-212, [arXiv:1009.2155].
16. "Spectral Energy Distribution of Markarian 501: Quiescent State vs. Extreme Outburst", VERITAS and MAGIC Collaboration (V.A. Acciari and M. Teshima et al.), *Astrophys. J.* 729, 2010, 2, [arXiv:1012.2200].
17. "Insights Into the High-Energy Gamma-ray Emission of Markarian 501 from Extensive Multifrequency Observations in the Fermi Era", FERMI, MAGIC, VERITAS and MAGIC Collaboration (A.A. Abdo and M. Teshima et al.), to be published in *Astrophys. J.*, [arXiv:1011.5260].
18. "Design Concepts for the Cherenkov Telescope Array", CTA Consortium (R. Enomoto, S. Inoue, M. Ohishi, M. Teshima, T. Yoshikoshi et al.), to be published in *Astro Particle Physics*, [arXiv:1008.3703].
19. "GRB100906A: Ashra-1 observation of early optical emission", Y. Asaoka et al., *GCN Circular*, 11291, 2010.
20. "Cosmic-ray energy spectrum around the knee obtained by the Tibet experiment and future prospects", M. Amenomori et al., *Advances in Space Research*, 47, 629-639, 2011.
21. "Cosmic-ray energy spectrum around the knee observed with the Tibet air-shower experiment", M. Amenomori et al., *Astrophysics and Space Sciences Transactions*, 7, 15-20, 2011.
22. "Expansion of Linear Range of Pound-Drever-Hall Signal", Shinji Miyoki, Souichi Terada, and Takashi Uchiyama, *Appl. Optics* 49, 5217, 2010.
23. "Optical properties measurement of an Al_2O_3 mirror substrate for the Large-Scale Cryogenic Gravitational Wave Telescope (LCGT)", M. Tokunari, et al., *Class. Quantum Grav.* 27, 185015, 2010.
24. "Status of LCGT", K. Kuroda (on behalf of the LCGT Collaboration), *Class. Quantum Grav.* 27, 084004, 2010.
25. "Keck Spectroscopy of Faint $3 < z < 7$ Lyman Break Galaxies: A High Fraction of Line Emitters at Redshift Six", Stark, D. P., R. S. Ellis, and M. Ouchi, *The Astrophysical Journal*, 728, L2, 2011, [arXiv:1009.5471 [astro-ph]].
26. "The Subaru Ly α blob survey: a sample of 100-kpc Ly α blobs at $z = 3$ ", Matsuda Y. et. al., *Monthly Notices of the Royal Astronomical Society*, 410, L13, 2011, [arXiv:1010.2877 [astro-ph]].
27. "Lyman- α Emitters and Lyman-Break Galaxies at $z = 3-6$ in Cosmological SPH Simulations", Nagamine K., M. Ouchi, V. Springel, and L. Hernquist, *Publications of the Astronomical Society of Japan*, 62, 1455, 2010, [arXiv:0802.0228 [astro-ph]].
28. "Statistics of 207 Ly α Emitters at a Redshift Near 7: Constraints on Reionization and Galaxy Formation Models", Ouchi M. et. al., *The Astrophysical Journal*, 723, 869, 2010, [arXiv:1007.2961 [astro-ph]].
29. "Global amount of dust in the universe", Fukugita M., [arXiv:1103.4191 [astro-ph]].
30. "Characterization of Sloan Digital Sky Survey Stellar Photometry", Fukugita M., N. Yasuda, M. Doi, J. E. Gunn, and D. G. York, *The Astronomical Journal*, 141, 47, 2011, [arXiv:1008.0510 [astro-ph]].
31. "Supernovae in the Subaru Deep Field: the rate and delay-time distribution of type Ia supernovae out to redshift 2", Graur O. et. al., [arXiv:1102.0005 [astro-ph]].
32. "Microwave Emission from the Edgeworth-Kuiper Belt and the Asteroid Belt Constrained from WMAP", Ichikawa, K. and M. Fukugita, to be published. [arXiv:1011.4796 [astro-ph]].
33. "The Sloan Digital Sky Survey Quasar Lens Search. IV. Statistical Lens Sample from the Fifth Data Release", Inada N., et. al., *The Astronomical Journal*, 140, 403, 2010, [arXiv:1005.5570 [astro-ph]].
34. "A complete calculation for direct detection of Wino dark matter", J. Hisano, K. Ishiwata and N. Nagata, *Phys. Lett. B* 690, 311, 2010, [arXiv:1004.4090 [hep-ph]].

35. "Reevaluation of Higgs-Mediated μ - e Transition in the MSSM", J. Hisano, S. Sugiyama, M. Yamanaka and M. J. S. Yang, *Phys. Lett. B* 694, 380, 2011, [arXiv:1005.3648 [hep-ph]].
36. "Gluon contribution to the dark matter direct detection", J. Hisano, K. Ishiwata and N. Nagata, *Phys. Rev. D* 82, 115007, 2010, [arXiv:1007.2601 [hep-ph]].
37. "Charge-Breaking Constraints on Left-Right Mixing of Stau's", J. Hisano and S. Sugiyama, *Phys. Lett. B* 696, 92, 2011, [arXiv:1011.0260 [hep-ph]].
38. "Right-handed sneutrino dark matter and big-bang nucleosynthesis", K. Ishiwata, M. Kawasaki, K. Kohri and T. Moroi, *Phys. Lett. B* 689, 163, 2010, [arXiv:0912.0781 [hep-ph]].
39. "Primordial Black Holes as All Dark Matter", P. H. Frampton, M. Kawasaki, F. Takahashi and T. T. Yanagida, *JCAP* 1004, 023, 2010, [arXiv:1001.2308 [hep-ph]].
40. "Numerical study of Q-ball formation in gravity mediation", T. Hiramatsu, M. Kawasaki and F. Takahashi, *JCAP* 1006, 008, 2010, [arXiv:1003.1779 [hep-ph]].
41. "Inflation from a Supersymmetric Axion Model", M. Kawasaki, N. Kitajima and K. Nakayama, *Phys. Rev. D* 82, 123531, 2010, [arXiv:1008.5013 [hep-ph]].
42. "Gravitational Waves from Collapsing Domain Walls", T. Hiramatsu, M. Kawasaki and K. Saikawa, *JCAP* 1005, 032, 2010, [arXiv:1002.1555 [astro-ph.CO]].
43. "Gravitational waves from kinks on infinite cosmic strings", M. Kawasaki, K. Miyamoto and K. Nakayama, *Phys. Rev. D* 81, 103523, 2010, [arXiv:1002.0652 [astro-ph.CO]].
44. "B-mode polarization induced by gravitational waves from kinks on infinite cosmic strings", M. Kawasaki, K. Miyamoto and K. Nakayama, *Phys. Rev. D* 82, 103504, 2010, [arXiv:1003.3701 [astro-ph.CO]].
45. "Kahler moduli double inflation", M. Kawasaki and K. Miyamoto, *JCAP* 1102, 004, 2011, [arXiv:1010.3095 [astro-ph.CO]].
46. "Destruction of ${}^7\text{Be}$ in big bang nucleosynthesis via long-lived sub-strongly interacting massive particles as a solution to the Li problem", M. Kawasaki and M. Kusakabe, *Phys. Rev. D* 83, 055011, 2011. [arXiv:1012.0435 [hep-ph]].
47. "Quantum Statistical Corrections to Astrophysical Photodisintegration Rates", G. J. Mathews, Y. Pehlivan, T. Kajino, A. B. Balantekin and M. Kusakabe, *Astrophys. J.* 727, 10, 2011, [arXiv:1012.0519 [astro-ph.SR]].
48. "Prospects for direct detection of inflationary gravitational waves by next generation interferometric detectors", S. Kuroyanagi, T. Chiba and N. Sugiyama, *Phys. Rev. D* 83, 043514, 2011, [arXiv:1010.5246 [astro-ph]].
49. "First very low frequency detection of short repeated bursts from magnetar SGR J1550-5418", Tanaka, Y. T., et al., *Astrophys. J.*, 721, L24-L27, 2010.
50. "Solar-type magnetic reconnection model for magnetar giant flares", Masada, Y., et al., *Pub. Astron. Soc. Japan*, 104, 1093-1102, 2010.
51. "Effect of the solar wind proton entry into the deepest lunar wake", Nishino, M. N., et al. *Geophys. Res. Lett.*, 37, L12106.1-4, 2010.
52. "In-flight performance and initial results of plasma energy angle and composition experiment (PACE) on SELENE (Kaguya)", Saito, Y., et al., *Space Sci. Rev.*, 154, 265-303, 2010.
53. "Synchronized Northern Hemisphere Climate Change and Solar Magnetic Cycles during the Maunder Minimum", Y.T. Yamaguchi et al., *PNAS*, 2010.
54. "Explosive volcanic eruptions triggered by cosmic rays: volcano as a bubble chamber", T. Ebisuzaki et al., *Gondwana Research*, 2010.
55. "Is the Sun heading for another Maunder Minimum? -Precursors of the grand solar minima", H. Miyahara et al., *Journal of Cosmology*, 8, 1970, 2010.
56. "Variations of Solar Activity and Climate during the Past 1200 Years", H. Miyahara, *Journal of Geography*, 119, 3, 510, 2010.

57. "Universality test of the charged Higgs boson couplings at the LHC and at B factories", Alan S. Cornell, et al., Phys. Rev. D81, 115008, 2010, [arXiv:0906.1652 [hep-ph]].

(b) Conference Papers

1. "Messenger of new physics", W. Rodejohann and M. Shiozawa, Proceeding of the Neutrino Oscillation Workshop (NOW2010), September, 2010, to be published in Nuclear Physics B Proceedings Supplement.
2. "Study of gamma-ray production in neutral-current neutrino-oxygen interactions and the detection of neutrinos from supernova explosion.", T. Mori, M. Sakuda, A. Tamii, H. Toki, M. Nakahata, and K. Ueno, AIP Conf.Proc. 1269, 418-420, 2010.
3. "Asian Facilities", M. Nakahata, Proceedings of Topical Workshop in Low Radioactivity Techniques (LRT2010), August, 2010.
4. "Low background techniques in XMASS", A. Takeda for the XMASS Collaboration, Proceedings of Topical Workshop in Low Radioactivity Techniques (LRT2010), August, 2010.
5. "Status of XMASS Experiment", S. Moriyama, Proceedings of identification of dark matter 2010 (IDM2010), July, 2010.
6. "XMASS", M. Yamashita, Proceedings of Patras Workshop on Axions, WIMPs, WISPs, July, 2010.
7. "Recent results on atmospheric neutrino oscillation from Super-Kamiokande", Y. Obayashi for the Super-Kamiokande Collaboration, Prepared for 35th International Conference on High Energy Physics: ICHEP 2010, Paris, France, 21-28 Jul 2010. Published in PoS ICHEP2010:313,2010.
8. "Search for Nucleon Decays in Super-Kamiokande", M. Miura for the Super-Kamiokande Collaboration, Prepared for 35th International Conference on High Energy Physics: ICHEP 2010, Paris, France, 21-28 Jul 2010. Published in PoS ICHEP2010:403,2010.
9. "Solar neutrino results from Super-Kamiokande", H. Sekiya for the Super-Kamiokande Collaboration, Prepared for 35th International Conference on High Energy Physics: ICHEP 2010, Paris, France, 21-28 Jul 2010. Published in PoS ICHEP 2010:330,2010.
10. "Construction and performance of XMASS 800kg detector", J. LIU for XMASS collaboration, Proceedings of 24th International Conference on Neutrino Physics and Astrophysics (Neutrino 2010), June, 2010.
11. "Radon Removal from Liquid Xenon", K. Martens for XMASS collaboration, Proceedings of 24th International Conference on Neutrino Physics and Astrophysics (Neutrino 2010), June, 2010.
12. "Large Underground Water Cherenkov Detectors", M. Shiozawa, Proceeding of the XXIV International Conference on Neutrino Physics and Astrophysics (Neutrino2010), June, 2010. to be published in Nuclear Physics B Proceedings Supplement.
13. "Commissioning of the new electronics and online system for the Super-Kamiokande experiment", S. Yamada, et. al. for the Super-Kamiokande Collaboration, Y. Arai, K. Ishikawa, A. Minegishi, and T. Uchida, IEEE Trans.Nucl.Sci.57:428-432, 2010.
14. "Status and prospect of atmospheric neutrinos and long baseline studies", T. Kajita, J. Phys. Conf. Ser. 203: 012012, 2010.
15. "The Telescope Array experiment: Status and Prospects", H. Tokuno et al. (Telescope Array Collaboration), Proceedings of 14th International Conference On Calorimetry In High Energy Physics (CALOR2010), 10-14 May 2010, AIP Conf. Proc.1238, 365-368, 2010.
16. "Measurement of UHECRs by the Telescope Array (TA) experiment", M. Fukushima for the Telescope Array Collaboration, Proceedings of XVI International Symposium on Very High Energy Cosmic Ray Interactions (ISVHECRI2010), 28 Jun - 2 Jul 2010.
17. "Results from the Telescope Array Experiment", D. Ikeda for the Telescope Array Collaboration, Proceedings of the 22nd European Cosmic Ray Symposium (ECRS2010), 3-6 Aug 2010.

18. "Recent Results from the Telescope Array Experiment", H. Sagawa for the Telescope Array Collaboration, Proceedings of the International Symposium on the Recent Progress of Ultra-high Energy Cosmic Ray Observation (UHECR2010), 10-12 Dec 2010.
19. "Absolute energy calibration of FD by an electron linear accelerator for Telescope Array", T. Shibata et al., Proceedings of UHECR2010, 10-12 Dec 2010.
20. "Energy measurement and spectrum by the Telescope Array", D. Ikeda for the Telescope Array Collaboration, Proceedings of UHECR2010, 10-12 Dec 2010.
21. "Measurement of UHECR composition by TA", Y. Tameda for the Telescope Array Collaboration, Proceedings of UHECR2010, 10-12 Dec 2010.
22. "Central Laser Facility Analysis at The Telescope Array Experiment", Y. Takahashi et al. (the Telescope Array Collaboration), Proceedings of UHECR2010, 10-12 Dec 2010.
23. "Comparison of CORSIKA and COSMOS simulation", S.Y. Roh et al., Proceedings of UHECR2010, 10-12 Dec 2010.
24. "Search for small clusters by auto-correlation analysis from Telescope Array", T. Okuda et al. (Telescope Array Collaboration), Proceedings of UHECR2010, 10-12 Dec 2010.
25. "An Event Reconstruction Method for the Telescope Array Fluorescence Detectors", T. Fujii et al. (Telescope Array Collaboration), Proceedings of UHECR2010, 10-12 Dec 2010.
26. "Large scale anisotropy of UHECRs for the Telescope Array", E. Kido for the Telescope Array Collaboration, Proceedings of UHECR2010, 10-12 Dec 2010.
27. "Heliospheric signatures seen in the sidereal anisotropy of high-energy galactic cosmic ray intensity", M. Amenomori et al., AIP Conf. Proc., 1302, 285-290, 2010.
28. "Cryogenic Advanced Gravitational Wave Detectors (LCGT)", K. Kuroda and LCGT Collaboration Proceedings of the Ninth Asia-Pacific International Conference on Gravitation and Astrophysics, Edit. Jun Luo, Ze-Bing Zhou, HsiChina, Hsien-Chi Yeh and Jong-Ping Hsu, Wuhan, China, 29 June-2 July 2009.
29. "Shocks in the Heliosphere", Terasawa, T., Chapter 12, IAGA Special Sopron Book Series vol. 4, "The Sun, the Solar Wind, and the Heliosphere", ed. by M. P. Miralles and J. S. Almeida, Springer, 2011.
30. "Anomalous deformation of the Earth's bow shock in the lunar wake: Joint observations by Chang'E-1 and SELENE", Nishino, M. N., et al., Proceedings of American Geophysical Union Fall meeting, Paper P54B-07, 2010.
31. "Effect of the solar-wind proton entry into the deepest lunar wake", Nishino, M. N., et al., Proceedings of EGU General Assembly, vol. 5, EPSC2010-473, 2010.
32. "VLF detection of ionospheric disturbance caused by a magnetar giant gamma-ray flare", Tanaka, Y. T., et al., Proceedings of 38th COSPAR Scientific Assembly, C11-0172-10, 2010.
33. "Effect of solar-wind proton entry into the deepest lunar wake", Nishino, M. N., et al., Proceedings of 38th COSPAR Scientific Assembly, B01-0061-10, 2010.
34. "Collisionless shock and particle acceleration", Terasawa, T., Proceedings of the IAU symposium 274, 2010.
35. "Identification of new physics and general WIMP search at the ILC", M.Asano, et al., to be published in proceedings of International Linear Collider Workshop 2010.
36. "Simulation Study of W Boson + Dark Matter Signatures for Identification of New Physics", T.Suehara, et al., to be published in proceedings of International Linear Collider Workshop 2010.

(c) ICRR Reports

1. ICRR-Report-568-2010-1
"A complete calculation for direct detection of Wino dark matter"
Junji Hisano, Koji Ishiwata, and Natsumi Nagata.
2. ICRR-Report-569-2010-2
"Reevaluation of Higgs-Mediated μ - e Transition in the MSSM"
Junji Hisano, Shohei Sugiyama, Masato Yamanaka, and Masaki Jung Soo Yang.
3. ICRR-Report-570-2010-3
"Gluon contribution to the dark matter direct detection"
Junji Hisano, Koji Ishiwata, and Natsumi Nagata.
4. ICRR-Report-571-2010-4
"Non-Gaussianity from Lifshitz Scalar"
Keisuke Izumi, Takeshi Kobayashi, and Shinji Mukohyama.
5. ICRR-Report-572-2010-5
"Decaying Dark Matter in Supersymmetric Model and Cosmic-Ray Observations"
Koji Ishiwata, Shigeki Matsumoto, and Takeo Moroi.
6. ICRR-Report-573-2010-6
"Inflation from a Supersymmetric Axion Model"
Masahiro Kawasaki, Naoya Kitajima, and Kazunori Nakayama.
7. ICRR-Report-574-2010-7
"Kähler moduli double inflation"
Masahiro Kawasaki, and Koichi Miyamoto.
8. ICRR-Report-575-2010-8
"Prospects for Direct Detection of Inflationary Gravitational Waves by Next Generation Interferometric Detectors"
Sachiko Kuroyanagi, Takeshi Chiba, and Naoshi Sugiyama.
9. ICRR-Report-576-2010-9
"Running Spectral Index from Inflation with Modulations"
Takeshi Kobayashi, and Fuminobu Takahashi.
10. ICRR-Report-577-2010-10
"Evolution of String-Wall Networks and Axionic Domain Wall Problem"
Takashi Hiramatsu, Masahiro Kawasaki, and Ken'ichi Saikawa.
11. ICRR-Report-578-2010-11
"Destruction of ${}^7\text{Be}$ in big bang nucleosynthesis vis long-lived sub-strongly interacting massive particles as a solution to the Li problem"
Masahiro Kawasaki, and Motohiko Kusakabe.
12. ICRR-Report-578-2010-12
"Improved estimation of radiated axions from cosmological axionic strings"
Takashi Hiramatsu, Masahiro Kawasaki, Toyokazu Sekiguchi, Masahide Yamaguchi, and Jun'ichi Yokoyama.
13. ICRR-Report-579-2010-13
"Cosmological constraints on dark matter models with velocity-dependent annihilation cross section"
Junji Hisano, Masahiro Kawasaki, Kazunori Kohri, Takeo Moroi, Kazunori Nakayama, and Toyokazu Sekiguchi.
14. ICRR-Report-580-2010-14
"Study of gravitational radiation from cosmic domain walls"
Masahiro Kawasaki, and Ken'ichi Saikawa.

D. Doctoral Theses

1. "Study of pulse shape discrimination and low background techniques for liquid xenon dark matter detectors",
K. Ueshima,
Ph.D. Thesis, Jan. 2011.
2. "Optical Properties of Type Ia Supernovae and their Host Galaxies",
K. Konishi, Ph.D. Thesis, Mar. 2011.

E. Public Relations

(a) ICRR News

ICRR News is a newspaper published quarterly in Japanese to inform the Institute's activities. This year's editors were Hideo Itoh. It includes :

1. reports on investigations by the staff of the Institute or made at the facilities of the Institute,
2. reports of international conferences on topics relevant to the Institute's research activities,
3. topics discussed at the Institute Committees,
4. list of publications published by the Institute [ICRR-Report, ICRR-Houkoku (in Japanese)],
5. list of seminars held at the Institute,
6. announcements,
7. and other items of relevance.

The main topics in the issues in 2010 fiscal year were:

No.73 (Sep 30, 2010)

- On the Study of Astrophysical Particle Acceleration, Toshio Terasawa.
- Status report of Telescope Array experiment, Hiroyuki Sagawa.
- Observation of Gamma Ray Bursts by Ashra, Kazuaki Ota.
- Staff reassignment.
- ICRR-Seminar.
- ICRR-Report.

No.74 (Nov 30, 2010)

- Development of a precise on-board gravity-gradiometer, Sachie Shiomi.
- Start operation of the Small electron linear accelerator for Absolute energy calibration of Telescope Array Experiment, Tatsunobu Shibata.
- Report on the training for ICRR technical staffs, Hiroyuki Sagawa.
- Beginning of the T2K experiment, Masato Shiozawa.
- Staff reassignment.
- ICRR-Seminar.

- ICRR-Report.

No.75 (Feb 28, 2011)

- Cosmic Reionization Probed with Subaru Telescope, Masami Ouchi.
- Cherenkov Telescope Array(CTA) project, Masahiro Teshima.
- Report on open campus 2009, Hideo Itoh.
- Staff reassignment.
- ICRR-Seminar.
- ICRR-Report.

No.76 (Mar 31, 2011)

- Report on the Meeting for Presenting the Results of Inter-University Research in JFY2010, Takanori Yoshikoshi.
- Axions from Axionic strings, Masahiro Kawasaki.
- Staff reassignment.
- ICRR-Seminar.
- ICRR-Report.

(b) Public Lectures

- "Detecting Dark Matter", Feb 26, 2011, Tokyo, Yoichiro Suzuki (ICRR, University of Tokyo).
- "Searching Dark Matter", Feb 23, 2011, Tokyo, Yoichiro Suzuki (ICRR, University of Tokyo).
- "GSA Science Cafe", Feb 12, 2011, Kamioka-cho, Hida-city, Gifu, Yoshinari Hayato (ICRR, University of Tokyo).
- "ICRR tour", Dec 10, 2010, ICRR, Chiba, Hideo Itoh (ICRR, University of Tokyo).
- "Detection of Gravity Wave predicted by Einstein", Nov 27, 2010, Kashiwa campus, University of Tokyo, Chiba, Masatake Ohashi (ICRR, University of Tokyo).
- "About Dark Matter", Nov 26, 2011, Kanazawa, Nishigawa, Yoichiro Suzuki (ICRR, University of Tokyo).
- "New age of Cosmic Ray Physics", Nov 20, 2010, Katsushika City Museum, Tokyo, Hideo Itoh (ICRR, University of Tokyo).
- "SSH Kainan High School", Nov 18, 2010, Kamioka-cho, Hida-city, Gifu, Jun Kameda (ICRR, University of Tokyo).
- "Weather of the Space and the Earth", Nov 14, 2010, University of Tokyo, Tokyo, Hiroko Miyahara (ICRR, University of Tokyo).
- "Observe the Universe through an Underground Huge Water Tank", Oct. 30, 2010, Kashiwa, Chiba, Yoshihisa Obayashi (ICRR, University of Tokyo).
- "Yoshiki High School", Sep 15, 2010, Toita Girl's Junior-Senior High School, Tokyo, Hideo Itoh (ICRR, University of Tokyo).
- "Investigation of the Universe using particle physics", Sep 14, 2010, Kamioka-cho, Hida-city, Gifu, Makoto Miura (ICRR, University of Tokyo).
- "SSH Toyounaka High School", Sep 6, 2010, Kamioka-cho, Hida-city, Gifu, Ko Abe (ICRR, University of Tokyo).
- "SSH Senior High School Attached to Kyoto University of Education", Aug 26, 2010, Kamioka-cho, Hida-city, Gifu, Jun Kameda (ICRR, University of Tokyo).
- "ICRR tour", Aug 24, 2010, ICRR, Chiba, Hideo Itoh (ICRR, University of Tokyo).

- "Visualisation of Radiation and Cosmic Ray", Aug 11, 2010, ICRR, Chiba, Hideo Itoh (ICRR, University of Tokyo).
- "JST Project for girl students to choose the science course", Aug 11, 2010, Kamioka-cho, Hida-city, Gifu, Yoshihisa Obayashi and Katsuki Hiraide (ICRR, University of Tokyo).
- "Particle physics and the Universe", Aug 10, 2010, ICRR, Chiba, Hideo Itoh (ICRR, University of Tokyo).
- "SSH Fujishima High School", Aug 10, 2010, Kamioka-cho, Hida-city, Gifu, Hiroyuki Sekiya (ICRR, University of Tokyo).
- "Yumeno Tamago Jyuku; Hida Academy Summer Seminar", Aug 6, 2010, Kamioka-cho, Hida-city, Gifu, Atsushi Takeda (ICRR, University of Tokyo).
- "SSH Takamatsu First High School", Aug 5, 2010, 5-1-5, Kashiwanoha, Kashiwa-city, Chiba, Shigetaka Moriyama (ICRR, University of Tokyo).
- "SSH Sanda Shoukan High School", Aug 5, 2010, Kamioka-cho, Hida-city, Gifu, Makoto Miura (ICRR, University of Tokyo).
- "Particle physics and the Universe", Aug 3, 2010, ICRR, Chiba, Hideo Itoh (ICRR, University of Tokyo).
- "Hirameki Tokimeki Science", Aug 3, 2010, Kamioka-cho, Hida-city, Gifu, Yoichiro Suzuki (ICRR, University of Tokyo).
- "Hirameki Tokimeki Science", Aug 2, 2010, Kamioka-cho, Hida-city, Gifu, Yoichiro Suzuki (ICRR, University of Tokyo).
- "Visualisation of Radiation and Cosmic Ray", Jul 30, 2010, ICRR, Chiba, Hideo Itoh (ICRR, University of Tokyo).
- "SSH Kawagoe High School", Jul 29, 2010, Kamioka-cho, Hida-city, Gifu, Atsushi Takeda and Yumiko Takenaga (ICRR, University of Tokyo).
- "Cosmic Ray Physics and ICRR", Jul 27, 2010, ICRR, Chiba, Hideo Itoh (ICRR, University of Tokyo).
- "Investigation of the Universe using particle physics", Jul 24, 2010, Niigata Prefectural Kokusai Joho High School, Niigata, Hideo Itoh (ICRR, University of Tokyo).
- "Investigation of the Universe using particle physics", Jul 13, 2010, Tokyo City University Junior and Senior High School, Tokyo, Hideo Itoh (ICRR, University of Tokyo).
- "Elementary Particles and Cosmic Rays", Jul 9, 2010, ICRR, Chiba, Hideo Itoh (ICRR, University of Tokyo).
- "SSH Shizuoka-kita High School", Apr 23, 2010, Kamioka-cho, Hida-city, Gifu, Ko Abe and Yumiko Takenaga (ICRR, University of Tokyo).

(c) Visitors

KASHIWA Campus (Total: 7 groups, 41 peoples)

- Chiba Advanced Technology Experience Program
- The Japan Society of Mechanical Engineers
- Induction course of the University of Tokyo
- Others: 4 groups

KAMIOKA Observatory (Total: 143 groups, 3028 peoples)

- Yumeno Tamago Jyuku (Hida Academy for High School Students)
- MEXT Super Science High School (SSH) project: total 7 schools
- Schools and Universities: total 29 groups
- Schools and Universities: total 21 groups
- Researchers: total 23 groups
- Others: 91 groups

F. Inter-University Researches

Numbers of Researchers

	Number of Applications	Number of Adoptions	Number of Researchers
Facility Usage			
Kamioka Observatory	37	36	874
Norikura Observatory	8	8	70
Akeno Observatory	8	8	181
Emulsion and Air Shower Facilities in Kashiwa	1	1	7
Low-level Radio-isotope Measurement Facilities in Kashiwa	6	6	25
Gravitational Wave Facilities in Kashiwa	3	3	29
Computer Facilities in Kashiwa	9	9	103
Over Sea Facilities	6	6	80
Others	18	18	382
Collaborative Researches			
Cosmic Neutrino Researches	28	27	739
High Energy Cosmic Ray Researches	43	43	682
Theoretical Researches or Rudimental Researches	20	20	289
Research Center for Cosmic neutrinos	5	5	40
Others			
Conferences	3	3	45

Research Titles

1. Development of low concentration radon detection system
2. Energy calibration for Super-Kamiokande
3. Study of solar neutrino energy spectrum
4. Neutrino workshop
5. Sidereal daily variation of $\sim 10\text{TeV}$ galactic cosmic ray intensity observed by the Super-Kamiokande
6. Study of Supernova Relic Neutrinos
7. Study in upward-going muons and high energy neutrinos
8. Precise measurement of Day/Night effect for B8 solar neutrinos
9. Study of Solar Neutrino Flux
10. Study of ambient gamma-ray and neutron flux at Kamioka Observatory
11. Study for the electron neutrino appearance search in the T2K experiment
12. Study of simulation for atmospheric neutrino
13. Study of nucleon decay $p \rightarrow \nu K$
14. Tokai to Kamioka Long Baseline Experiment T2K
15. 3-flavor Oscillation study in atmospheric neutrinos
16. Study of atmospheric neutrinos and neutrino oscillations

17. Neutrino interaction study using accelerator data
18. Development of the new online DAQ system for Super-Kamiokande
19. Study for Supernova monitor
20. Search for proton decay via $e^+\pi^0$ mode
21. R&D of a Mton water Cherenkov Hyper-Kamiokande
22. Analysis of Spatial Distribution of Radon Family Underground and Its Dosimetry
23. Direction-sensitive dark matter search experiment
24. Development of metal composites loaded liquid scintillator for measurement of solar neutrinos and neutrinoless $\beta\beta$ decay
25. Development of InP detector for measurement of solar pp/7Be ν
26. Study for lowering backgrounds of radioisotopes in large volume detectors
27. Study for upgrade of XMASS detector
28. Study for double beta decay of ^{48}Ca
29. Integration of crustal activity observation around the Atotsugawa fault
30. A study on emission spectrum of liquid xenon
31. Seismic classification of underground facilities for low frequency ground based gravitational wave detectors
32. A search for Dark Matter using Liquid Xenon Detector
33. Design and Construction of Purification system for XMASS 800kg detector
34. Multi-Color Imager for Transients, Survey and Monstrous Explosions
35. Production and calibration of surface detectors for the Telescope Array experiment
36. A study of the hybrid trigger for the Telescope Array experiment
37. Observation of Galactic Cosmic ray by the Large Area Muon Telescope
38. R&D for a Small Atmospheric Cherenkov Telescope in Akeno Observatory
39. Observation of solar neutrons in solar cycle 24
40. Vegetation survey of alpine plants on Mt.Norikura
41. Observation of total ozone and UV solar radiation with Brewer spectrophotometer on the Norikura mountains
42. Space weather observation using muon hodoscope at Mt.Norikura
43. Study of particle acceleration in electric field using x and gamma rays from lightning and thunderclouds
44. Ecophysiological studies of alpine plants
45. Observation of the highest energy Solar Cosmic Rays
46. Observation of nightglow and its reflected and scattered light on the mountain
47. Study of the composition of cosmic-rays at the knee
48. Observation of high-energy cosmic-ray electrons with emulsion chambers
49. Experimental Study of High-energy Cosmic Rays in the Tibet AS γ experiment
50. Development of advanced photon counter for the future IACT
51. Development of the optical fiber image transfer system for Ashra
52. Study of Galactic Diffuse Gamma Rays

53. Study of absolute energy calibration air shower by compact Electron LINAC
54. Sidereal daily variation of 10TeV galactic cosmic-ray intensity observed by the Tibet air shower array
55. Study on High Energy Cosmic-Ray source by Observation Using Long Duration Balloon
56. Basic Study to Establish the CTA Japan Consortium
57. Cosmic ray interactions in the knee and the highest energy regions
58. A study on variation of interplanetary magnetic field with the cosmic-ray shadow by the sun
59. Acceleration processes: Comparative study of 1st and 2nd order processes
60. Observation of TeV gamma-ray spectra from galactic objects
61. Bolivian Air Shower Joint Experiment
62. A R&D for a new atmospheric monitoring system
63. Improvement of characteristics of the image sensor used in Ashra
64. Study on the Ultra-high Energy Cosmic Ray Future Projects
65. Observation of very-high-energy gamma-rays in Australia
66. Data Analysis of the UHECR data for the Auger Project III
67. Multiwavelength observation of extragalactic gamma-ray objects with CANGAROO telescope and Fermi gamma-ray space telescope
68. Development of an atmospheric transmittance meter for the site survey of Cherenkov telescopes
69. Workshop on High Energy Gamma-Ray Astronomy
70. Data analysis of nearby galaxies and clusters of galaxies and their non-thermal radiation models
71. Observation with All-sky Survey High Resolution Air-shower detector Ashra
72. Monte Carlo simulation for the Tibet air shower array
73. Radiation and environment Measurement while thunder storm at TA site
74. Study of radio detection of highest energy cosmic rays
75. Study of Extremely-high Energy Cosmic Rays by Telescope Array
76. Development of an optical cavity to stabilize ultranarrow lasers
77. Development of Local Suspension Point Interferometer for CLIO (II)
78. Gravitational Wave Detector in Kamioka (IX)
79. Development of an intensity stabilization system for a high-power laser for CLIO
80. Research of the Earth's free oscillations based on simultaneous observations with a laser strainmeter and a superconducting gravimeter
81. data analysis using CLIO data
82. Development of DC-readout system for CLIO interferometer
83. Study of a LCGT cryostat toward ultra-high vacuum operation
84. Development of Sapphire Mirror Suspension for LCGT (VI)
85. R&D and Design of large-scale cryogenic gravitational wave telescope (XI)
86. Development of Local Suspension Point Interferometer for CLIO (XII)
87. Evolution of the universe and particle physics

88. Comprehensive Researches on Cosmic Dusts
89. Detection of time variations for cosmogenic Be-7
90. Detection of low level radioisotopes in tree rings
91. Study of solar activity, cosmic rays and climate change based on the analysis of cosmogenic nuclides and stable isotopes
92. Chemical study for Antarctic micrometeorites
93. Determination of ^{26}Al in Antarctic meteorite samples
94. Continuous Measurement of Underground Laboratory Environment
95. Deposition Rate variation of natural activities ^7Be and ^{210}Pb
96. Simulation Study for the IceCube Neutrino Observatory
97. Precise calculation of the atmospheric neutrino flux
98. Future plan symposium for cosmic ray research

G. List of Committee Members

(a) Board of Councillors

KAJITA, Takaaki	ICRR, University of Tokyo
TERASAWA, Toshio	ICRR, University of Tokyo
KURODA, Kazuaki	ICRR, University of Tokyo
NAKAHATA, Masayuki	ICRR, University of Tokyo
YAMAGATA, Toshio	University of Tokyo
MATSUMOTO, Yoichiro	University of Tokyo
NISHIKAWA, Koichiro	KEK
EGUCHI, Toru	YITP, Kyoto University
MIYAMA, Shoken	National Astronomical Observatory
TORII, Shoji	Waseda University
MASAIKE, Akira	Kyoto University
MURAKI, Yasushi	Konan University
MAKINO, Fumiyoshi	Institute of Space and Astronautical Science
SATO, Katsuhiko	IPMU, University of Tokyo
KOMAMIYA, Yukio	ICEPP, University of Tokyo

(b) Advisory Committee

KAJITA, Takaaki	ICRR, University of Tokyo
NOJIRI, Mihoko	KEK
SAITO, Naohito	KEK
YAMAMOTO, Hitoshi	Tohoku University
AIHARA, Hiroaki	University of Tokyo
ITOW, Yoshitaka	STEL, Nagoya University
MORI, Masaki	Ritsumeikan University
KAJINO, Fumiyoshi	Konan University
MUNAKATA, Kazuoki	Shinshu University
TOTANI, Tomonori	Kyoto University
FUKUSHIMA, Masaki	ICRR, University of Tokyo
SUZUKI, Yoichiro	ICRR, University of Tokyo
KURODA, Kazuaki	ICRR, University of Tokyo
TERASAWA, Toshio	ICRR, University of Tokyo
NAKAHATA, Masayuki	ICRR, University of Tokyo
KAWASAKI, Masahiro	ICRR, University of Tokyo

(c) Inter-University Research Advisory Committee

NISHIJIMA, Kyoshi	Tokai University
OHASHI, Hideo	Tokyo University of Marine Science and Technology
KANDA, Nobuyuki	Osaka City University
MUNAKATA, Kazuki	Shinshu University
TASAKA, Shigeki	Gifu University
TAMURA, Tadahisa	Kanagawa University
YAMAMOTO, Tokonatsu	Konan University
OGIO, Shoichi	Osaka City University
FUKUSHIMA, Masaki	ICRR, University of Tokyo
OHASHI, Masatake	ICRR, University of Tokyo
TAKITA, Masato	ICRR, University of Tokyo
YOSHIKOSHI, Takanori	ICRR, University of Tokyo
SHIOZAWA, Masato	ICRR, University of Tokyo

H. List of Personnel

Director	KAJITA, Takaaki		
Vice-Director	FUKUSHIMA, Masaki		
Kamioka Observatory (Neutrino and Astroparticle Division)			
Scientific Staff	NAKAHATA, Masayuki, MORIYAMA, Shigetaka, ABE, Ko, KISHIMOTO, Yasuhiro, MIURA, Makoto, OGAWA, Hiroshi, TAKEDA, Atsushi,	SUZUKI, Yoichiro, SHIOZAWA, Masato, HIRAIDE, Katsuki, KOBAYASHI, Kazuyoshi, NAKAYAMA, Shoei, SEKIYA, Hiroyuki, TOMURA, Tomonobu,	HAYATO, Yoshinari, YAMASHITA, Masaki, KAMEDA, Jun, KOSHIO, Yusuke, OBAYASHI, Yoshihisa, TAKEUCHI, Yasuo, YAMADA, Satoru
Administrative Staff	TAKAKURA, Koji		
Technical Staff	KANBE, Tomio, ONOE, Tatsuya	KUMAMARU, Seiichi,	NOZAWA, Noriyuki,
Research Fellow	TAKENAGA, Yumiko		
Secretary	MAEDA, Yukari,	OKURA, Yoko,	TAKAMATSU, Midori
Research Center for Cosmic Neutrinos (Neutrino and Astroparticle Division)			
Scientific Staff	KAJITA, Takaaki, OHASHI, Hideo	KANEYUKI, Kenji,	OKUMURA, Kimihiro,
Technical Staff	SHINOHARA, Masanobu		
Research Fellow	KAJI, Hiroshi,	LAING, Andrew Brian	
Secretary	KITSUGI, Atsuko,	WATANABE, Keiko	
High Energy Cosmic Ray Division			
Scientific Staff	FUKUSHIMA, Masaki, RUBTSOV, Grigory, TERASAWA, Toshio, TESHIMA, Masahiro, OISHI, Michiko, TAKITA, Masato, SASAKI, Makoto,	NONAKA, Toshiyuki, SAKURAI, Nobuyuki, LEE, Martin Alan, ENOMOTO, Ryoji, ONISHI, Munehiro, ASAOKA, Yoichi	TAKEDA, Masahiro, SHIBATA, Tatsunobu, SCHOLER, Manfred, YOSHIKOSHI, Takanori,
Technical Staff	KOBAYASHI, Takahide, AOKI, Toshifumi, KOIZUMI, Chikako,	HOSHI, Noboru, MORIMOTO, Yusuke,	IKEDA, Kiriko, NAKADA, Yuichiro
Research Fellow	IKEDA, Daisuke, CHEN, Ding, AITA, Yuichi,	KONDO, Yoshimi, KAWATA, Kazumasa, MASUDA, Masataka,	TAMEDA, Yuichiro,
Secretary	OKAMURA, Takako, TATSUMI, Fusako, KOKUBUN, Yayoi, FUKUI, Misa,	OKI, Kaoru, TOJO, Kaori	OTA, Kazuaki
Akeno Observatory (High Energy Cosmic Ray Division)			
Scientific Staff	SAGAWA, Hiroyuki		
Technical Staff	OOKA, Hideyuki,	SHIMIZU, Kanetoshi	
Norikura Observatory (High Energy Cosmic Ray Division)			
Technical Staff	AGEMATSU, Yoshiaki, USHIMARU, Tsukasa,	ISHITSUKA, Hideki, YAMAMOTO, Kuniyuki	SHIMODAIRA, Hideaki,

Astrophysics and Gravity Division

Scientific Staff	KAWAMURA, Seiji, MIYOKI, Shinji, MIYAKAWA, Osamu, NAKATANI, Ichiro, KIMURA, Nobuhiro, FUKUGITA, Masataka, MIYAHARA, Hiroko, KAWASAKI, Masahiro,	KURODA, Kazuaki, UCHIYAMA, Takashi, OISHI, Naoko, SAITO, Yoshio, OUCHI, Masami, HISANO, Junji,	OHASHI, Masatake, TANNER, David Burham, TAKAHASHI, Ryutaro, SUZUKI, Toshikazu, MENARD, Brice, IBE, Masahiro
Research Fellow	SHIOMI, Sachie, KUROYANAGI, Sachiko, SEKIGUCHI, Toyokazu	KUSAKABE, Motohiko,	ISHIWATA, Koji,
Secretary	KIKUCHI, Rie,	MASHIMA, Chieko,	SAKAI, Akiko

Graduate Students

Doctor	KIDO, Eiji, LEE, Ka-pik, UESHIMA, Kota, SAITOH, Takanori, KAWAKAMI, Etsuko, RYO, Masaki, KONISHI, Kohki, MIYAMOTO, Hideaki,	McLACHLAN, Thomas Fukuei, YOKOZAWA, Takaaki, KOBAYASHI, Takeshi, SAIKAWA, Kenichi, OBI, Yoshio	UENO, Ko, MIYAMOTO, Koichi, SUGIYAMA, Shohei,
Master	TAKAHASHI, Yoshiaki, TOYAMA, Takeshi, INOUE, Daisuke, ITOH, Takashi, IYOGI, Kazuki, HIRANO, Shigetoshi, SAKAKIBARA, Yusuke, KITAJIMA, Naoya, TAKESAKO, Tomohiro, NAGATA, Kumiko	SODA, Takashi, HIRAI, Shun, NISHIIE, Hironori, SEKIGUCHI, Takanori, NAGATA, Natsumi, YAMAMOTO, Yusuke,	YOSHIGOE, Koichi, SHINOZAKI, Akihiro, TAKEDA, Naoyuki,

Administration Division

Scientific Staff	ITOH, Hideo		
Administrative Staff	MATSUZAWA, Noboru, ARIDOME, Ryutaro, AKIYAMA, Makiko, SAITO, Akiko,	SETO, Mikako, OGURA, Satoshi, FUJIE, Tamiko, TAKANO, Eri,	SASADA, Takaaki, KANEKO, Saho, MARUMORI, Yasuko, YAMAGUCHI, Akiko